

# **The Use of Confocal Raman Microscopy for the Evaluation of *In-Vitro* Biofilm Model Structures**

von der Fakultät 4 Energie-, Verfahrens- und Biotechnik der  
Universität Stuttgart zur Erlangung der Würde eines Doktors der  
Naturwissenschaften (Dr. rer. nat.) genehmigte Abhandlung

vorgelegt von

**Lukas Simon Kriem**

aus Ludwigsburg

Hauptberichter: apl. Prof. Dr. Steffen Rupp

1. Mitberichter: Prof. Dr. Roland Kontermann

Tag der mündlichen Prüfung: 21.11.2022

Institut für Grenzflächenverfahrenstechnik und Plasmatechnologie der  
Universität Stuttgart

2022



## **Publications**

This work was funded in parts by the European Union's Horizon 2020 research innovation programme under grant agreement No. 722871 in the scope of the Marie Skłodowska-Curie Action ITN BioClean. P&G and other partners contributed time, industrial supervision, training and technical guidance/expertise, access to equipment, placements in industry and coauthored and reviewed associated papers.

As part of the grant, agreement parts of this work were already published in peer-reviewed journals and can be found here:

Kriem, L.S., Wright, K., Ccahuana-Vasquez, R.A., Rupp, S., 2020. Confocal Raman microscopy to identify bacteria in oral subgingival biofilm models. PLOS ONE 12, e0232912. <https://doi.org/10.1371/journal.pone.0232912>

Kriem, L.S., Wright, K., Ccahuana-Vasquez, R.A., Rupp, S., 2021. Mapping of a subgingival dual-species biofilm model using Confocal Raman Microscopy. Front. Microbiol. doi: 10.3389/fmicb.2021.729720

Additionally, this work has been shared publicly at several national and international conferences and meetings. A complete list can be found in the Chapter 8.1 (Appendix) of this work.

### Abstract

In nature, the majority of microorganisms grow and accumulate on surfaces. These microorganisms are in general surrounded by an extracellular matrix, also generating a biofilm. Extensive research has been done to further understand these biofilms, especially those that cause human diseases such as subgingival biofilms where their accumulation on teeth over time can cause gingivitis and periodontitis. While dynamics, formation and composition of these biofilms are well known, techniques for continuously monitoring the formation of subgingival biofilm are limited. In recent years, advancements in the field of optical spectroscopic techniques have provided an alternative for analyzing three-dimensional microbiological structures, in addition to the traditional destructive or biofilm staining techniques. In this work, it was demonstrated that the use of confocal Raman spectroscopy, coupled with multivariate analysis, provides an approach to differentiate common subgingival bacteria. In addition, a workflow was developed that allows for the spatial differentiation of bacteria in an *in vitro* model simulating a subgingival biofilm, a technique which was also confirmed by mapping a second mixed species *in vitro* biofilm found on medical devices.

The present work demonstrates the use of confocal Raman Microscopy to differentiate common subgingival bacterial species (*Actinomyces naeslundii*, *Fusobacterium nucleatum*, *Streptococcus mutans*, *Veillonella dispar* and *Prevotella nigrescens*) and including their identification in unknown samples. In a second step, a workflow was established to evaluate and differentiate bacterial species in two dual-species *in vitro* biofilm models, using confocal Raman microscopy. The first biofilm model comprised of *Actinomyces denticolens* and *Streptococcus oralis* was cultured using the ‘Zürich *in vitro* model’. *Candida albicans* and *Pseudomonas aeruginosa* were cultured as a second dual-species biofilm to confirm the established workflow. Both biofilms were then analyzed using confocal Raman Microscopy. Cluster analysis was used to spatially differentiate and map the biofilm models over a specified area. To confirm species clustering within the cultured biofilms, confocal laser scanning microscopy was coupled with fluorescent *in-vitro* hybridization. Furthermore, dense bacteria interface area samples, as an artificial model of clusters in a biofilm, were used to test the developed multivariate differentiation model. This confirmed model was successfully used to differentiate species in a dual-species biofilm that were additionally compared and confirmed by morphology analysis. The results show that the developed workflow was able to identify main clusters of bacteria based on spectral ‘fingerprint region’ information acquired from confocal Raman microscopy. Using this workflow, it was demonstrated that confocal Raman microscopy can be used to spatially analyze dual-species *in vitro* biofilms, thus providing an alternative technique to map biofilm models.

### Zusammenfassung

In der Natur akkumulieren die meisten Mikroorganismen mit Hilfe einer extrazellulären Matrix auf Oberflächen. Diese Akkumulation von Mikroorganismen ist auch als Biofilme bekannt. Zahlreiche Forschungsarbeiten wurden zu diesen Biofilmen durchgeführt, insbesondere zu denjenigen, die beim Menschen Krankheiten hervorrufen. Hierzu gehören subgingivale Biofilme, die durch ihre Ansammlung auf Zähnen im Laufe der Zeit zu Gingivitis und Parodontitis führen kann. Während Dynamik, Bildung und Zusammensetzung dieser Biofilme bekannt sind, gibt es nur wenige Methoden, die eine kontinuierliche Überwachung des Wachstums von subgingivalen Biofilmen ermöglichen. Fortschritte im Bereich der optischen Spektroskopie führten zu einer Alternative zur klassischen Analyse dreidimensionaler mikrobiologischer Strukturen, wie destruktive Methoden oder Biofilm-Färbetechniken. In dieser Arbeit wurde gezeigt, dass der Einsatz der konfokalen Raman-Spektroskopie in Verbindung mit einer multivariaten Analyse einen Ansatz zur Differenzierung gängiger subgingivaler Bakterien bietet. Darüber hinaus wurde ein Workflow entwickelt, der die räumliche Differenzierung von Bakterien in einem subgingivalen *In-vitro* Biofilmmodell ermöglicht. Dieser Prozess wurde an einem weiteren medizinisch relevanten *In-vitro* Biofilmmodell, bestätigt.

In der vorliegenden Arbeit wurde der Einsatz der konfokalen Raman-Mikroskopie zur Differenzierung gängiger subgingivaler Bakterienarten (*Actinomyces naeslundii*, *Fusobacterium nucleatum*, *Streptococcus mutans*, *Veillonella dispar* und *Prevotella nigrescens*) und die Identifikation von Arten in unbekanntem Proben demonstriert. In einem zweiten Schritt wurde ein Workflow zur Bewertung und Unterscheidung von Bakterienarten in zwei unterschiedlichen *In-vitro* Biofilmmodellen mit zwei Spezies unter Verwendung der konfokalen Raman-Mikroskopie entwickelt. Das erste Biofilmmodell, bestehend aus *Actinomyces denticolens* und *Streptococcus oralis*, wurde mit dem "Zürich *in vitro* Modell" kultiviert. *Candida albicans* und *Pseudomonas aeruginosa* wurden ebenfalls gemeinsam als Biofilm kultiviert, um den etablierten Workflow zu bestätigen. Beide Biofilme wurden mit konfokaler Raman-Mikroskopie analysiert. Mit Hilfe der Clusteranalyse wurden die Biofilmmodelle räumlich differenziert und dargestellt. Zur Validierung wurde die konfokale Laser Scanning Mikroskopie mit fluoreszierender *In-vitro* Hybridisierung eingesetzt. Darüber hinaus wurden Proben mit Bakteriengrenzflächen als Modell von Clustern in einem Biofilm verwendet, um das entwickelte multivariate Differenzierungsmodell zu testen. Dieses Modell wurde erfolgreich zur Differenzierung von Organismen in einem Zwei-Organismen Biofilm verwendet. Zusätzlich wurden die erhaltenen Ergebnisse mittels Morphologie-Analysen verglichen und bestätigt. Die Ergebnisse zeigen, dass der entwickelte Workflow geeignet war, die untersuchten Bakterien durch konfokale Raman-Mikroskopie zu identifizieren. Dies basiert auf den „Fingerprint Regionen“, die charakteristisch für verschiedene Spezies sind. Mit Hilfe dieses Workflows konnte gezeigt werden, dass die konfokale Raman Mikroskopie Zwei-Organismen Biofilme *in vitro* räumlich analysieren und darstellen kann und somit eine alternative Technik zur Darstellung von Multi-Organismen Biofilmmodellen darstellt.

### Acknowledgments

I would like to thank the following people, without whom I would not have been able to complete this research, and without whom I would not have made it through my dissertation!

I would like to thank...

... **apl. Prof. Dr. Rupp** for his guidance, support and mentoring over the past few years, especially when communication and scientific exchange weren't made easy due to the COVID-19 pandemic.

... **Prof. Dr. Kontermann** for his willingness to be my second referee to evaluate this thesis.

... **Dr. Kevin Wright** and **Dr. Renzo Vasquez** from P&G for their continuous input, scientific conversations and insights into the industrial work environment, that inspired me to continue this research and challenge me to be successful in this project.

... **Dr. Iris Trick** and **Dr. Ursula Schließmann** for believing in me and my abilities and giving me the opportunity to work on this project.

... my colleagues at the Fraunhofer IGB **Bryan Lotz, Ilka Derwenskus, Gerhard Gottschling** and **Hedwig Pilgram** for the motivating, enjoyable work environment and the scientific discussions.

... all **students and professors from the Bioclean Network** for the great scientific exchange, help and numerous exciting meetings over the past few years.

... the **colleagues at the former Greater London Innovation Center** in Egham for their support, welcoming arms and great work environment throughout my secondment.

... Finally, I would not be where I am today without my friends and family. I would like to thank my girlfriend, **Laney** for taking this journey through graduate school with me. I would also like to thank my mother, **Marion**, my father, **Gerhard** and my sister **Sarah** for their endless love and support.

...the **SARS CoV-2** virus for teaching me what's important in life and forcing me to take the time to successfully finish this thesis.

## Table of Contents

<b>Abstract</b> .....	<b>I</b>
<b>Zusammenfassung</b> .....	<b>II</b>
<b>Acknowledgments</b> .....	<b>III</b>
<b>List of Abbreviations</b> .....	<b>VI</b>
<b>List of Figures</b> .....	<b>VIII</b>
<b>List of Tables</b> .....	<b>X</b>
<b>1 Introduction</b> .....	<b>1</b>
1.1 Microorganisms and biofilms.....	3
1.1.1 Physiology and biochemistry of microorganisms.....	3
1.1.2 Development of biofilms.....	5
1.1.3 Oral subgingival bacteria and biofilms.....	9
1.1.4 Bacterial and fungal biofilms with clinical relevance.....	12
1.2 Methodology of identification of microorganisms.....	13
1.3 Raman Spectroscopy Instrumentation.....	16
1.3.1 The Raman effect.....	16
1.3.2 Molecular vibrations of molecules and resulting Raman peaks.....	18
1.3.3 Information-rich spectral regions of microorganisms.....	19
1.3.4 Raman-based methods for biofilm analysis.....	22
1.4 Mathematical Methods and Data Analysis.....	24
1.5 Insights and results from previous studies.....	26
<b>2 Objectives</b> .....	<b>28</b>
<b>3 Material and Methods</b> .....	<b>29</b>
3.1 Materials.....	29
3.1.1 Instruments.....	29
3.1.2 Software.....	31
3.1.3 Microorganisms.....	31
3.1.4 Consumables.....	32
3.2 Methods.....	32
3.2.1 Cultivation and sample preparation of planktonic bacteria.....	32
3.2.2 Cultivation and sample preparation of biofilms.....	35
3.2.3 Optimization of oral biofilm cultivation methods.....	36
3.2.4 Sample preparation for different analysis methods.....	37
3.3 Raman signal processing and multivariate analysis.....	40
3.3.1 Data processing.....	41
3.3.2 Statistical modelling.....	45
3.3.3 Biofilm distribution mapping using CA.....	51
<b>4 Results</b> .....	<b>53</b>
4.1 Differentiation of oral bacteria.....	53
4.1.1 Raman spectra for five subgingival bacterial species.....	53
4.1.2 Influence of the growth phase of bacteria on the Raman spectra.....	56
4.1.3 Influence of sample preparation on the Raman spectra.....	57
4.1.4 Multivariate analysis of species.....	61

## TABLE OF CONTENTS

---

4.1.5	Identification of bacteria with Raman .....	64
4.2	Analysis of biofilm structure .....	67
4.3	Model development for spatial mapping of biofilms .....	68
4.3.1	Calibration of planktonic bacteria and mono-species biofilms using Renishaw inVia™ Qontor .....	69
4.3.2	Multivariate analysis of calibration datasets .....	72
4.3.3	Evaluation of mapping analysis model .....	74
4.3.4	Mapping of dual-species biofilms .....	76
4.3.5	Comparison of different mapping technologies to CRM .....	80
4.4	Application of the used model for other biofilms.....	83
4.4.1	Formation of calibration datasets for <i>C.albicans</i> and <i>P.aeruginosa</i> .....	83
4.4.2	Multivariate analysis of biofilm calibration datasets .....	84
4.4.3	Mapping of dual-species biofilms .....	85
<b>5</b>	<b>Discussion .....</b>	<b>88</b>
5.1	CRM method development.....	88
5.2	Use of CRM for mapping of dual-species biofilms.....	92
5.3	Comparison of Raman mapping to other methods .....	98
5.3.1	Fluorescent and morphological mapping techniques .....	98
5.3.2	Laser-induced vibrational mapping technique .....	99
5.3.3	Mapping techniques based on chemometric profiles .....	101
5.3.4	Combination of techniques for mapping with CRM .....	102
<b>6</b>	<b>Conclusion and Outlook.....</b>	<b>104</b>
<b>7</b>	<b>References.....</b>	<b>109</b>
<b>8</b>	<b>Appendix.....</b>	<b>123</b>
8.1	Outreach activities .....	123
8.2	Raman spectra of different biological molecules .....	124
8.3	Media recipes.....	125
8.3.1	Modified Fluid Universal Medium in Sørensen’s buffer (pH 7.2): .....	125
8.3.2	Saliva and artificial saliva preparation and evaluation.....	127
8.4	Fluorescent <i>in-situ</i> hybridization .....	130
8.5	Raman spectra.....	131
8.5.1	Borosilicate glass spectrum .....	131
8.5.2	Hydroxyapatite disc spectrum .....	131
8.5.3	Peak assignment of Raman spectra for medical microorganisms .....	132
8.6	RT-PCR calibration curves.....	132
8.7	Individual images of FISH staining .....	133
8.8	Bacteria coverage for different samples that were analyzed through morphology and Raman analysis .....	134
	<b>Declaration of Authorship .....</b>	<b>135</b>



## List of Abbreviations

Abbreviation	Unit	Description
	°C	temperature
	µg, g	mass
	µL, mL	volume
	bp	base pairs
	cm <sup>-1</sup>	wavelength unit
	cm <sup>2</sup>	area
	mM	milli Molar
	nm, µm	length
	rfu	relative fluorescent units
	rpm	rotations per minute
	sec, min, h	time
(w/v)		weight to volume ratio in %
<b>6-FAM</b>		6-Carboxyfluorescein fluorescent dye
<b>ACT476</b>		Name of the specific fluorescent dye sequence for <i>Actinomyces</i>
<b>AFM</b>		Atomic Force Microscopy
<b>An</b>		<i>A.naeslundii</i>
<b>Ar-Laser</b>		Argon Laser
<b>ATCC</b>		American Type Culture Collection (strain number)
<b>ATR-FTR</b>		Attenuated Total Reflectance-Fourier Transform Infrared
<b>BHI</b>		Brain Heart Infusion Medium
<b>CA</b>		Cluster Analysis
<b>CCD</b>		Charge-coupled Device Camera
<b>CDC</b>		Center of Disease Control
<b>CE</b>		Confidence Ellipse
<b>CLSM</b>		Confocal Laser Scanning Microscopy
<b>CRM</b>		Confocal Raman Microscopy
<b>Cy3</b>		Cyanine fluorescent dye
<b>DBIA</b>		Dense Bacteria Interface Area
<b>DMM</b>		Defined Medium Mucin
<b>DNA</b>		Deoxyribonucleic Acid
<b>DSM</b>		DSMZ- German Collection of Microorganisms and Cell Culture GmbH (strain number)
<b>EPS</b>		Extracellular polymeric substance
<b>ESEM</b>		environmental scanning electron microscopy
<b>FA</b>		Formamide
<b>FISH</b>		Fluorescence <i>in-situ</i> hybridization
<b>Fn</b>		<i>F.nucleatum</i>
<b>FT-IR</b>		Fourier transform infrared spectroscopy
<b>HCA</b>		Hierarchical Cluster Analysis
<b>He-Ne-Laser</b>		Helium/Neon Laser
<b>ID</b>		Identification
<b>IGB</b>		Fraunhofer Institute for Interfacial Engineering and Biotechnology

## LIST OF ABBREVIATIONS

---

<b>IR</b>	Infrared Spectroscopy
<b>K++</b>	specific algorithm for data analysis
<b>LB</b>	Lysogeny broth
<b>LDA</b>	Linear Discriminant Analysis
<b>MALDI-TOF</b>	Matrix Assisted Laser Desorption/Ionization, Time Of Flight Mass Spectrometer
<b>mFUM</b>	modified Fluid Universal Medium
<b>MIT447</b>	Name of the specific fluorescent dye sequence for <i>Streptococcus</i>
<b>NaCl</b>	Sodium chloride
<b>O2PLS-DA</b>	Orthogonal Two-Way Partial Least Square Analysis with Discriminant Analysis
<b>OD600</b>	Optical Density at 600nm
<b>OPLS</b>	Orthogonal Partial Least Square
<b>PBS</b>	Phosphate-buffered saline
<b>PC</b>	Principal Component
<b>PCA</b>	Principal Component Analysis
<b>PC-LR</b>	Principle Component with Linear Regression analysis
<b>PFA</b>	Paraformaldehyde
<b>PLS</b>	Partial Least Square
<b>Pn</b>	<i>P.nigrescens</i>
<b>qPCR</b>	quantitative Polymer Chain Reaction
<b>RM</b>	Raman Microscopy
<b>RNA</b>	ribonucleic acid
<b><i>rpoS</i></b>	RNA polymerase, sigma S gene
<b>rRNA</b>	ribosomal ribonucleic acid
<b>RT-PCR</b>	Real-time Polymer Chain Reaction
<b>SEM</b>	Scanning Electron Microscopy
<b>SERS</b>	Surface Enhanced Raman Spectroscopy
<b>Sm</b>	<i>Streptococcus mutans</i>
<b>SVM</b>	Super Vector Machine
<b>TE</b>	Solution made from Tris and EDTA
<b>TERS</b>	Tip-Enhanced Raman Spectroscopy
<b>UV</b>	Ultra violet light
<b>Vd</b>	<i>V.dispar</i>
<b>VWR</b>	American chemicals distributor
<b>w/o</b>	without
<b>YNBNP</b>	Yeast Nitrogen Base w/o amino acids and ammonium sulfate broth
<b>YPD</b>	Yeast Extract-Peptone-Dextrose broth

---

## List of Figures

Figure 1: Number of publications with the terms 'Biofilm' and 'Biofilm mapping' .....	1
Figure 2: Schematic of a eukaryotic cell (left) and a prokaryotic cell (right) .....	4
Figure 3: Stages of biofilm formation .....	8
Figure 4: Composition of subgingival biofilms.....	11
Figure 5: Summary of different characterization technologies for biofilms .....	14
Figure 6: Jablonski diagram of possible scattering interactions between an incident photon (green) and a Raman active molecule.....	17
Figure 7: The different types of Raman-active vibrational modes for the molecule $O=CH_2$ . .....	19
Figure 8: Example of Raman spectra with an extended range ( $103.3-3205\text{ cm}^{-1}$ ) .....	20
Figure 9: Raman spectra of amino acids with a non-cyclic R side chain.....	21
Figure 10: Comparison of spectral peaks of two Raman instruments with V.dispar .....	29
Figure 11: Schematic of sample preparation for the calibration of planktonic bacteria.....	34
Figure 15: Raw Raman spectrum. ....	41
Figure 16: Spectrum after truncation.....	42
Figure 17: Spectrum after Cosmic Ray removal. ....	42
Figure 18: Spectrum after background removal. ....	43
Figure 19: Spectrum after baseline correction.....	43
Figure 20: Spectrum after noise filtering.....	44
Figure 21: Spectrum after smoothing. ....	44
Figure 22: Spectrum after normalization.....	45
Figure 23: Spectrum after differentiation. ....	45
Figure 21: Examples of relative coverages and approaches of determination. ....	52
Figure 22: Averaged processed Raman signal (84 spectra total per species) from five different subgingival species of the calibration group with standard deviations .....	53
Figure 23: Average spectra for five different species at four different growth phases .....	59
Figure 24: Average spectra for five different species in a hydrated and dehydrated state including the standard deviation.....	60
Figure 25: Multivariate Analysis of selected oral bacteria show the distribution of the same set of spectra (84 spectral samples for each strain) for A. PCA Analysis and B. O2PLS-DA Analysis.....	62
Figure 26: O2PLS-DA analysis of planktonic cell spectra for three species shows the distribution of spectra.....	65
Figure 27: O2PLS-DA analysis of mono-species biofilm spectra .....	66
Figure 28: CLSM image of the FISH-stained dual-species biofilm.....	68
Figure 29: Experimental design setup for the differentiation and confirmation of Raman mapping in a dual-species biofilm model. ....	69

## LIST OF FIGURES

---

Figure 30: Averaged processed Raman signals (300 spectra for each dataset) before Savitsky-Golay differentiation for <i>S.oralis</i> and <i>A.denticolens</i> and their standard deviations.....	70
Figure 31: PCA Analysis of selected oral bacteria show the distribution of the 2nd order derivative of spectra.....	73
Figure 32: Distribution of <i>A.denticolens</i> and <i>S.oralis</i> in a DBIA sample .....	75
Figure 33: Distribution of <i>A.denticolens</i> (red areas) and <i>S.oralis</i> (green areas) in 15 dual-species biofilms.....	77
Figure 34: Coverage distribution was calculated from samples shown in Figure 33 for morphology and Raman analysis using ImageJ.....	79
Figure 35: Specific Coverage distribution based on the blue areas in Figure 33 that were calculated based on the specific differences at each location using ImageJ. The red line indicates the average difference of the 15 samples with 26.71 % . .....	80
Figure 36: Averaged processed Raman signal (300 spectra total) for <i>P.aeruginosa</i> and <i>C.albicans</i> mono-species biofilms after processing without differentiation. ....	83
Figure 37: PCA Analysis in the form of a score plot of two selected medically relevant bacteria .....	84
Figure 38: Distribution of <i>C.albicans</i> and <i>P.aeruginosa</i> in a biofilm .....	86
Figure 39: Peak intensity at 1525 $\text{cm}^{-1}$ using CRM with standard deviation. ....	94
Figure 40: Peak intensity at 982 $\text{cm}^{-1}$ using CRM with standard deviation. ....	95
Figure 41: Total concentration of bacteria in a multi-species biofilm consisting of <i>A.denticolens</i> , <i>S.oralis</i> and <i>V.dispar</i> . ....	129
Figure 42: Ratio of bacterial species within a biofilm cultivated with different types of saliva .....	129

---

## List of Tables

Table 1: Macromolecules that can be found in a bacterial cell .....	5
Table 2: human infections that are associated to biofilms.....	7
Table 3: Different functionalities of the EPS components and role within a biofilm .....	9
Table 4: Overview of Raman-based technologies.....	23
Table 5: Used Microorganisms and species ID.....	32
Table 6: Primer sequences used for the quantification of multi-species biofilms.....	38
Table 7: Product fragment sequence formed with the use of primer sequences described previously.	38
Table 8: Prepared master mix for qPCR application per sample. ....	39
Table 9: qPCR cycle settings.....	39
Table 10. Sequence and formamide concentrations for fluorescence in-situ hybridization probes .....	40
Table 11: List of collected spectra for the different analysis setups in this research. ....	41
Table 12: Application of different statistical methods .....	50
Table 13: Parameters that can be selected as part of the WiRe 5.2.....	52
Table 14: Specific peak assignments for the different species and their presence or absence compared to other species .....	54
Table 15: Comparison of the performance of species identification using the O2PLS-DA model for planktonic cells.....	65
Table 16: Comparison of the performance of species identification using the O2PLS-DA model for mono-species biofilm spectra.....	66
Table 17: Comparison of relevant imaging techniques that consider the mapping of multi-species biofilms.....	82
Table 18: Quantitative results of bacterial and fungal coverage .....	87

# 1 Introduction

On our planet, most microorganisms live in multicellular communities consisting of bacteria, archaea, protozoa, algae and fungi. These are embedded to varying degrees in a hydrated biopolymer matrix almost always composed of extracellular polymeric substances, polysaccharides, proteins, nucleic acid and lipids, and form so-called biofilms (Branda et al., 2005). Historically, however, microorganisms were initially studied in their planktonic phases and research was focused mostly on the investigation and characterization of this growth phase of microorganisms. Even though biofilms were first described in 1936 (Zobell and Anderson, 1936), it took much longer until this research field was recognized and further explored, a fact made evident by the vastly increasing number of publications on this topic over the past two to three decades (Figure 1).

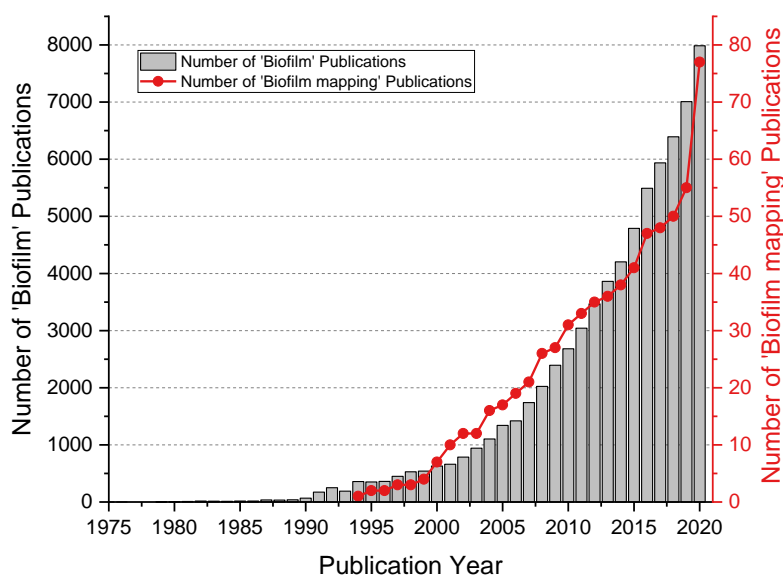


Figure 1: Number of publications with the terms 'Biofilm' and 'Biofilm mapping' per year between 1975 and 2020 (<https://www.webofscience.com/wos/woscc/basic-search>)

The formation of biofilms occurs on phase boundaries. The areas on which biofilm growth appears are at the interface from liquid to a solid, liquid to gaseous or solid to gaseous phase (Flemming and Wingender, 2010). Here, microorganisms tend to attach, assemble, proliferate and form clusters on surfaces, enabling their survival under many different conditions. Some examples of such biofilm formations are biofilms on rocks in rivers (liquid and solid phase) or biofilms on building facades (air and solid phase).

Biofilms typically have a negative connotation because they can have a harmful effect on human health. Especially biofilms in a medical setting have high importance. It is estimated that these biofilms can be accounted for approximately 65% of all bacterial infections (Lewis,

2001). They are usually the result of *Streptococci sp.*, *Staphylococci sp.*, gram negative bacteria, and/or fungal infections (Kokare et al., 2009). Of the many biofilm varieties studied, medical biofilms on implants are of high concern due to their resilience to antibiotics, which can result in recurring infections and the failure of treatments (Bryers, 2008; Whiteley et al., 2002).

Oral biofilms, as an example of such medical biofilms, have been studied in relation to oral diseases, like gingivitis and periodontitis (Tanner et al., 1996). Subgingival biofilms are specifically important because they grow in the subgingival sulcus and are in direct contact with both the tooth surface and tissue cells, where bacteria accumulation could lead to gingivitis or the development of other periodontal infections (Marsh and Martin, 2009; Zijng et al., 2012). Both infections have a high impact on the human health and their corresponding treatment costs are high as a result of their resistance to treatment (Costerton, 1999; Römling et al., 2014; Wolcott et al., 2010).

Bacterial distribution in biofilms have been widely identified and quantified over the past few decades. However, in recent years, the effect of the architecture of oral biofilms on the extent of disease has been identified as a factor that can have an influence on the behavior and damage exerted to the host. For this reason, it is to no surprise that research on biofilm mapping has increased, parallel to biofilm research in general (Figure 1) and underlines the demand to further understand the architecture of biofilms in different settings. In comparison to all biofilm publications, research on biofilm mapping is still very limited, making up only 0.01% of publications including the word 'biofilm' in the title.

For oral biofilms specifically, the most common mapping technique to analyze biofilms is the use of fluorescence *in-situ* hybridization (FISH) combined with confocal laser scanning microscopy (CLSM) (Kommerein et al., 2017; Thurnheer et al., 2019; Xiao et al., 2017). This technique has had a large impact in understanding the dynamics of oral biofilms, because it enabled researchers to view biofilms with good resolution and allowed for characterization. Nevertheless, the complex preparation procedure, the cost of materials and equipment and the time associated to this technique demands for new ways of analyzing biofilms (Pantanella et al., 2013).

Recently, with the technical advancements in optical spectroscopy it became possible to identify specific chemical components with high spectral resolution (Rzhevskii, 2019). Confocal Raman Microspectroscopy (CRM) is a combination of Raman Spectroscopy with confocal optical microscopy. Due to its unique technical characteristics, it allows for a non-

destructive and non-invasive analysis of a sample with no to little sample preparation, a spatial resolution of 1  $\mu\text{m}$  and the opportunity to continuously evaluate a sample (Liu et al., 2022). CRM measures scattered radiation and sample specific energy shifts from samples that have been excited with a laser beam. With the technology improvements of specific filters to inhibit scattered light to enhance the Raman signal, the development of more specific detectors, and the establishment of intensity strong laser sources to receive increased Raman counts, it has greatly increased the importance of CRM in biofilm research in recent years.

As a result of these improvements, CRM has been used successfully for the spatial resolution of biomedical environments like tissue samples or bacterial cells (Cals et al., 2018; Gualerzi et al., 2017; Rebrošová et al., 2017; Sil et al., 2017; Strola et al., 2013). However, the acquired signals from these biomedical components are highly complex (Colniță et al., 2017; Stöckel et al., 2016; Tewes, 2019). Therefore, differentiation based on Raman spectra has had significant limitations up to now (Beier et al., 2012, 2010; Cepeda-Pérez et al., 2016; Rebrošová et al., 2017; Zhu et al., 2004). For this reason, CRM has only been used a few times for the analysis of environmental biofilms thus far. The focus of these studies was based on molecular details of spectra 1. of single species biofilms (Gieroba et al., 2020; Kusić et al., 2015; Ramirez-Mora et al., 2019; Wickramasinghe et al., 2020), 2. over time (Carey et al., 2017; Chao and Zhang, 2012; Keleştemur et al., 2020; Liu et al., 2020) or 3. under the influence of stress, mostly chemicals (Daood et al., 2020; Jung et al., 2014). In all cases, spatial mapping was not yet considered in these settings. However, the results showed great opportunities for the development of mapping techniques using Raman-based technologies.

## 1.1 Microorganisms and biofilms

### 1.1.1 Physiology and biochemistry of microorganisms

Microorganism is a basic term for unicellular organisms and can further be divided into eukaryotes and prokaryotes (Figure 2). Bacteria and archaea belong to the prokaryote group, because they are simple-built unicellular organisms without a separated nucleus from the rest of the cell. In this work the focus is on various bacterial species which are *Actinomyces spp.*, *Fusobacterium nucleatum*, *Streptococcus spp.*, *Veillonella dispar*, *Prevotella nigrescens* and *Pseudomonas aeruginosa*. Cells that have a separated nucleus are grouped as eukaryotes, including fungi, algae and protozoa. In this work *Candida albicans* was used as a fungal organism pathogenic to human and involved in biofilm formation on medical devices. Besides the difference in cellular organization, there are more distinctions between the two kingdoms



## INTRODUCTION

of species. Both show four common structures: 1. the plasma membrane, that forms a barrier between the interior of a cell and their living environment, consisting of approximately 50% lipid and 50% protein by weight; 2. the cytoplasm, a viscous substance inside the cell that contains macromolecules important for different functions within the cell that is mainly composed of water, salts, and proteins; 3. nucleic acids, the genetic material of the cell; and 4. ribosomes, that facilitate protein synthesis, typically containing 40% protein and 60% RNA. The chemical composition of cells is especially important for the use of Raman spectroscopy and will be further discussed in the next chapters.

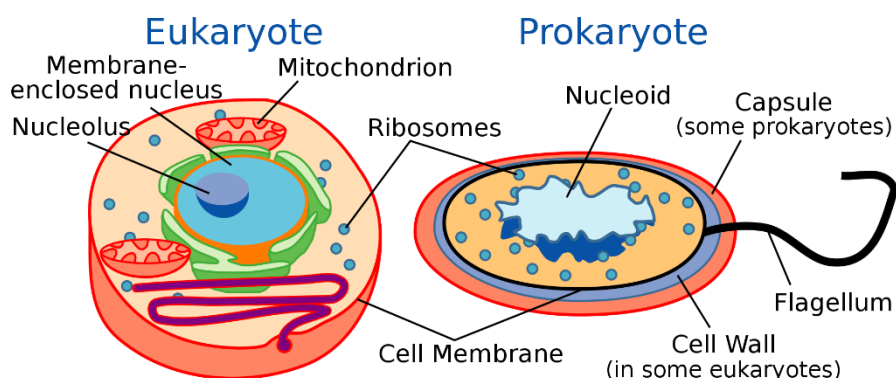


Figure 2: Schematic of a eukaryotic cell (left) and a prokaryotic cell (right) with main components of the cell (National Center for Biotechnology Information).

Prokaryotes come in various shapes, but many fall into three categories: 1. cocci (spherical), 2. bacilli (rod-shaped), and 3. spirilli (spiral-shaped). These shapes can be helpful for cell differentiation based on microscopic images. While the shape of a cell exhibits unique features, so does the macromolecular composition of a cell. As for most eukaryotic cells the main component in a bacterial cell is water – approximately 70% of the total cell weight. The remaining amounts are components that include mostly macromolecules, small monomer quantities and inorganic ions. With macromolecules making up around 96% of the dry weight, they are very important in terms of Raman spectra and Raman-active compounds that are discussed in the next chapters. Common macromolecules, monomeric subunits, and their locations in the cells including ratios are found in Table 1. Depending on species, growth state, metabolism, or whether they are part of a biofilm, these ratios can change (Wan et al., 2018).

Chapter 1.3.3 will show in detail that different molecular structures show unique Raman spectra. Using this information together with the knowledge about overall macromolecular compositions shown in Table 1, certain predictions can be made to differentiate species. This will be introduced in the next chapters. While Table 1 shows differences in the presence, absence and concentration of molecules between prokaryotes and eukaryotes (such as absence

## INTRODUCTION

of lipopolysaccharides or reduced RNA concentration in fungi), it will also be important to determine how differences within multiple bacterial species can be determined using Raman spectra.

*Table 1: Macromolecules that can be found in a bacterial cell with their monomers, location within the cell and percentage of dry cell weight. Numbers are based on Escherichia coli and Salmonella typhimurium (bacteria) and C.albicans chlamydo spores (fungi) (applied from Madigan et al., 2018; Jansons and Nickerson, 1970)*

Macromolecule	Primary subunit (monomer)	Location in a cell	Percentage of dry weight	
			Bacteria	Fungi
Proteins	amino acids	cell wall, cell membrane, pili, flagella, ribosomes, as enzymes in the cytoplasm.	55%	32%
Lipids	fatty acids	membranes, storage depots	9%	20-25%
Polysaccharides	sugars (carbohydrates molecules)	cell wall, capsule, inclusions (energy and carbon storage)	5%	35-40%
Lipopolysaccharides	sugars and fatty acids	membranes	3.4%	-
RNA	nucleotides	ribosomes	20.5%	6.2%
DNA	nucleotides	nucleoid, plasmid	3.1%	3-5%

### 1.1.2 Development of biofilms

Whenever microorganisms attach, assemble, proliferate and form clusters on surfaces to improve their survival under different conditions, they are referred to as biofilms. According to Jefferson (2004) three potential incentives can drive the formation of biofilms: 1. protection from harmful conditions (for example host defense), 2. sequestration to a nutrient-rich area (colonization), 3. utilization of cooperative benefits (community).

More than 99% of microorganisms worldwide organize themselves in multi-cellular communities. They are found at the interfacial regions solid-liquid (such as aquatic biofilms on rocks), liquid-gaseous (such as ‘floating biofilms’), and solid-gaseous (such as biofilms on building facades). Biofilms are comprised of a whole range of microorganisms such as Gram-negative and Gram-positive bacteria, archaea, protozoa, algae or fungi which are integrated differently in the biopolymer matrix consisting of extracellular polymeric substances (EPS), polysaccharides, proteins, nucleic acids and lipids. Biofilm structures provide protection to the inhabiting populations from chemical and physical environmental agents such as disinfectant solutions, biocides, antibiotics or radiation. Furthermore, the architecture and robustness of biofilms do not allow removal from the surface even with vigorous rinsing.

## INTRODUCTION

---

For that reason, biofilms are omnipresent in nature where nutrients are available and have specific roles in the habitats where they form. They play a key role in global chemical cycles such as the oxygen cycle, the carbon cycle and nitrogen cycle. They also function as natural filters in water bodies by purifying water through biodegradation of toxic organic and inorganic compounds and thereby reduce pollution. Humankind have used these specific characteristics to their advantage. For example, biofilms are used for the treatment of wastewater or for biologically cleaning oil spills in oceans (Brooijmans et al., 2009; Wuertz et al., 2005). In recent years, however, biofilms have tended to have a negative connotation, stemming from contaminations in water, foods, cosmetics or in production processes, as well as in hospitals (Hall-Stoodley et al., 2004). Especially in production processes, microbial growth causes damage to materials or impairs the function of technical equipment, resulting in increased energy consumption, reduced production efficiencies and costly downtimes (Di Pippo et al., 2018).

Biofilms are also found on and within humans where they can have positive and/or negative effects for the human host. When biofilms are part of a natural flora such as skin, mouth or gut flora, they can be rather beneficial because they inhibit the formation of pathogenic biofilms and support the digestion. In addition, they contribute to vitamins. They can additionally function as a protection layer against the colonization of pathogenic microorganisms, reducing the chance of diseases.

However, when biofilms are discussed in a medical and human context, a lot of these biofilms are harmful and require medical attention. Some of the infections associated to biofilms are summarized in Table 2, with the most prominent example being biofilms found on a tooth surface, a prerequisite for periodontitis or gingivitis or biofilms on medical devices.

According to Lewis in 2001, 65% of all human infections from microorganisms have their roots in biofilms. Fighting these infections can require substantial economical investments. Thorpe et al. (2018) concluded that the costs to treat bacterial infections in the US in 2014 was around \$2.2 billion, highlighting the need to increase research in this field. In fact, biofilms are up to 1000-fold more resistant to antibiotics and disinfection than planktonic bacteria (Mah, 2012), making efficient and cost-effective treatment very difficult and therefore increasing the hospital costs of patients fighting these bacterial infections.

## INTRODUCTION

*Table 2: Summary of human infections that are associated to biofilms with specific bacteria that are comprising these biofilms (applied from Purschke, 2012)*

<b>infections or disease</b>	<b>associated microorganisms</b>
caries	<i>Streptococcus spp.</i> , acid-forming cocci, <i>Candida spp.</i> , anaerobic bacteria
periodontitis	anaerobic bacteria
otitis media	<i>Haemophilus influenza</i>
chronic tonsillitis	different species
cystic fibrosis pneumonia	<i>Pseudomonas aeruginosa</i> , <i>Burkholderia cepacia</i>
endocarditis	<i>Streptococcus viridans</i> , staphylococci
necrotizing fasciitis	Group A Streptococci
musculoskeletal system	Gram-positive cocci
Osteomyelitis	different species
bile duct infection	gut bacteria
infectious liver stones	gram-negative rod bacteria
bacterial prostatitis	gram-negative bacteria
<b>infections associated to medical devices</b>	
contact lenses	<i>Pseudomonas aeruginosa</i> , Gram-positive cocci
stitch	staphylococci
respiration-associated pneumonia	gram-negative rod bacteria
prosthetic heart valve	staphylococci, <i>Enterococcus spp.</i> , <i>Candida albicans</i>
arterial prosthetic	staphylococci, <i>P. aeruginosa</i> , <i>C. albicans</i> , <i>Klebsiella pneumoniae</i>
endovascular catheters	staphylococci, <i>Candida spp.</i>
cerebrospinal fluid shunt	staphylococci, <i>C. albicans</i> , <i>Cryptococcus</i>
peritoneal dialysis peritonitis	different species
bladder catheter infection	<i>P. aeruginosa</i> , <i>Klebsiella pneumoniae</i> , <i>Enterococcus spp.</i> ( <i>E. coli</i> ), staphylococci, <i>Candida spp.</i>
intrauterine device	<i>Actinomyces israelii</i> , <i>S. aureus</i> , <i>C. albicans</i> , <i>Enterococcus spp.</i> , staphylococci
orthopedic prosthetics	staphylococci, <i>C. albicans</i> , <i>Enterococcus spp.</i> , <i>P. aeruginosa</i>

The interesting question arises: why do bacterial biofilms cause such a great resistance to external factors, not only antibiotics and disinfections, but also environmental changes such as nutrient availability, temperature or pH changes? The formation of biofilms is divided in five different phases from an initial bacterial attachment to a surface, to the dispersion of bacteria from a biofilm. The different stages are summarized in Figure 3.

In the first step, cells attach reversibly on inorganic or organic surface structures. This process is highly dependent on the material and structure of the surface. Biofilms will develop faster on rougher and hydrophobic materials than on smooth and/or hydrophilic surfaces (Pringle and Fletcher, 1983). However, many surfaces are coated by a fluidic milieu creating an environment of different chemical properties on the surface that adds to attachment of cells. Typically, Gram-negative are the first bacteria that are able to attach to a surface because they show the polar

charge (which makes them hydrophilic) on the outside of their cells allowing for easy attachment in the second step. After some time, as a third progression, individual cells produce an EPS which attaches them to the surface and allows them to protect themselves from external forces and adverse conditions. Additionally, cells start to produce adhesins which function as molecular anchor proteins that additionally interact with the surface to strengthen attachment (Lawrence et al., 1987).

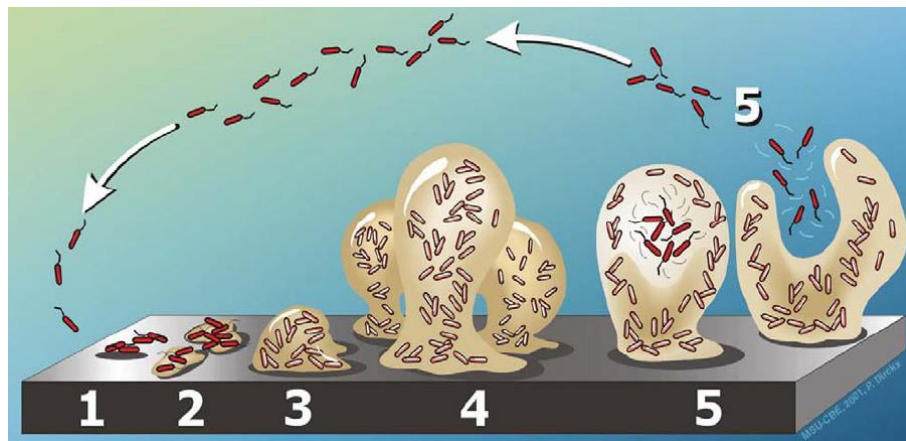


*Figure 3: Stages of biofilm formation. 1) initial surface attachment, 2) production of extracellular polymeric substance (EPS) and adhesins that lead to irreversible surface attachment, 3) formation of bacterial microcolonies, 4) biofilm maturation, 5) bacterial dispersion from the biofilm (Stoodley et al., 2002)*

Particularly the formation of EPS of attached bacteria has a large effect on the resistance to external forces. Although EPS consists of up to 98% of water, it is also comprised of polysaccharides, proteins, nucleic acids and lipids, creating an environment where microorganisms can get embedded in (Flemming, 2011). The composition of the EPS matrix, also known as ‘matrixome’, is an assembly of chemical and functional diverse biomolecules that can be grouped into either the category of molecules associated with the cell surface or molecules secreted extracellular. For biofilm formation, EPS plays a key role in the structural and functional properties of a biofilm that are not predictable or identifiable through the study of planktonic bacteria (Karygianni et al., 2020). These properties include surface adhesion-cohesion, chemical heterogeneity, spatial organization, physical and social interactions and increased tolerance to antimicrobials. Forming the three-dimensional framework of biofilms, EPS allows the adhesion to surfaces, aggregation of cells and sorption of organic and inorganic compounds and ions (Flemming and Wingender, 2010), but can take on many more functions that are summarized in Table 3. Because of their broad and versatile functions within a biofilm, the EPS matrix is important for the survival of the biofilm. Depending on the embedded microorganisms, the nutrient availability and growth conditions, the composition of the EPS-matrix varies.

## INTRODUCTION

*Table 3: Different functionalities of the EPS components and role within a biofilm (applied from Flemming et al., 2007).*

Effect of EPS component	Nature of EPS component	Role in biofilm
Constructive	Neutral polysaccharides Amyloids	Structural component Structural component
Sorptive	Charged hydrophobic polysaccharides	Ion exchange, sorption
Active	Extracellular enzymes	Polymer degradation
Surface-active	Amphiphilic Membrane vesicles	Interface interactions Export from cell, sorption
Informative	Lectins Nucleic acids	Specificity, recognition Genetic information, structure
Redox active	Bacterial refractory polymers	Electron donor or acceptor?
Nutritive	Various polymers	Source of C, N, P

The three-dimensional framework allows the increased proliferation of bacteria and the continuous growth of microorganisms in layers. It is also noteworthy that within the biofilm forming process, bacteria that do not form individual biofilms are now able to live synergetically with biofilm-forming bacteria and use their EPS architecture for attachment (Tsuneda et al., 2003). Additionally, a large number of genes of microorganisms living in biofilms are regulated differently than in planktonic living cells. This sometimes leads to strongly pronounced phenotypic and physiological differences within the same species and also changes the specific macromolecular composition within cells (Sánchez et al., 2019). Once biofilms reach a certain maturation level, individual cells or microcolonies detach to colonize new locations and habitats. This dispersion and continuous colonization is the result of nutrient limitations or shear forces from fluidic flows (Stoodley et al., 2002).

### 1.1.3 Oral subgingival bacteria and biofilms

In dental medicine, biofilms are divided into two different groups depending on their location on a tooth: supragingival and subgingival biofilms. Supragingival biofilms are bacteria that adhere to a tooth surface above the gingiva while biofilms below the gingiva are called subgingival and are in direct contact with the gingival sulcus. Because of their varying growth conditions, different compositions of bacteria in a biofilm can appear. Here, accumulations of bacterial populations that prefer oxygen availability (aerobe or facultative anaerobe) are found in the supragingival area while populations that prefer no oxygen (anaerobe and obligate

## INTRODUCTION

---

anaerobe) are found in the subgingival area (Shi et al., 2015; Ximenez-Fyvie et al., 2000). Several bacterial species are able to also colonize both areas (facultative anaerobe).

Because subgingival biofilms tend to be the driving force of gingivitis and periodontitis (Tanner et al., 1996), increased focus is put on the understanding of the dynamics of these bacterial biofilms and their architecture. Key subgingival microorganisms were identified previously by Socransky et al. in 1998 and were further specified by Abusleme et al. in 2013. Socransky et al. defined a model which explained the inter-relationship of bacterial species within a subgingival biofilm, associating specific organisms with health and disease status and placing these consortia into ‘Socransky’s complexes’ (Figure 4A). Examples of the Socransky complexes showed prevalence of *A. naeslundii* in the microbiota of a healthy periodontal region, whereas the prevalence of *Veillonella spp.* was more associated with the plaque present in periodontitis (Figure 4B). Abusleme et al. (2013) also identified subgingival species in periodontal healthy patients and patients with periodontitis.

One unique characteristic of subgingival biofilms is the high complexity of bacterial species that are involved in the formation of biofilms (Ramberg et al., 2003; Ximenez-Fyvie et al., 2000). Additionally, certain bacterial species colonize the surface early in the biofilm formation process (also known as early colonizers) while others tend to colonize at a later time point (also known as late colonizers) (Aruni et al., 2015). Early colonizers are able to colonize the pellicle coated tooth surface and are almost exclusively Gram-positive facultative anaerobic bacteria. Here, specific macromolecules such as adhesins in pellicles on the surface allow the interaction with bacterial receptor resulting in attachment (Marsh et al., 2011). In addition, early colonizers are also able to interact with each other resulting in even greater bacterial attachment (Marsh and Martin, 2009).

Examples of early colonizers are *Streptococci spp.* and *Actinomyces spp.* (Figure 4C). Secondary colonizers such as *P. intermedia*, *P. loescheii*, *Capnocytophaga spp.* and *F. nucleatum* are able to adhere to the early colonizers that are already present and later attracting late colonizers such as *P. gingivalis* (Kolenbrander and London, 1993). The process of bacteria adhering to one another is a process also known as ‘coaggregation’ where specific interactions of proteins and carbohydrates on the bacterial cell surface (in addition to hydrophobic, electrostatic and van der Waals forces) allow the bacteria-bacteria interactions forming the characteristic biofilm structure (Lemon et al., 2008).

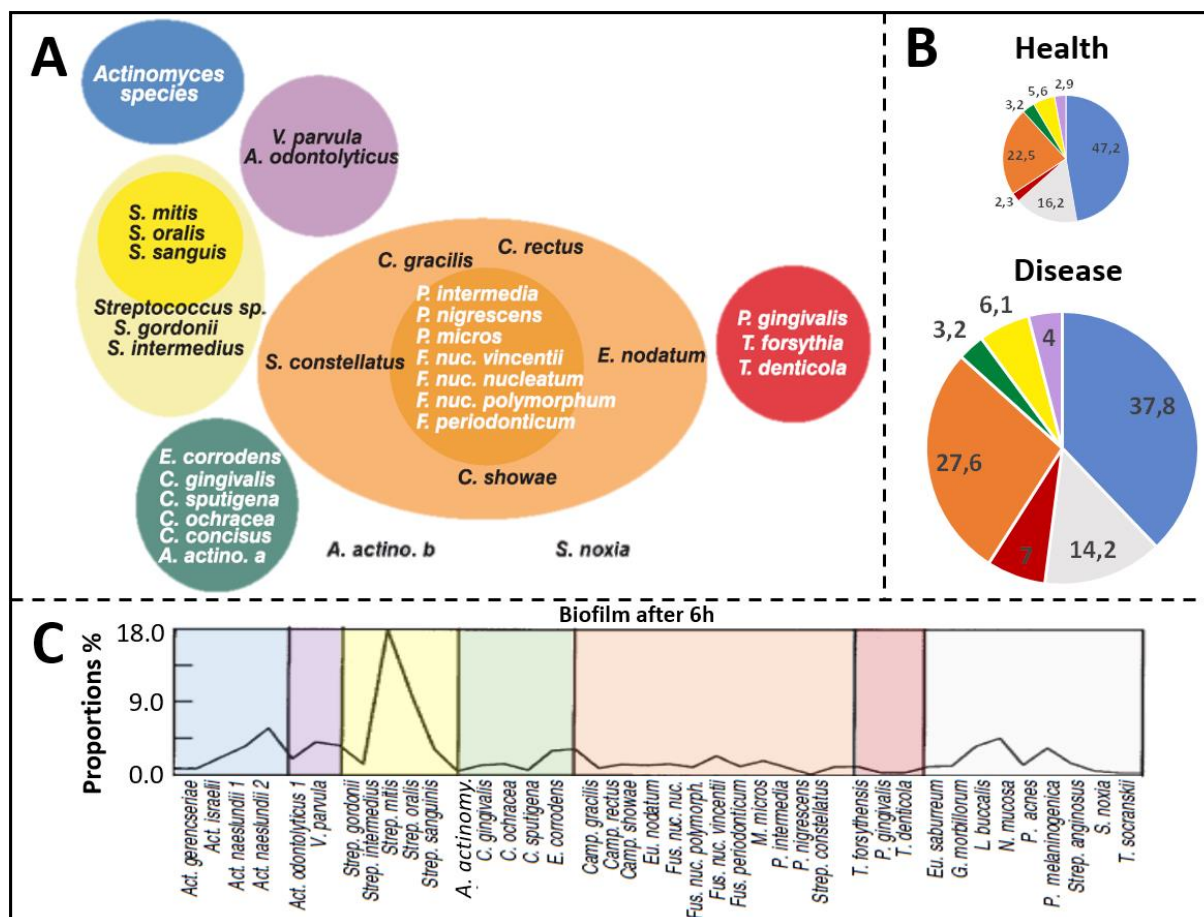


Figure 4: Composition of subgingival biofilms. A) ‘Socransky’ diagram representation of the relationships of species within microbial complexes and between the microbial complexes (Socransky et al., 1998), B) Pie chart of mean % probe count of microbial ‘Socransky’ groups in subgingival biofilm samples from 22 periodontally healthy and 23 periodontitis subjects (Ximenez-Fyvie et al., 2000), C) Averaged relative counts (%) of microbial ‘Socransky’ groups of initial biofilms after 6h from 15 subjects (Li et al., 2004).

Ximenez-Fyvie et al. demonstrated in 2000 that all species defined in the ‘Socransky’ groups were present in subgingival biofilms with varying concentrations (Figure 4B). For instance, the two major groups of healthy and disease biofilms consisted of *Actinomyces spp.* and bacteria from the orange complex, making up 69.7% in healthy biofilms and 65.4% in diseased individuals, thus making them key members in the abundance and architecture of oral biofilms. Other noteworthy groups were also bacteria from the red complex and *Streptococci spp.* complex (Figure 4B). The analyzed biofilms in Figure 4B and their composition were based on fully matured biofilms. In comparison, species distribution in the initial subgingival biofilm process shows high proportions of mainly *Streptococci spp.* and *Actinomyces spp.* species (Figure 4C) with 5.97% *A.naeslundii*, 18.53% *S.mitis*, 10.48% and *S.oralis* (Li et al., 2004). Other bacteria that were found in substantial amounts in initial biofilms were *Veillonella spp.*, *Gemella spp.*, *Rothia spp.* or *Neisseria spp.* (Diaz et al., 2006).



Due to the role of early and late colonizers in the formation of subgingival biofilms, different species are found at different locations within the biofilm. As a result, it has been shown that many microorganisms tend to form clusters in subgingival biofilms, with dense ‘hotspot’ areas composed of only one of the species (Guggenheim et al., 2009; Zijng et al., 2012).

### **1.1.4 Bacterial and fungal biofilms with clinical relevance**

While gingival biofilms are formed almost exclusively from bacterial species, some biofilms in a clinical relevant setting are composed of bacteria and fungi (Puiu et al., 2017; Santus et al., 2021). This makes them interesting to analyze for different reasons, for instance large structures such as the formation of hyphae or increased drug resistance. Additionally, fungi can act as a biotic surface that bacteria can attach to. In this work, bacteria-fungi biofilms were used to test the applicability of the developed Raman mapping workflow using other medically relevant biofilms beyond the oral environment such as biofilms on different types of prosthetics. These biofilms often proliferate on medical device surfaces as well as on and in the human body and for that reason are labeled as medical biofilms.

Within the microbial population colonizing humans, *C. albicans* and *P. aeruginosa* are often identified coexisting in a human host (Peleg et al., 2010) and can be found in bladder catheter infections, endovascular catheters or on arterial and orthopedic prosthetics (Table 2). While oral biofilms tend to show synergistic behavior, conversely biofilms consisting of bacteria and fungi, such as *P.aeruginosa* and *C.albicans*, may also show antagonistic behavior (Hogan and Kolter, 2002). Most research focuses on pathogenesis or quorum sensing of and within these biofilms (Grainha et al., 2020).

Nevertheless, the influence of the architecture of biofilms on the pathogenesis of these dual-species biofilms has not been considered much to this day (Rather et al., 2021). One example of linking architecture to survival strategies of *P.aeruginosa* in biofilms containing *C.albicans* was evaluated by Purschke et al. in 2012. Here, experiments were conducted determining the secretome at different time points in early biofilm development. Since both microorganisms are in direct competition for binding sites and nutrients, changes in proteomic composition and biofilm architecture appear over time (Purschke, 2012). In this study *P.aeruginosa* sequestered iron in the media by producing pyocyanin and 1-hydroxyphenazine to block growth of *C.albicans* (Kerr et al., 1999).

Both microorganisms were also previously identified as contributors to oral candidiasis (Bandara et al., 2013) in the context of oral biofilm research. Additionally, they are both present

in substantial amounts in samples collected by oral swabbing (Hermann et al., 1999). The majority of research done on these biofilms have rather had a general medical background (not dental background, as shown in Table 2). Bridier et al. (2017) described the close relationships between the architecture of a biofilm and its functional properties, emphasizing the need to better describe and understand cell behavior, from single cell to multicellular scale, during biofilm structure development and maturation. Understanding the architecture of clinical relevant biofilms may ultimately help to treat biofilms better which is one of the motivations of this thesis.

### **1.2 Methodology of identification of microorganisms**

In many different areas such as medicine, biology or technical processes, the characterization and identification of biofilms, including their biochemical composition, is highly important. Particularly for development of strategies to prevent and inhibit biofilms, this information is extremely valuable. While the microbial composition of biofilms in the medical field plays a key role in diseases, the architecture of the biofilm has an important role in understanding the disease mechanism.

Several techniques have been used in the analysis of biofilms (Huang et al., 2020) under consideration of different factors such as microbial cells, metabolic activity, available nutrients and varying physico-chemical conditions (temperature, flow, pH, etc.). A summary of used mapping technologies for biofilms can be found in Figure 5. In general, mapping technologies can be placed into three main groups depending on the properties that are mapped by the technology. These include: 1. physical, 2. physico-chemical and 3. chemical properties. Depending on the question asked, some techniques are more qualified to be used than others are. For the analysis of biofilms, the understanding of physical characteristics and chemical properties of involved compounds and microorganisms is important, whereas physico-chemical analysis mostly refers to the attachment of bacteria and then ultimately biofilms but is not able to evaluate the architecture of samples.

Common techniques used in understanding architecture include confocal laser scanning microscopy (CLSM), atomic force microscopy (AFM), scanning electron microscopy (SEM) and Fourier transform infrared spectroscopy (FT-IR).

To date, fluorescence in-situ hybridization (FISH) coupled with CLSM is seen as the state-of-the-art technique for oral biofilm architecture analysis because it allows the analysis of biofilm

## INTRODUCTION

structures, while at the same time also considering species composition and localization within the structure (Kommerein et al., 2017; Thurnheer et al., 2019; Xiao et al., 2017). CLSM allows the collection of spatial information through a structural non-destructive and three-dimensional technique to visualize the architecture of biofilms (Lawrence et al., 1998). Even though this techniques shows good resolution over a large sampling window of interest, detailed local resolution is limited and biofilm development cannot be analyzed over time (Barranguet et al., 2004). Furthermore, sample preparation for the analysis is complex, expensive and requires extensive knowledge in the technique.

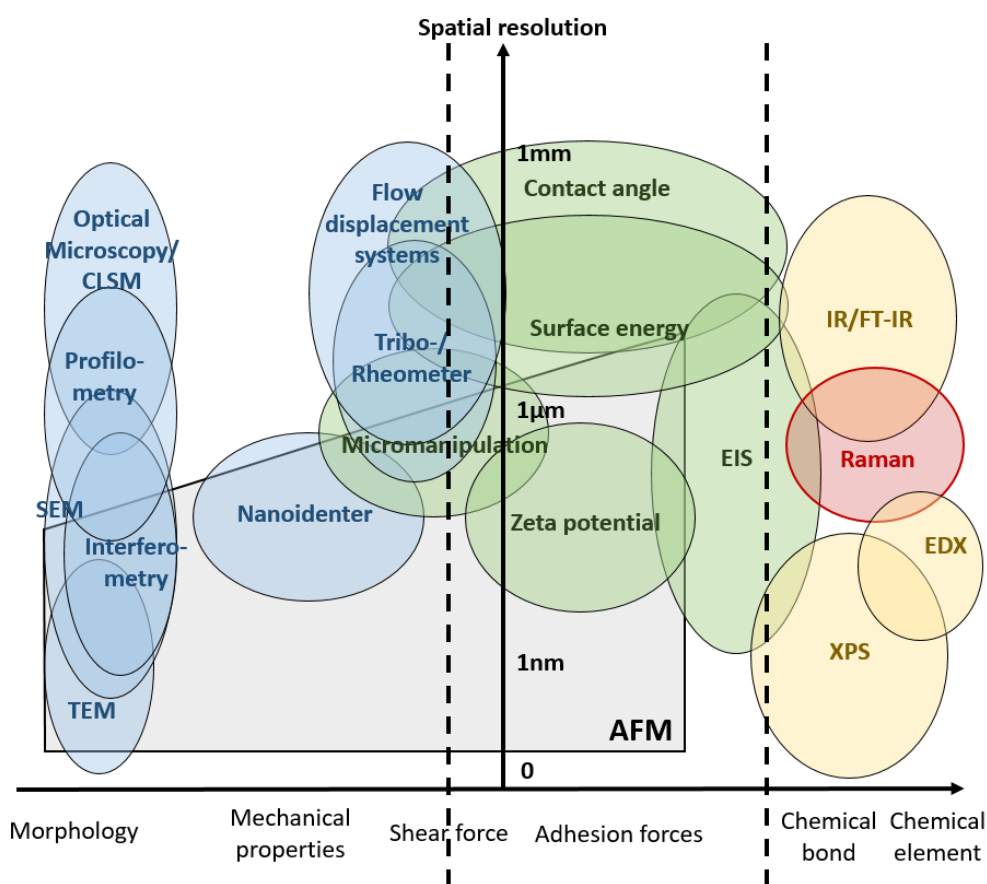


*Figure 5: Summary of different characterization technologies for biofilms. CLSM = Confocal laser scanning microscopy, SEM = scanning electron microscopy, AFM = atomic force microscopy, TEM = transmission electron microscopy, EIS = electrochemical impedance spectroscopy, IR = infrared spectra, FTIR = Fourier-transform infrared spectroscopy, EDX = energy-dispersive X-Ray spectroscopy, XPS = X-Ray photoelectron spectroscopy (applied from Huang et al., 2020)*

In contrast, SEM allows a much better resolution with an improved biofilm visualization. Sample preparation, however, requires fixation or drying of the sample which can have an influence on the structure and morphology of biofilms, reducing reproducibility, as well as the authenticity of the acquired images (Alhede et al., 2012). Recent improvements in sample preparation such as Cryo-SEM (Wille et al., 2017) and environmental scanning electron

microscopy (ESEM) (Fernández-Delgado et al., 2015) now allow for the analysis of un-fixed samples and thus improves biofilm analysis.

Similar to SEM, AFM also allows the visualization of biofilm in the nanometer range and has been widely used for the analysis of topography examination due to its high resolution and sensitivity (Wright et al., 2010). For analysis, the required fixation methods can still have an effect on the integrity of the biofilms sample. With AFM being a sample-touching technique due to its scanning tip, the disruption can lead to detachment of cells from the biofilms having additional effects on the biofilm structure (James et al., 2016).

For the above described visualization technologies for characterization of the species within a biofilm, sampling and staining are required, a process that can compromise the samples integrity and kill all living cells. Hence, there is a current lack of a simple, non-destructive, and cheap preparation procedures for biofilm visualization (Pantanella et al., 2013). In addition, with the exception of FISH, all other techniques don't allow differentiation of bacteria unless the cell morphology is different and permits visual identification.

Chemometric information based techniques, on the other hand, are able to produce information that allows for the distinction of microorganisms. Chemometric systems use mathematical, statistical and other methods to provide a maximum of chemical information in order to analyze chemical data. In this work, microorganisms are identified using specific vibrations of chemicals and compounds within a sample which, combined with chemometric systems, are able to differentiate different microorganisms. FTIR and CRM are techniques that fall into this group that collect chemical vibrations. Both methods deliver complementary information about the characteristics of a biofilm based on a molecular perspective (Gieroba et al., 2020; Sharma and Prakash, 2014). Here, these spectroscopic methods are based on the change of dipole moments (IR) or the polarization of molecules (CRM). These vibrations are excited through absorption of infrared light for FTIR or inelastic scattering of photons from a laser source (CRM). Due to the physical characteristics of these two methods, the same bond is excited differently resulting in diverse peak intensities. The most prominent example is the O-H stretch of water that shows a very prominent peak in IR spectra, due to their dipole moment, something that is only slightly visible in Raman spectra allowing for the analysis of samples in water.

Compared with physical mapping techniques, the microspectroscopic approach allows a fast, non-destructive and label-free analysis of biofilms and can be seen advantageous for the analysis of the three-dimensional architecture and differentiation of biofilms. Because CRM

also allows the analysis of liquid samples, it can be advantageous for the analysis of biofilms samples and is, therefore, used in this thesis.

### **1.3 Raman Spectroscopy Instrumentation**

By definition, Raman spectroscopy can be described as the analysis of molecules and crystals using inelastic scattering of light. The fundamental principle was first described by Adolf Smekal in 1923 (Smekal, 1923) and was proven by Chandrasekhara V. Raman five years later (Raman and Krishnan, 1928), winning him the Nobel Prize in 1930.

It took, however, until the introduction and improvement of lasers, semiconductor detectors, more sensitive amplifiers and computer-based analysis tools to apply Raman-based technologies in common analysis procedures. While Raman spectroscopy has been used for the chemical characterization of different materials, the described advancements together with statistical methods now also allows the use of Raman for the study of biological samples as well.

#### **1.3.1 The Raman effect**

Monochromatic light, usually a laser source, is used in Raman spectroscopy to analyze a sample similar to infrared spectroscopy (IR). In both cases, a sample shows interactions with photons from the laser. In IR, the photons are absorbed by the sample and the energy of absorbed IR photons can be measured and visualized.

For Raman spectroscopy, the scattering of photons is analyzed where two different types of scattering can be observed: 1. elastic scattering with the same frequency as the induced light - also known as Rayleigh-scattering and 2. inelastic scattering resulting in a different, shifted frequency - also known as Raman-scattering (Kudelski, 2008). Elastic scattering occurs when no loss of energy of the incident photon can be observed, while inelastic scattering causes a loss of energy due to interactions with the sample. Only around 1 out of  $10^8$  photons of all scattered light is scattered inelastically as Raman-scattering (Hamasha, 2011).

The interaction of a photon with the energy  $h\nu_0$  with a molecule causes a virtual absorption of the photon while moving the molecule's energy level to a virtual state that can be found between a ground state and an excited state. This virtual state, however, although only short-lived, results in the scattering of a photon when moving to its original state. The interaction of the molecule

and the induced light can result in three different scattering scenarios that are also summarized in a Jablonski diagram in Figure 6.

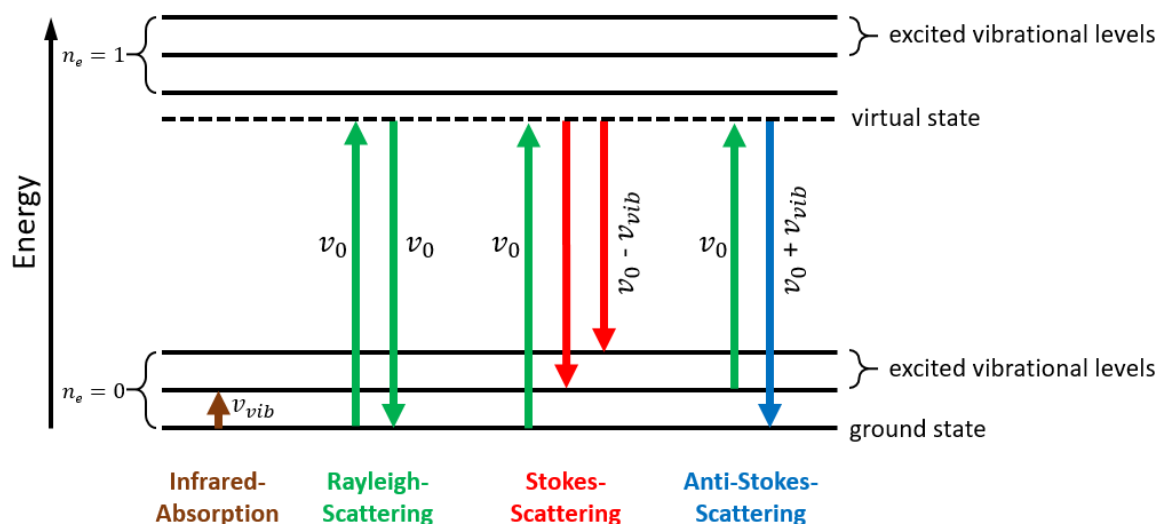


Figure 6: Jablonski diagram of possible scattering interactions between an incident photon (green) and a Raman active molecule.

As mentioned, the most common interaction is Rayleigh scattering, where the induced photon energy  $h\nu_0$  moves the molecule to a virtual state but the same energy  $h\nu_0$  is again emitted and for that reason the molecule doesn't take up any energy nor does it change the frequency between the induced and emitted frequency.

Additionally to Rayleigh scattering, Stokes-scattering can appear, although at lower frequency of 1 per every  $10^8$  occasions. In this case, the induced and emitted frequency is different because the molecule emits a photon with the energy  $h(\nu_0 - \nu_{vib})$  so the molecule accepts energy putting it into an excited vibrational state and thus the scattered photon has a  $h\nu_{vib}$  lower energy. If the molecule is already in an excited vibrational level then after the excitation by a photon, the molecule falls back to the ground state thus having a  $h\nu_{vib}$  higher energy than the induced light resulting in a frequency of  $h(\nu_0 + \nu_{vib})$ . Out of the three scenarios, this anti-Stokes scattering is the least likely because much less molecules are in an excited, rather than the ground state. For the analysis using Raman spectroscopy, these two events of inelastic scattering of the photons from a molecule are of interest (Rostron et al., 2016). The scattered photon with a  $h\nu_{vib}$  lower energy, also known as the Raman shift, is able to be detected and visualized by a Raman instrument using a CCD detector. Depending on the molecular structure and thus vibrational properties of the analyzed sample, the scattered photon has multiple different energy levels resulting in many different peaks at different wavelengths.

### 1.3.2 Molecular vibrations of molecules and resulting Raman peaks

The presence of inelastic scattering is dependent on the polarizability of a sample. Changes in the polarization of molecules can be detected by Raman spectroscopy and appear due to molecular vibrations. They are based on the individual movements of atoms within the molecule. Vibrations appear from the excitation of the molecules through photons of induced light from the laser as described in Chapter 1.3.1. For Raman spectroscopy, polarization describes how easily or difficult an electron cloud around a molecule can be distorted by a photon. Here, the polarization depends on the specific atoms, their masses and their bond strength. Depending on the structure and atom interactions of the molecule it comprises a very unique vibrational spectrum that is detected by Raman spectroscopy as the result of energy changes.

In general, atoms within a molecule show periodic motion even if the molecule doesn't show rotational or translational motions, which is termed molecular vibration and their frequency is termed vibrational frequency. These molecular vibrations can additionally be induced through the photons from a laser source generating scattering. For this scattering, normal oscillation modes are considered. During a normal oscillation mode, all atoms within a molecule oscillate at the same frequency. A molecule comprised of  $N$  atoms has  $3N-6$  normal modes, while a linear molecule has  $3N-5$  normal modes (Landau and Lifshitz, 1976). Because the frequency of a normal mode depends on the bond-strength and the mass of the specific molecules, distinctive frequencies of these Raman specific active vibrational modes can be detected. This can be seen as peaks in a spectral readout and are measured in the units of wavenumbers ( $\text{cm}^{-1}$ ) (Harris and Bertolucci, 1978).

For the analysis of molecules, two different modes are Raman-active and can be detected: 1. stretching modes and 2. bending modes. Within the stretching mode, it can further be differentiated between symmetric and asymmetric stretch, where both types show a change in bond length between two atoms. When the bond length remains unchanged, but the angle between two bonds change then they are considered bending modes. Within the bending mode, it can further be differentiated between scissoring, rocking, twisting and wagging depending on the direction of atom bending. For simplicity, the different vibrational modes are shown in Figure 7.

The molecule's Raman spectrum is able to give information about a molecular structure. This information includes the Raman energy shift of a peak, the intensity of a peak and thus the

concentration present in the sample and the polarization properties of a peak that is linked to the molecule's specific symmetry. Because microorganisms are comprised of many different molecular groups with many different vibrational modes, a broad range of spectral peaks are expected, often making a specific molecule identification difficult due to the overlapping of peaks. Nevertheless, certain chemical compounds show unique peaks that can be assigned to specific compounds and will be discussed in the next chapter.

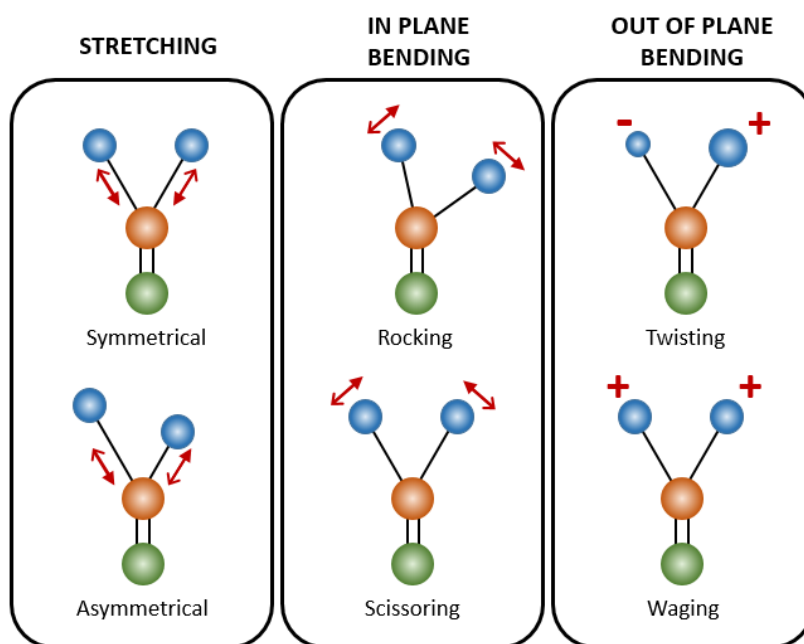


Figure 7: The different types of Raman-active vibrational modes for the molecule  $O=CH_2$ .

### 1.3.3 Information-rich spectral regions of microorganisms

As described in Chapter 1.2, bacteria are comprised of different macromolecules besides water. These compositions can be species specific, offering an opportunity to differentiate species based on their specific macromolecular compositions. However, signals from these molecules can be very complex and can be superpositioned in a Raman spectra due to the similar vibrations within the molecule. For that reason, it is not trivial to attribute specific peaks to a molecular structure of a macromolecule. For the development of prediction and mapping models, the collection of many spectral information are essential to locate the areas that show the most significant differences.

In a preliminary experiment, the full spectral range between  $103.3\text{-}3205\text{ cm}^{-1}$  and a total of 1950 wavenumbers were recorded (Figure 8) to determine information-rich areas within the spectrum. Here, two areas with peaks can be identified. In comparison, the peaks in the area  $600\text{-}1800\text{ cm}^{-1}$  are lower in intensity than the peak between  $2840\text{-}3000\text{ cm}^{-1}$ . Additionally, it



can be seen that the area between 600 and 1800  $\text{cm}^{-1}$ , also known as the ‘fingerprint region’, shows varying peaks and can be used for the identification and differentiation of microorganisms (Lorenz et al., 2017; Sato and Martinho, 2018; Socrates, 2001) and thus builds the basis for the developed workflow in this thesis.

The spectral peaks in the area between 2840-3000  $\text{cm}^{-1}$  can be directly associated to symmetric and asymmetric stretch vibrations of C-H<sub>3</sub> and C-H<sub>2</sub> bonds of fatty acids in phospholipids as well as proteins (Neugebauer et al., 2007). Because these macromolecules make up the majority of macromolecules within a cell, these vibrations are Raman active and due to their high concentrations of over 60% are large in their count, thus skewing the peak identification in the fingerprint area.

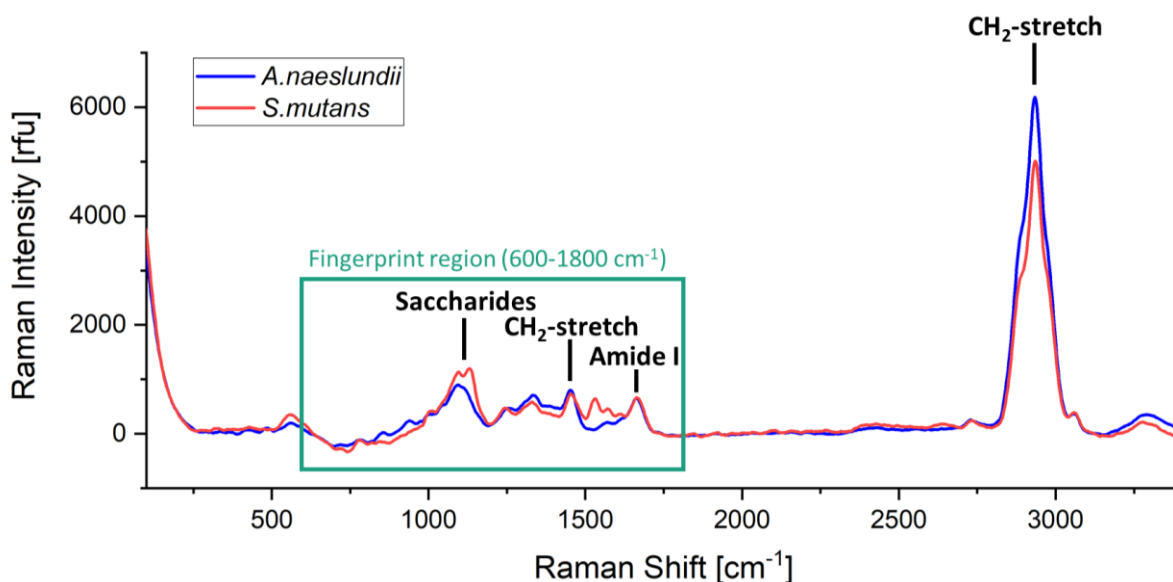


Figure 8: Example of Raman spectra with an extended range (103.3-3205  $\text{cm}^{-1}$ ) with *S. mutans* and *A. naeslundii*.

In order to understand the chemical profile of microorganisms, it is important to know the individual spectra of the components present within a cell. While some compounds show unique spectral profiles that allow simple identification, many others show similar peaks and make identification difficult due to their overlap.

Proteins, for example, are described as chains of amino acids that are linked by peptide bonds. With a total of 20 amino acids, the individual spectra can be very unique depending on their side chains that can be Raman active. A total of eleven structures could be identified that showed unique peak features while the other nine showed similar spectra to the other eleven and weren't individually pictured. The exemplary spectra are shown in Figure 9.

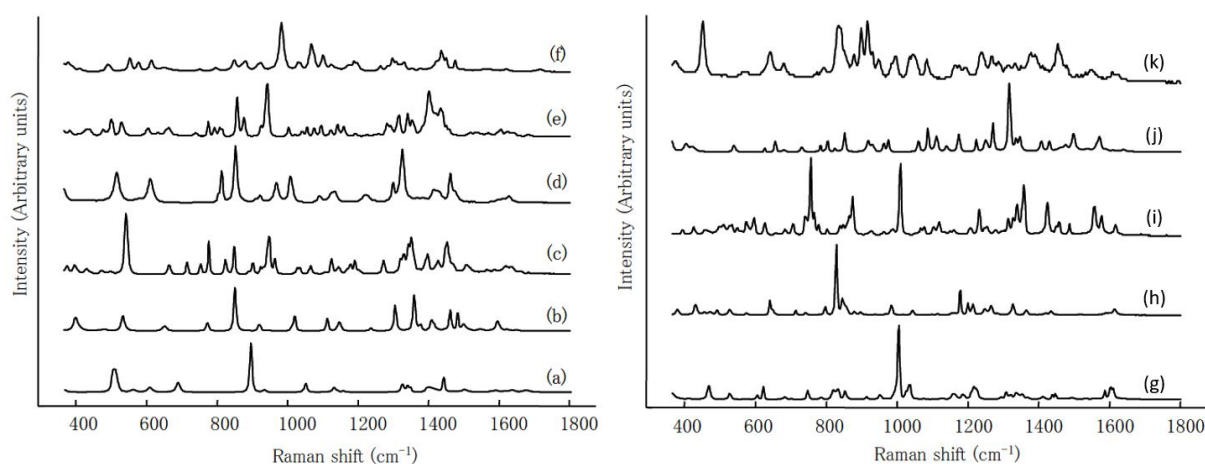


Figure 9: Raman spectra of amino acids with a non-cyclic R side chain: (a) glycine, (b) L-alanine, (c) L-valine, (d) L-serine, (e) L-glutamate, (f) L-arginine and with a cyclic R side chain: (g) L-phenylalanine, (h) L-tyrosine, (i) L-tryptophan, (j) L-histidine, (k) L-proline (applied from De Gelder, 2008).

Fatty acids as lipids make up the cell membrane of a microbial structure, but can also be found inside a cell as lipopolysaccharides and as a storage depot. Here, simple triglycerides are made up of three fatty acids and glycerol. In comparison, phospholipids are made of triglycerides and other components such as nitrogen or phosphorous compounds. Because the available lipids are known and can also be species specific, they can be used for classification. Examples of linear unbranched saturated fatty acids can be found in Chapter 8.2 of the Appendix and can be used as a reference for lipid identification in Raman spectra. In comparison to amino acid spectra, fatty acids show less spectral peaks because they show fewer vibrational modes that are Raman active. Nevertheless, they also show unique spectral peaks that allow differentiation.

Polysaccharides are another important component group because they can be found as part of the capsule structure of bacteria, but they are also extensively present in EPS especially when forming biofilms. Glucanes, for example, are the major group of polysaccharides of EPS formed by *S.mutans* (Klein et al., 2015). The structure of polysaccharides are made of chain sugar monomers that can be found in different compositions based on individual bacteria. For simplicity, five major saccharides and their Raman spectra are shown in Chapter 8.2 in the Appendix that can be frequently found in biofilm and bacteria related questions.

The last group of macromolecules that are present in higher abundance in microorganisms are nucleic acids in the form of DNA or RNA. They are composed of polymers of nucleotides where the nucleotides are attached to a sugar by a glycosidic bond and phosphate. The sequence is comprised of combinations of five different nucleotides which are adenine, cytosine, guanine and thymine (for RNA it is uracil instead). These nucleotides also show unique Raman spectra found in Chapter 8.2 of the Appendix.

Even though the microorganism's molecular composition may be interesting in answering questions that require insights into the molecules present in a microorganism, it is not always necessary to know the exact composition, but rather to focus on the underlying differences between microorganism's spectra. Understanding the absence or presence of certain peaks will, however, help the classification and understanding of microorganisms. Combined with robust training, calibration datasets and algorithms it allows differentiation. These statistical models will be discussed in Chapter 1.4.

### **1.3.4 Raman-based methods for biofilm analysis**

Several Raman-based methods that allow the analysis of biological samples are available and are summarized in Table 4. The Raman-based technology described above refers to the classic analysis method using Raman Microscopy (RM) and can be seen as the basis for all the other analyses. All other technologies are variations of this method and offer substantial advantages in their application compared to RM and for that reason have their own specific applications that amplifies certain peaks of a spectra (Kudelski, 2008; Rostron et al., 2016). For simplicity, methods are put in relation to the analysis of biological samples and how they fit into the consideration of this thesis.

Resonance Raman-Microspectroscopy, for example, uses a laser that generates incident photons close to the electronic transitions of a compound. Because of this, the quantum yield of the Raman effect is greatly improved, allowing for the reduction of acquisition time. While this characteristic is helping the acquisition of biofilms, the method requires the detection and use of chromophores such as cytochrome c (Viridis et al., 2014), carotenoid (Li et al., 2012) or rhodopsin (Bruun, 2013). Because these compounds are not naturally found in oral and other medical biofilms, these compounds would need to be incorporated in biofilms artificially, which may alter the structure of the sample. Instead, using a different laser source such as a UV-Light laser could allow the analysis of biofilm samples without the alteration of the sample. However, the laser would only allow for the amplification of aromatic amino acids or nucleic acids (Manoharan et al., 1990). Because these chemical components are present in all microorganisms of interest, this technology doesn't allow the use for differentiation of bacterial species for mapping because spectral information are not species specific enough.

Because biological samples typically show high fluorescence and only small peak characteristics, amplification methods that amplify peaks and thus reduce the fluorescent signal have been of interest. One of these methods is SERS. Fleischmann et al. first explained in 1974

## INTRODUCTION

the Raman signal amplification effect by showing the increased pyridine signal on a silver-based electrode. It was shown that that due to the nanoscale roughness of metal surfaces, the signal of a laser is amplified. For SERS, either the use of a metallic surfaces or the attachment of particles to the analyte can be used for amplification (Ivleva et al., 2010). Nowadays, typical metals, like gold or silver are used, which can be attached to a surface by electrochemical roughening, coating of nano-structured substrates or the deposition of metallic nanoparticles usually in a colloidal form (Mikac et al., 2015). Previously, SERS was successfully used for the analysis of chemical variation of different biofilm stages (Chao and Zhang, 2012), location of specific compounds within a biofilm (Colniță et al., 2017) or biofilm characterization (Seda Keleştemur et al., 2018). While SERS is a great method for the acquisition of specific bands and demonstrated success in the analysis of biofilms it, again, requires a rather extensive sample preparation similar to resonance RM which limits the application for biofilm mapping. Additionally, not all component peaks are amplified in the same manner which can make species differentiation difficult (Zeiri et al., 2002).

*Table 4: Overview of Raman-based technologies that can be used for the analysis of microbiological samples and biofilms (applied from Kubryk, 2017).*

<b>Technique</b>	<b>Advantages</b>	<b>Disadvantages</b>	<b>Application</b>
<b>Raman-Microspectroscopy</b>	<ul style="list-style-type: none"> <li>• Molecular/chemical Fingerprint</li> <li>• Water independent</li> <li>• Lateral resolution in <math>\mu\text{m}</math></li> <li>• Marker-free</li> </ul>	<ul style="list-style-type: none"> <li>• Interference from fluorescence</li> <li>• Long measurement times</li> <li>• Low resolution</li> </ul>	<ul style="list-style-type: none"> <li>• Biochemical imaging</li> <li>• Identification and characterization of single microorganisms and EPS</li> <li>• Analysis of biofilm formation</li> </ul>
<b>Resonance Raman-Microspectroscopy</b>	<ul style="list-style-type: none"> <li>• High resolution and selectivity</li> <li>• Fast analysis</li> </ul>	<ul style="list-style-type: none"> <li>• Chromophores are required</li> <li>• Photo-bleaching</li> </ul>	<ul style="list-style-type: none"> <li>• Biochemical imaging</li> <li>• Fast identification and characterization of microorganisms</li> <li>• Cell sorting</li> </ul>
<b>Surface enhanced Raman-Spectroscopy (SERS)</b>	<ul style="list-style-type: none"> <li>• Signal amplification</li> <li>• Deletion of fluorescence signal</li> <li>• Fast analysis</li> </ul>	<ul style="list-style-type: none"> <li>• Reproducibility of spectra difficult</li> <li>• Dependent on analyte and point of absorption</li> </ul>	<ul style="list-style-type: none"> <li>• Biochemical imaging</li> <li>• Fast identification and characterization of microorganisms and EPS</li> <li>• Analysis of quorum sensing</li> </ul>
<b>Tip-enhanced Raman-Spectroscopy (TERS)</b>	<ul style="list-style-type: none"> <li>• Lateral resolution below the optical diffraction limit</li> <li>• Correlation between structural and topographic data</li> </ul>	<ul style="list-style-type: none"> <li>• Difficult production of tips</li> <li>• Contamination of tips</li> </ul>	<ul style="list-style-type: none"> <li>• Biochemical imaging</li> <li>• Characterization of single microorganisms</li> <li>• Analysis of cell surface dynamics</li> </ul>

In contrast to resonance Raman Microspectroscopy and SERS, TERS has the unique advantage that the technique can be used without any sample preparation and thus ensures the integrity of a sample. Additionally, the tip enhancement has the valuable benefit that a resolution of up to

20 nm is possible. Schmid et al. (2010) demonstrated that TERS allowed the mapping of a sample area as small as 10-50 nm in diameter. TERS, being similar to SERS, uses a metal-covered tip, allowing a more precise sample positioning in the near field and also amplifying Raman signals. Previous studies showed that, due to the non-invasive and non-destructive analysis of samples, TERS was able to be used for the analysis of structures of polysaccharides and peptides within bacterial cells (Neugebauer et al., 2007; Pahlow et al., 2012). For that reason, TERS offers solutions to all described disadvantages of the other Raman-based methods including classic CRM. Nevertheless, while the advantages are clear, the production of such tips can be difficult and complex. This prevents TERS to be used more regularly, especially for mapping research using Raman techniques. It is due to the difficulty of manufacturing such tips that this technology was not considered in this thesis.

## **1.4 Mathematical Methods and Data Analysis**

As pictured in Chapter 1.3.3, Raman spectra of microbiological samples contain Raman-signals from all macromolecules present in the cell that are: 1. Raman-active and 2. in the focus of the laser. As shown in Chapter 1.1, these discussed major macromolecules are present in all microbial cells and thus their specific Raman-active bonds from nucleic acids, proteins or lipids create similar Raman spectra, making the visual differentiation of spectra difficult. Additionally, bacteria in subgingival biofilms occupy the same habitat and, therefore, show even more similar chemical compositions. Even though differences in spectral fingerprint patterns of oral bacteria have been shown to be minor, they still allow differentiation between species to be made (Beier et al., 2012; Berger and Zhu, 2003). Conversely, microorganisms from different domains such as *P.aeruginosa* being a prokaryote and *C.albicans* being an eukaryote show more diverse peak profiles in their spectra, simplifying the differentiation of these microorganisms (Keleştemur et al., 2020).

In order to extract useful information from spectral profiles, statistical and chemometric approaches are essential to gain inside knowledge into chemical composition and differentiation, also looking at their applicability for biofilm mapping. To deliver good informational output for these approaches, the nature of Raman spectra, such as fluorescent background or noise, hinders these processes from performing well. These need to be combined with common processing steps discussed in Chapter 3.3.1. Because Raman spectra of microorganisms are more complex than classic chemical samples, processing is crucial to

extract the full potential of statistical analysis and give the opportunity to use it for mapping approaches (Bocklitz et al., 2011).

Within multivariate analysis, a broad spectrum of methods are available to analyze a large dataset with high amounts of samples (here Raman spectra in general) that show large numbers of variables (Raman peaks and their adjacent intensities) (Dillon and Goldstein, 1984). The purpose of these multivariate methods are to minimize dimensions of the data and find patterns and groups that allow discrimination and classification of species. For the analysis of microbiological data from Raman spectra, two basic methods are typically used: 1. unsupervised and 2. supervised classifications, whereas analysis models were previously also used in a combination of both types of classifications.

With the unsupervised method, learning from the statistical model refers to creating underlying patterns from an unspecific dataset without any reference data to labeled outcomes or predictions. Such examples are principle component analysis (PCA) (Almarashi et al., 2012; Colniță et al., 2017; Gualerzi et al., 2017; Lu et al., 2011; Samek et al., 2015; Sil et al., 2017), cluster analysis (CA) (Bonifacio et al., 2010; Hutchings et al., 2010; Maitra et al., 2020; Parthasarathy et al., 2008) or hierarchical cluster analysis (HCA) (Cheeseman et al., 2021; Harz et al., 2005; Kniggendorf et al., 2011). In analytical statistics, unsupervised methods treat all variables in a database the same and use high-dimensional points for classification, but do not consider assigned classifications of variables. This makes the model efficient and easy to use and generates good output especially in models that require classifications into two groups.

For more complex systems, supervised methods may be advantageous. Examples being partial least square analysis (PLS) (El Senousy et al., 2014; Fanesi et al., 2018; Feng et al., 2019; Villa et al., 2019), support vector machines (SVM) (Jung et al., 2014; Kusić et al., 2014) or linear discriminant analysis (LDA) (Krafft and Popp, 2019; Potter et al., 2020). Often, combinations of these systems are also used. Conversely to unsupervised methods, supervised methods require and use annotated classifications to maximize inter-class variance. However, these methods require knowledge of the dataset before examination, such as calibration datasets to be able to identify and group samples which can be problematic in some cases.

For that reason, PCA is normally used for simple and linear dimensionality reduction while PLS is used for classification of different sample groups. In this thesis, three statistical approaches were used: 1. PCA and 2. CA as unsupervised approaches and 3. a variation of PLS

and LDA as a supervised method. These methods and their applicability for the different questions are introduced and discussed in Chapter 3.3.2.

## 1.5 Insights and results from previous studies

Publications that use CLSM as the mapping method of choice remain the majority in topics that require mapping techniques in a biofilm setting. The advantages over other mapping techniques have been discussed previously. CLSM shows good results when answering questions related to biofilm architecture. Because CLSM is a destructive technique that doesn't allow continuous observation of growth of the same biofilm, new techniques are evolving that allow that.

Nowadays, through advancements in technology, optical spectroscopy techniques offer the opportunity to identify chemical compounds in high spectral and spatial resolution (Rzhevskii, 2019). In addition, it is also possible to combine the power of 3D sample analysis with focused chemical composition. CRM is one of these emerging techniques. For this reason, previous studies were able to demonstrate that the use of CRM is able to spatially differentiate complex biomedical sample in a tissue or bacteria setting (Cals et al., 2018; Gualerzi et al., 2017; Rebrošová et al., 2017; Sil et al., 2017; Strola et al., 2013).

To the best of my knowledge, CRM has only been used a few times for the analysis of environmental biofilms thus far, but never as a mapping technology. Instead, the focus of these studies were based on extracting information to evaluate molecular details of spectra 1. of single species biofilms (Gieroba et al., 2020; Kusić et al., 2015; Ramirez-Mora et al., 2019; Samek et al., 2015; Wickramasinghe et al., 2020), 2. over time (Carey et al., 2017; Chao and Zhang, 2012; Keleştemur et al., 2020; Liu et al., 2020) or 3. under the influence of stress, mostly chemicals (Daood et al., 2020; Jung et al., 2014). While they give insights into the use and applicability of CRM in a microbiological setting, the acquired data is not suitable for answering questions with regard to the architecture of the analyzed samples. While SERS remains promising as a modified Raman microscopy technique (Chao and Zhang, 2012; Keleştemur et al., 2020; Seda Keleştemur et al., 2018) with the potential for higher levels of discrimination spectra, it only allows the cultivation of biofilms on specified SERS-active surfaces or modifications through nanoparticles. Because the focus of this thesis is on *in-vitro* models and chemically un-modified biofilm samples, classic CRM is considered in this research.

## INTRODUCTION

---

Nonetheless, a limited number of research groups have looked at chemometric information for the spatial distribution of bacteria in biofilms. For example, Beier et al. (2010) were able to demonstrate that it is possible to differentiate two *Streptococci sp.* in a pseudo-biofilm sample (term used by the author) and were able to confirm differentiation of species by PC-LR. This was the first time CRM appeared as an option for potential biofilm mapping. However, this analysis was based on modified bacteria by crystal violet staining of one species and the biofilms were not based on cultured biofilms over time. Gieroba et al., (2020) was able to use chemical maps to locate glucans and Amide I for different *Streptococci sp.*. While they were able to determine concentrations of different chemical compounds in a specified area, the research's focus was not on the differentiation of species in a multi-species biofilms based on their chemometric spectra and was lacking the statistical evaluation that resulted in the chemical maps. Horiue et al., (2020) was able to map bacterial species in biofilms grown near drains of household bathrooms (known as pink biofilms due to their color) using specific pigment spectral bands and statistical methods. While differentiation of areas was possible, the study was unable to associate clusters to specific bacterial species. Lastly, Kniggendorf and Meinhardt-Wollweber, (2011) were able to demonstrate that resonance Raman spectroscopy was able to identify and locate different microbial species on granules samples from sequencing batch reactors for anaerobic ammonium oxidation. This method was not able to be applied in this work though because, as shown in Chapter 1.3.4, resonance Raman microscopy requires chromophores (cytochrome-c in the work), which are not expected in biofilms cultured in this thesis.



## 2 Objectives

Previous scientific publications already suggested the use of CRM for differentiation of microorganisms based on their unique chemometric profiles (see Chapter 1.5). A vast majority of the research focuses on the analysis of natural microbiological and biofilm samples (Lee et al., 2021; Pezzotti, 2021), while only a few consider medical and oral biofilms (Gieroba et al., 2020; Rebrošová et al., 2019). Additionally, spatial mapping of biofilms has not yet been evaluated in the context of using Raman technologies.

The goal of this thesis is the development of a workflow to spatially map *in-vitro* biofilms (subgingival and other medically relevant biofilms) using chemometric profiles acquired from confocal Raman technologies.

In the first step, it is hypothesized that using CRM with specific prediction models allow the differentiation of common oral bacteria from different Socransky complexes (Socransky et al., 1998). These oral bacteria are part of the core subgingival microbiome and are additionally confirmed and quantified as such by Abusleme et al. (2013). Specifically, the core species evaluated were *Fusobacterium nucleatum*, *Streptococcus mutans*, *Veillonella dispar*, *Actinomyces naeslundii* and *Prevotella nigrescens*. Here, for the analysis of the identity of microorganisms, both planktonically and biofilm grown species were analyzed and compared by multivariate statistical models. In this first step the purpose was to lay the groundwork for the use of CRM in *in-vitro* research for subgingival biofilm models and establish the application of artificial subgingival biofilm models.

In a second step, it is then hypothesized that CRM, coupled with multivariate analysis techniques such as a PCA and CA, are able to predict and differentiate subgingival bacteria in a biofilm model. To develop and confirm this approach, different datasets, samples and analysis technologies were used to confirm: 1. species clustering in the *in-vitro* grown subgingival dual-species biofilm model, 2. the use of a multivariate analysis model in a mapping setup and 3. the use of chemometric information from Raman spectra for the mapping of *in-vitro* dual-species biofilm models. Distribution analysis using CRM in combination with multivariate analysis was performed with dense bacteria interface area (DBIA) samples using planktonic bacteria and was further compared to morphology and CLSM. Lastly, artificially grown *in-vitro* dual-species biofilms were then mapped using the previously developed workflow and were also compared to morphology measurements of the biofilm. The developed method was then applied to additional medically relevant biofilms consisting of bacteria (*P.aeruginosa*) and fungi (*C.albicans*) to demonstrate the applicability of the developed method.

## 3 Material and Methods

### 3.1 Materials

#### 3.1.1 Instruments

Studies were performed at Procter&Gamble Greater London Innovation Centre in Egham, UK and Fraunhofer IGB in Stuttgart, Germany.

##### *Raman Microscopy*

At Procter&Gamble the instrument used for analysis was a ThermoFisher Scientific DXR2xi (ThermoFisher Scientific, Waltham, Massachusetts, USA), which was equipped with a 50x long working distance objective, a 532 nm filter and a 532 nm laser to capture a full spectral range of 50-3500  $\text{cm}^{-1}$ . Data acquisition was performed using a 25  $\mu\text{m}$  confocal pinhole setup, 5.0 mW laser power, 0.25 sec exposure time, 100 scans, a low baseline correction and a spectral detection range from 600-1800  $\text{cm}^{-1}$  (Kriem et al., 2020).

At Fraunhofer IGB, a Renishaw inVia™ Qontor (Renishaw plc, Wotton-under-Edge, UK), equipped with a 100 $\times$  objective, a 532 nm filter and a 532 nm laser was used to capture a spectral range of 282.8-2016.2  $\text{cm}^{-1}$  and 1015 collection points using a CCD camera. Data acquisition was performed using 50% laser power (equivalent to 25 mW), 1 sec exposure time and 10 accumulations (8 accumulations for biofilm mapping) (Kriem et al., 2021).

Unless otherwise indicated, all spectral acquisitions have been acquired using the settings described above.

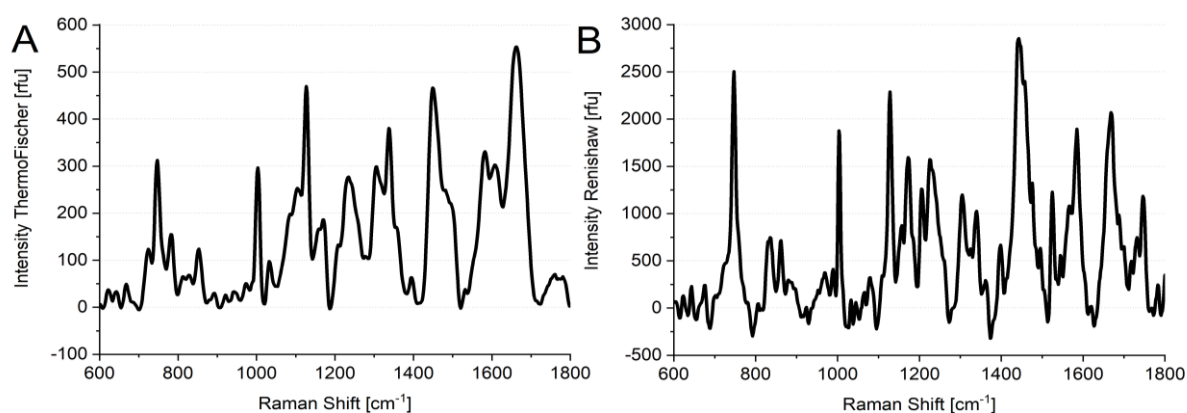


Figure 10: Comparison of spectral peaks of two Raman instruments with *V.dispar*. (A) shows the average Raman spectra (from 96 spectra) generated with a ThermoFisher Scientific DXR2xi and (B) shows the Raman spectra (from 300 spectra) generated with a Renishaw inVia™ Qontor. Note that counts from the Renishaw instrument are generally around 5-fold higher than the counts from the ThermoFisher instrument.

*V.dispar* was used to display spectral peak differences of the two instruments. Average spectra are shown in Figure 10. Differences appear in the counts of peaks with Renishaw inVia™ Qontor counts being roughly a 5-fold higher than ThermoFisher Scientific DXR2xi. As seen in the acquisition settings, the Renishaw inVia™ Qontor is equipped with a more powerful laser allowing a 5-fold increased laser strength that results in the equivalent increased signal count.

Because the objectives of this work are on the differentiation of spectral information, there is a dependency on the spectral information that can be accumulated. Figure 10 shows, that the Renishaw inVia™ Qontor is able to also detect minor peaks that improves the information available that can be used for statistical analysis and differentiation of species. Furthermore, Figure 10 shows that both systems are able to detect major peaks that are also specified in the peak assignment table of Table 14 (724 cm<sup>-1</sup>: Adenine; 1004 cm<sup>-1</sup>: Phenylalanine; 1127 cm<sup>-1</sup>: C-C, C-N stretch of proteins; 1174 cm<sup>-1</sup>: -; 1230 cm<sup>-1</sup>: Amide III; 1308 cm<sup>-1</sup>: -; 1339 cm<sup>-1</sup>: Tryptophan; 1447 cm<sup>-1</sup>: CH<sub>2</sub> deformation; 1580 cm<sup>-1</sup>: Amide II; 1665 cm<sup>-1</sup>: Amide I). The comparison of the two systems showed that both systems can be used for Raman spectra evaluations in this work. The use of two different Raman systems and the similar peak detection also shows that repetitive results can be generated on different systems while Renishaw inVia™ Qontor shows increased detection of weaker peaks as well and for that reason was further used for biofilm mapping applications.

### *Confocal Laser Scanning Microscopy (CLSM)*

An inverted microscope Zeiss LSM710 (Zeiss, Oberkochen, Germany) fitted with an Axio Observer Z1, a UV laser, an Ar-Laser (Lasos, Jena, Germany), a He-Ne laser (Zeiss, Oberkochen, Germany) and a computer-operated confocal laser scanning system was used for the analysis of biofilm architecture using FISH staining. Due to the species specific fluorescent stains, filters were set to 500-540 nm for detection of 6-FAM and 570–630 nm for Cy3. Images were obtained with a 100× oil immersion objective.

### *Microscopic imaging*

Microscopic images using a Renishaw inVia™ Qontor were obtained as well, to obtain microscopic images as well as Raman spectra of the same image field simultaneously. Morphological analysis was done based on the shape of bacteria as described in Chapter 1.1.1. While *S.oralis* is cocci shaped, *A.denticolens* is rod shaped simplifying the differentiation process on the microscopic image. For differentiation an ImageJ (Rasband) plugin with the name *MorphoLibJ* was used (Morphological segmentation). This allowed for a rapid and un-

biased differentiation of microbial shapes that can be used for comparison of distributions determined based on Raman mapping.

### *Quantitative Polymer Chain Reaction (qPCR)*

A LightCycler® (Roche, Basel, Switzerland) RT-PCR instrument was used with settings described in Methods.

### **3.1.2 Software**

Raman data acquisition with the ThermoFisher Scientific DXR2xi was performed using OMNICxi Version 1.6.0.26 (ThermoFisher Scientific, Madison, WI, USA). Raman data acquisition with the Renishaw inVia™ Qontor was performed using WiRe Version 5.3 and 5.4 (Renishaw plc, Wotton-under-Edge, United Kingdom). Data processing of spectral data from both instruments was done using WiRe 5.2 (Wotton-under-Edge, United Kingdom). The specific applied processing steps are described in Chapter 3.3.1.

Statistical multivariate analysis was achieved with two different software programs: Origin 2019b (OriginLab Corporation, Northampton, MA, USA) and SIMCA15 (Umetrics, Umea, Sweden). PCA analysis was done using Origin 2019b and PLS analysis was done using SIMCA 15.

CA and mapping was performed using Renishaw WiRe 5.2 through a multivariate data analysis module. Details on the specific analysis in this work can be found when the principles of cluster analysis are discussed in Chapter 3.3.2.

CLSM analysis with FISH staining was done using Zeiss ZEN Version 2.3 (Oberkochen, Germany). Images from CLSM were then processed and recombined using ImageJ (Rasband, 1997).

Additionally, all graphs and figures were created using Origin 2019b.

### **3.1.3 Microorganisms**

Table 5 shows the different microorganism species used for the experiments. Before the experiments, species were confirmed using MALDI-TOF or PCR.

Table 5: Used Microorganisms and species ID.

Species	ID
<i>Actinomyces naeslundii</i>	ATCC 12104
<i>Fusobacterium nucleatum</i>	ATCC 25586
<i>Porphyromonas nigrescens</i>	ATCC 33563
<i>Streptococcus mutans</i>	ATCC 35668
<i>Veillonella dispar</i>	ATCC 17748
<i>Actinomyces denticolens</i>	DSM 20671
<i>Streptococcus oralis</i>	DSM 20066
<i>Veillonella dispar</i>	DSM 20735
<i>Candida albicans</i>	ATCC 10231
<i>Pseudomonas aeruginosa</i>	DSM 22644

### 3.1.4 Consumables

All chemicals were purchased from Sigma Aldrich (St. Louis, MO, USA) or VWR (Radnor, PA, USA) unless otherwise indicated. All bacteria strains were purchased from ATCC (Manassas, VA, USA) or DSMZ (Braunschweig, Germany). Primer sequences and gene fragments (gBlocks™) for RT-PCR quantification were obtained from Integrated DNA Technologies (Leuven, Belgium). gBlocks™ assembly was developed with Luka Kadovic and Marta Rubio Texeira from Integrated DNA Technologies. Oligonucleotides for FISH staining were purchased from biomers.net GmbH (Ulm, Germany).

## 3.2 Methods

Some of the methods mentioned have already been described in previous peer-reviewed publications by Kriem et al. in 2020 and 2021.

### 3.2.1 Cultivation and sample preparation of planktonic bacteria

#### *Cultivation of oral bacteria*

Bacteria were available as glycerol stocks (25% glycerol (v/v)) stored at -80 °C. Brain Heart Infusion (BHI) medium (Sigma-Aldrich) was used for initial cultivation to ensure constant conditions for all experiments. Bacterial species used were *A.naeslundii*, *A.denticolens*, *F.nucleatum*, *P.nigrescens*, *S.mutans*, *S.oralis* and *V.dispar* (see Table 5 for strain IDs). Classic cultivation methods for the used bacterial strains suggest the use of defibrinated sheep blood as an enrichment of nutritional properties. However, cultivation was done without defibrinated sheep blood to avoid differences due to changing blood batches having an effect on spectral peaks. All species were incubated under anaerobic conditions (80% N<sub>2</sub>, 15% CO<sub>2</sub>, 5% H<sub>2</sub>) at 37 °C in anaerobic jars (schuett-biotec GmbH, Göttingen, Germany). Sample handling was done under aerobic conditions.

## MATERIAL AND METHODS

---

First, bacterial stocks were thawed, streaked onto individual BHI agar plates with an inoculation loop and incubated anaerobically for 48 h. Then, a few colonies were selected and transferred to 15 mL Falcon tubes containing BHI medium and incubated anaerobically for an additional 72 h. After that, the bacterial solutions were again diluted at a 1:100 ratio with fresh BHI medium, separated into three tubes and incubated anaerobically for an additional 96 h. In comparison, the solutions for the calibration of biofilms for mapping were diluted into five 15 mL Falcon tubes containing modified fluid universal medium (mFUM) instead of BHI medium. This process of incubation was repeated for a total of three times per species. mFUM was prepared based on Gmür and Guggenheim, 1983. A detailed recipe for mFUM can also be found in Chapter 8.3.1 of the Appendix.

For the acquisition of calibration spectra and the analysis of growth phase and state, every 24 h 1500  $\mu\text{L}$  of sample solution was put in Eppendorf tubes, centrifuged at 5000 rpm for 5 min and the supernatant was removed. Samples were resuspended in 1000  $\mu\text{L}$  of 0.9 % NaCl (w/v) (for calibration spectra of biofilm mapping DI water was used instead of NaCl solution) and centrifuged for an additional 5 min. The supernatant was removed and the bacterial pellet was vortexed for 15 sec in order to suspend the pellet. 3  $\mu\text{L}$  were then dispensed on a borosilicate glass slide (VWR) and air dried for 10 min under a laminar flow bench for confocal Raman spectral analysis (the analysis of hydrated samples was done immediately after dispensing without air drying). For the comparison of hydrated and dehydrated samples, the 24 h bacterial samples were also measured at 48 h, 72 h and 96 h to evaluate possible deterioration of the peaks over time. A schematic of sample analysis is shown in Figure 11.

For the confirmation of the statistical biofilm mapping method, 3  $\mu\text{L}$  of concentrated *S.oralis* bacteria solution were dispensed on a borosilicate slide (VWR) and air dried until visibly dry. Then 3  $\mu\text{L}$  of concentrated *A.denticolens* solution was dispensed in very close proximity to the *S.oralis* spot, generating a natural transition area with two dense unmixed areas of each species. For simplicity purposes, these samples are labeled as DBIA samples in the following chapters.

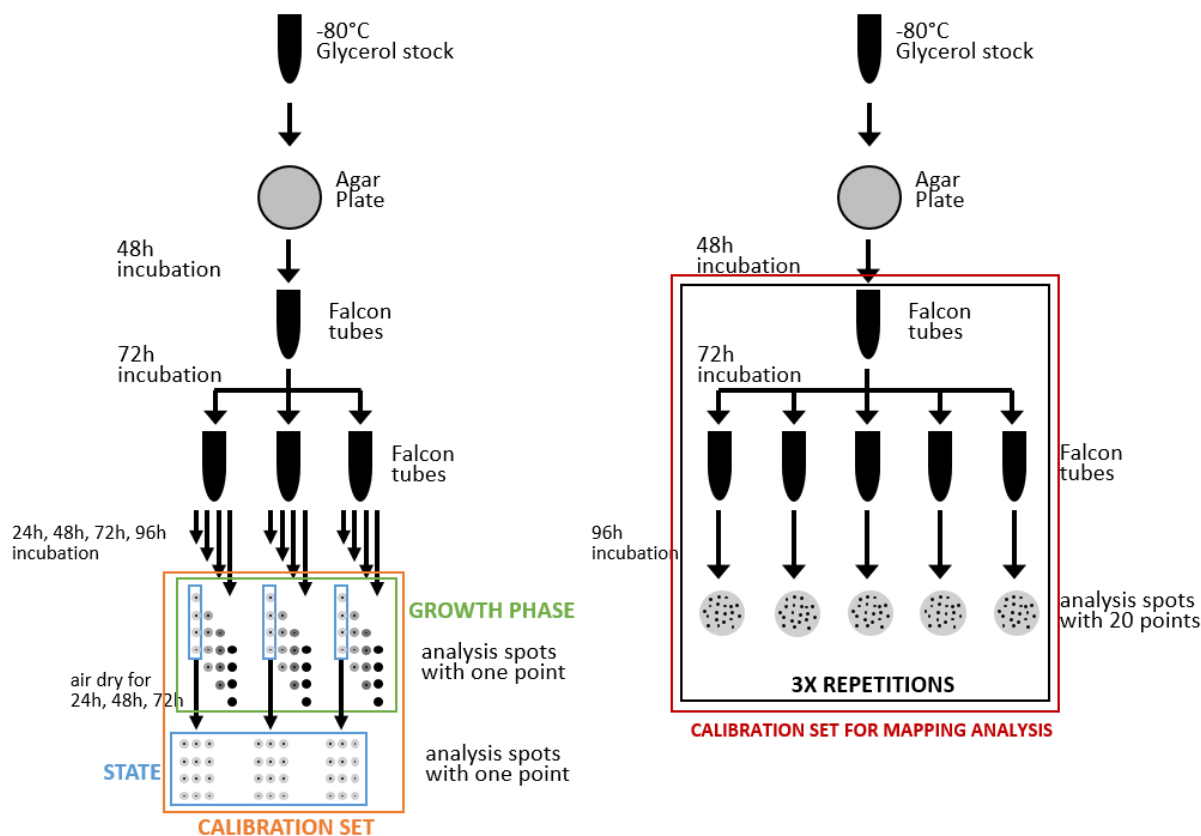


Figure 11: Schematic of sample preparation for the calibration of planktonic bacteria and which sample were used for which analysis.

#### Cultivation of microorganisms also found in other medical settings

To cultivate the bacteria commonly found in medically relevant biofilms, *C.albicans* and *P.aeruginosa* (see Table 5 for strain IDs) were available as glycerol stocks (25% glycerol (v/v)) stored at -80°C. Although the organisms have different optimized growth media, YNBNP-Medium (1,7 g / 1 Yeast Nitrogen Base w/o amino acids and ammonium sulfate, 25 mM Phosphate buffer pH 7,0, 2,5 mM N-Acetylglucosamine (Hogan and Kolter, 2002)) was used for cultivation in order to prevent the possibility of differences due to chemical modifications in the medium. Cultivation was done under normal aerobic conditions at 32 °C on a shaking platform set to 175 rpm.

First, stocks were thawed, streaked onto individual LB agar plates for *P.aeruginosa* and YPD agar plates for *C.albicans* and were incubated for 48 h at 32°C. Then, a few colonies were selected and transferred to 15 mL Falcon tubes containing YNBNP medium and incubated for an additional 24 h at 32°C. This solution was used for calibration spectra acquisition and biofilm growth experiments.

For the acquisition of calibration spectra 1500 µL of sample solution of each species was put in Eppendorf tubes after 24 h incubation time, centrifuged at 5000 rpm for 5 min and the

supernatant was removed. Samples were resuspended in 1000  $\mu\text{L}$  of DI water and centrifuged for an additional 5 min. The supernatant was removed and the microbial pellet was vortexed for 15 sec in order to suspend the pellet. 3  $\mu\text{L}$  were then dispensed on a borosilicate glass slide (VWR) and air dried for 10 min under a laminar flow bench for confocal Raman spectral analysis.

### 3.2.2 Cultivation and sample preparation of biofilms

#### *Cultivation of oral biofilms*

Mono-species biofilms for the ThermoFisher Scientific DXR2xi were grown on sterilized CDC reactor glass discs (Biosurface Technologies Corporation, Bozeman, MN, USA) in 24-well polystyrene cell culture plates (Nunc A/S, Roskilde, Denmark). For biofilms cultivated for Renishaw inVia™ Qontor, 1  $\text{cm}^2$  glass discs were cut from borosilicate glass slides (VWR) and sterilized. For the optimization of biofilm growth conditions, sterile sintered hydroxyapatite discs (Clarkson Chromatography Products Inc., South Williamsport, PA, USA) were implemented as a tooth alternative. Three different artificial saliva alternatives (Hahnel, DMM and PBS) were tested and compared to natural saliva (results shown in Chapter 3.2.3). Detailed recipes and preparation procedures can be found in the Chapter 8.3.2 of the Appendix. Finally, cultivation of biofilms was performed in 24-well polystyrene cell culture plates (VWR).

Biofilm cultivation methods have been applied from Gmür and Guggenheim (1983) and have been mentioned in previous publications by the author. All cultivations of biofilms were done under anaerobic conditions (80%  $\text{N}_2$ , 15%  $\text{CO}_2$ , 5%  $\text{H}_2$ ) at 37 °C while sample handling was done under aerobic conditions.

First, individual species were cultured anaerobically in 15 mL Falcon tubes containing BHI medium for approximately 65 h. Next, bacteria solutions were diluted using mFUM medium at a ratio 1:25 and were incubated anaerobically in 15 mL Falcon tubes for an additional 24 h. After 24 h, the solution was diluted again in 15 mL Falcon tubes with mFUM medium at a ratio of 1:1 and incubated anaerobically for 5 h. Before the formation of biofilms, discs were preincubated in 800  $\mu\text{L}$  saliva (or artificial saliva) for 4 h at room temperature under shaking radial conditions at 100 rpm to insure pellicle formation. At this point, species solutions were also adjusted to  $\text{OD}_{600}$  1.0 by dilution with mFUM medium.

To initiate biofilm formation, discs were placed into wells containing 800  $\mu\text{L}$  saliva (or artificial saliva) and 800  $\mu\text{L}$  mFUM medium. Immediately following, wells were inoculated with bacteria solutions (200  $\mu\text{L}$  for mono-species biofilms, 100  $\mu\text{L}$  *S.oralis* and 100  $\mu\text{L}$  *A.denticolens*



for dual-species biofilms, multi-species biofilms of *S.oralis*, *A.denticolens* and *V.dispar* for a total of 200  $\mu\text{L}$  at a ratio 1:1:1) and mixed carefully in the well by up-and-down pipetting of the solution. 24 h and 48 h after incubation start, the growth medium was removed and discs were dip washed three times with 0.9 % NaCl (w/v) solution and placed back in the well. The medium was then carefully replaced (800  $\mu\text{L}$  saliva (or artificial saliva) and 800  $\mu\text{L}$  mFUM medium) to not disrupt the forming biofilm. Harvesting of the biofilm occurred after 65h of total incubation time. Again, the medium was removed and discs dip washed three times with 0.9 % NaCl (w/v) solution (for mono-species and dual-species biofilm mapping discs were dip washed in DI water). For RT-PCR and CLSM analysis of biofilms, more harvesting steps were necessary. These steps are discussed in Chapter 3.2.4.

### *Cultivation of C.albicans and P.aeruginosa biofilms*

Methods from Purschke, 2012 were applied for the cultivation of mono-species and mixed biofilms found on catheters or open burn wounds (Hermann et al., 1999). They are labeled as medically relevant biofilms due to their clinical relevance. 1  $\text{cm}^2$  borosilicate glass coupons cut from glass slides (VWR) were used. After cultivation in 50 mL Falcon tubes for 24 h as described in Chapter 3.2.1, 10 mL of each solution was centrifuged for 10 min at 5000 rpm. Supernatant was then removed and replaced by new YNBNP medium and mixed for washing. The samples were centrifuged for another 10 min at 5000 rpm and the supernatant was again removed. Then, both solutions were set to  $\text{OD}_{600}$  1.0 (ca.  $3 \times 10^7$  cells / mL for *C.albicans*; ca.  $1 \times 10^9$  cells / mL for *P. aeruginosa*) by dilution with YNBNP medium.

For mono-species biofilm formation, discs were placed into a well of 24-well plates with 1000  $\mu\text{L}$  of either *C.albicans* or *P.aeruginosa* solution (for cultivation of dual-species biofilm organisms were mixed at 1:1 ratio resulting in 500  $\mu\text{L}$  of each solution) and incubated aerobically in static conditions at 32 °C for 90 min. After initial incubation, the medium was removed and replaced by fresh YNBNP medium and incubated in static conditions aerobically at 32 °C for an additional 48 h. Finally, the medium was removed, the discs were dip washed three times in DI water, and were then air dried for 10 min in a laminar flow bench for Raman analysis.

### **3.2.3 Optimization of oral biofilm cultivation methods**

Oral biofilms were cultivated using the ‘Zürich model’ (described in detail in Chapter 3.2.2). This method calls for a 50:50 mixture of mFUM medium and natural saliva for the cultivation of these biofilms. For the reproduction of results, the use of natural saliva can be problematic

as saliva for scientific studies show variances of the complex biochemical and electrophysical properties between individuals and in an individual over time (Darrene and Cecile, 2016; Hannig and Joiner, 2006; Lendenmann et al., 2000; Lyng Pedersen and Belstrøm, 2019). The variability of natural saliva reduces reproducibility of results which might have an impact on the Raman spectra and peaks. For this reason, the use of artificial saliva, as a replacement for natural saliva in the 50:50 ratio, was evaluated for this work. A full analysis of the use of artificial saliva can be found in Stöhrer, 2020. The analysis of different saliva alternatives demonstrated that PBS mixed with mFUM at a ratio of 50:50 shows the lowest difference to natural saliva with mFUM and, therefore, was used for future work and the cultivation of oral biofilm models (see Chapter 8.3.2 (Appendix) for evaluation of artificial saliva).

### **3.2.4 Sample preparation for different analysis methods**

Throughout this thesis different analytical methods were used. RT-PCR was used for the evaluation of artificial saliva for oral biofilm cultivation (see Chapter 3.2.3). FISH, being the state-of-the-art method, coupled with CLSM measurements was used for the evaluation of biofilm architecture (see Chapter 4.2). Microscopy was used for the determination of success of Raman mapping and evaluation of the use of Raman for biofilm structure identification based on microorganism architecture (see Chapter 4.3 and 4.4). The methodologies of the three methods are described below.

#### *RT-PCR*

Sample and analysis procedure is also described in Stöhrer, 2020. After biofilm cultivation, biofilm discs were transferred to a 15 mL falcon tube containing 1 mL PBS. The falcon tubes were sonicated for 30 min at room temperature to remove the biofilm from the surface and generate single bacteria in solution. The detached biofilm was analyzed quickly to avoid agglutination. For analysis, 100  $\mu$ L were used to quantify the composition of bacterial species in a multi-species biofilm based on different saliva.

After biofilm detachment, 100  $\mu$ L of the multi-species biofilm solution was transferred to a lysis tube from the DNA isolation and purification kit ('innuSPEED Bacteria/Fungi DNA Kit', AnalytikJena AG, Jena, Germany). At this point, DNA extraction was performed as described in the manual of the mentioned kit, where DNA was dissolved in 75  $\mu$ L of solution.

For the analysis of multi-species biofilms consisting of *S.oralis*, *A.denticolens* and *V.dispar*, RT-PCR was carried out in three individual wells in duplicates with species specific primers. This resulted in three different product fragments. Primer sequences are described in Table 6

## MATERIAL AND METHODS

and the resulting product fragments are shown in Table 7. This procedure ensures the analysis of multi-species biofilms and their quantification by individual species.

*Table 6: Primer sequences used for the quantification of multi-species biofilms purchased from IDT-DNA (Leuven, Belgium).*

Organism	Primer type	Sequence (5'-3')
<i>S.oralis</i>	Forward	accaggtccttgacatccctctgacc
	Reverse	accacctgtcacctctgtcccg
<i>A.denticolens</i>	Forward	tattgggCGTAAAGGGCTTGTAGGC
	Reverse	tctcctgatatctgCGCATTCCAC
<i>V.dispar</i>	Forward	ctgagaggatgaacggccacattg
	Reverse	gctccgTCAGACTTTCGTCcattg

*Table 7: Product fragment sequence formed with the use of primer sequences described previously.*

Organism	Product fragment (5'-3')	Fragment length (bp)
<i>S.oralis</i>	accaggtccttgacatccctctgaccgctctagagatag agtttcccttcgggacagaggtgacaggtggt	70
<i>A.denticolens</i>	tattgggCGTAAAGGGCTTGTAGGCggctggtcgcgtc tgccgtgaaaatccttcggcttaaccgggggcttgCGG tgggtacgggCGGCTTgagtgCGGTAGGGGaggctgg aattcctggtgtagCGGTGGAATGCGCAGATATCAGGA gga	150
<i>V.dispar</i>	ctgagaggatgaacggccacattgggactgagacacgg cccagactcctacgggaggcagcagtggggaatcttcc gcaatggacgaaagtctgacggagc	101

For the quantification of species, calibrations were established at different concentrations ranging from  $10^1$  to  $10^9$  templates/ $\mu$ L. For this calibration, a specific template containing all three product fragments was created in collaboration with IDT-DNA. Therefore, the following gBlock™ was generated with primer sequences underlined and DNA spacers highlighted in bold:

CTGAGAGGATGAACGGCCACATTGGGACTGAGACACGGCCAGACTCCTACGGGAGGCAGCAGTGGGGAATCTTC  
CGCAATGGACGAAAGTCTGACGGAGCTGCATGATCTACGTGCGTCACATGCAGTACTATTGGGCGTAAAGGGCTT  
GTAGGCGGCTGGTTCGCGTCTGCCGTGAAAATCCTTCGGCTTAACGGGGGCTTGCGGTGGGTACGGGCCGGCTTG  
AGTGCGGTAGGGGAGGCTGGAATTCCTGGTGTAGCGGTGGAATGCGCAGATATCAGGAGGACACTAGCTCAGATT  
CAGTAGACCGCTGTTGACCAGGTCTTGACATCCCTCTGACCGCTCTAGAGATAGAGTTTTCCTTCGGGACAGAGG  
TGACAGGTGGT

For the analysis, wells were prepared using a qPCR Sygreen Master Mix (Nippon Genetics, Düren, Germany) with specific mixing ratios (Table 9). Samples were then run under specific cycle settings as described in Table 8.

## MATERIAL AND METHODS

Table 8: qPCR cycle settings.

Step	Temperature (°C)	Ramp Rate (°C/sec)	Time	Cycles
Pre-incubation	95	4.4	2 min	1
Denaturation	95	4.4	5 sec	1
Amplification	95	4.4	15 sec	40
	65	2.2	30 sec	
	72	4.4	30 sec	
Melting curve	95	4.4	5 sec	1
	40	2.2	1 min	
	97	0.06	∞	
Cooling	40	1.5	10 sec	1

Table 9: Prepared master mix for qPCR application per sample.

Content	Volume (μL)
qPCRBio Sygreen Mix Separate-Rox 500, Nippon Genetics, Germany	10
Forward Primer	0.8
Reverse Primer	0.8
DNA Sample Template	1
Sterile ultrapure water	7.4

DNA concentration per biofilm was recalculated based on the fact that 100 μL of a 1 mL biofilm suspension was used for DNA extraction, and DNA was diluted in 75 μL. Consequently, the results in copies/μL were multiplied by the factor  $75 \cdot \frac{100}{75} \cdot 10 = 1000$ .

### *Fluorescent in-situ hybridization (FISH) for confocal Laser Scanning Microscopy*

The structural analysis and comparison to Raman Microscopy were done using fluorescence *in-situ* hybridization (FISH). The staining was performed according to the protocol previously described by Thurnheer et al. in 2004 using the probe combinations listed in Table 10 and was further detailed in in Kriem et al. (2021). Compositions of the chemicals used can be found in Chapter 8.4 in the Appendix.

Biofilms were fixed using ice-cold 4% paraformaldehyde (PFA) and incubated at 4 °C for a time of 60 min with biofilms fully submersed in PFA. After fixation, the PFA solution was removed by dip washing the sample disc three times in 0.9 % NaCl (w/v). After dip washing, the discs were incubated again with lysozyme solution (1 mg/mL) for 8 min at room temperature and then dip washed twice with 0.9 % NaCl (w/v) for the permeabilization of biofilms.

*Table 10. Sequence and formamide concentrations for fluorescence in-situ hybridization probes purchased from biomers.net GmbH (Ulm, Germany)*

Organism	Name	Label	FA <sup>a</sup> (%)	NaCl <sup>b</sup> (mM)	Probe concentration (µg/ml of hybridization buffer)	Sequence (5'→3')	Source
<i>Streptococcus oralis</i>	MIT447	6-FAM	30	102	20	CAC CCG TTC TTC TCT TAC A	(Thurnheer et al., 2004)
<i>Actinomyces denticolens</i>	ACT476	Cy3	30	102	20	ATC CAG CTA CCG TCA ACC	(Gmür and Lüthi-Schaller, 2007)

<sup>a</sup> Formamide concentration in the hybridization buffer

<sup>b</sup> Concentration of NaCl used in the washing buffer

Prior to first use, FISH probes were dissolved in TE-buffer for working concentrations of 20 µg/mL for 6-FAM and 10 µg/mL for Cy3. Biofilm samples were pre-hybridized in hybridization buffer at 46 °C for 15 min without oligonucleotide probes with the samples fully submersed in the buffer. Biofilm disc were then transferred from the pre-hybridization buffer onto a tissue paper that was placed in a small Petri dish. 65 µl of hybridization buffer with probe was added onto the biofilm and the dish was sealed with Parafilm. The biofilms were then hybridized in the dark for 90 min at 46 °C.

After hybridization, samples were washed in washing buffer (that was pre-heated to 48 °C in a waterbath) for 45 min at 48 °C. For CLSM analysis the samples were washed with 0.9 % NaCl (w/v), then fixed onto glass slides using nitrocellulose dissolved in butyl acetate (commonly known as nail polish) (Essence shine last&go!, cosnova, Frankfurt, Germany) and embedded in Mowiol® 4-88. Sample slides were then stored at 4 °C for at least 24 h but not more than 7 days in order for the antifadent to dry and then be used for analysis.

In total, 15 fluorescent labeled coupons (and 5 coupons of DBIA samples) were analyzed using an inverted microscope Zeiss LSM710 (Zeiss, Oberkochen, Germany) described in Chapter 3.1.1.

### *Raman and Microscopy*

All planktonic and biofilm samples were able to be used for analysis directly after sample preparation described in Chapters 3.2.1 and 3.2.2.

## **3.3 Raman signal processing and multivariate analysis**

Spectral acquisitions of samples were done using one of the instruments described in Chapter 3.1.1 with their specific acquisition settings. For ThermoFisher Scientific DXR2xi, spectra were pre-corrected using low baseline correction in spectral acquisition mode.

For planktonic samples and dual-species biofilms, random locations away from the sample border were chosen. For DBIA samples, a random border area between the two species was selected. For dual-species and DBIA sample acquisitions, microscopic images were taken for morphology analysis of the same area.

Depending on the analysis question, different numbers of spectra were collected. These are specified in Figure 11. To perform spectral processing, all spectra of one analysis group was grouped together and the same processing steps were applied to the group. Unless otherwise indicated, all processing steps and settings remained identical for all groups to reduce noise effects and spectral variations due to spectral sample collection and processing. All reprocessing steps were performed using Renishaw WiRE 5.2 (Renishaw plc, Wotton-under-Edge, UK).

Table 11: List of collected spectra for the different analysis setups in this research.

Type of analysis		Bacteria	Samples	Spots	Points	Total Spectra per bacteria species or sample
<b>Growth phase</b>	<b>24 h</b>	5	3	4	1	<b>12</b>
	<b>48 h</b>	5	3	4	1	<b>12</b>
	<b>72 h</b>	5	3	4	1	<b>12</b>
	<b>96 h</b>	5	3	4	1	<b>12</b>
<b>State</b>	<b>Hydrated</b>	5	12	4	1	<b>48</b>
	<b>Dehydrated</b>	5	12	4	1	<b>48</b>
<b>Calibration set for differentiation</b>		5	21	4	1	<b>84</b>
<b>Planktonic bacteria prediction</b>		3	9	1	4	<b>36</b>
<b>Mono-species Biofilm prediction</b>		3	5	1	6	<b>30</b>
<b>Calibration set for mapping</b>		2	15	1	20	<b>300</b>
<b>Mapping confirmation</b>		2	3	Area: 15 x 15 $\mu\text{m}$		<b>225</b>
<b>Oral Biofilm mapping</b>		2	15	Area: 18 x 18 $\mu\text{m}$		<b>324</b>
<b>Medical Biofilm mapping</b>		2	3	Area: 35 x 35 $\mu\text{m}$		<b>625</b>

### 3.3.1 Data processing

A number of steps had to be performed in order to translate a raw Raman spectrum into a spectrum that allows comparison between the different species. This is largely because the raw spectrum shows too much noise and fluorescence, preventing analysis based on species-specific peak characteristics. These processing steps are specified below. To better visualize the effect of the processing steps, a mono-species *A.denticolens* biofilm spectra was used and is shown in Figure 12 to Figure 20.

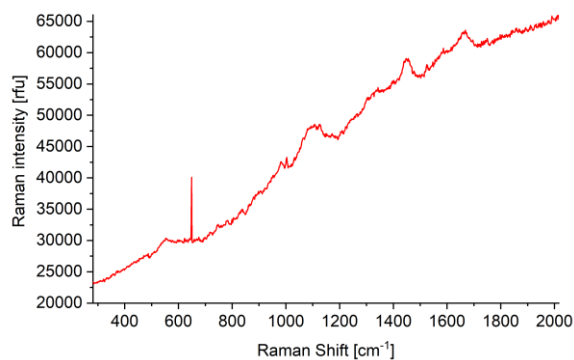


Figure 12: Raw Raman spectrum.

### *Truncation*

For the analysis and differentiation of bacterial species, the spectra between 600-1800  $\text{cm}^{-1}$ , also known as the ‘fingerprint region’, 706 data points were collected to show differences in molecular composition. While the ThermoFisher Scientific DXR2xi is able to collect spectra over this range, the Renishaw inVia™ Qontor collects a spectral range of 282.8-2016.2  $\text{cm}^{-1}$  and 1015 data points. For that reason, all spectra were truncated to a uniform range from 600-1800  $\text{cm}^{-1}$  with 706 data points. Wavenumber data points were unified to ensure that statistical analysis tools can be executed properly. A shift in wavenumbers between spectra of one dataset would have resulted in insufficient statistical analysis because these tool require a uniform spectral range.

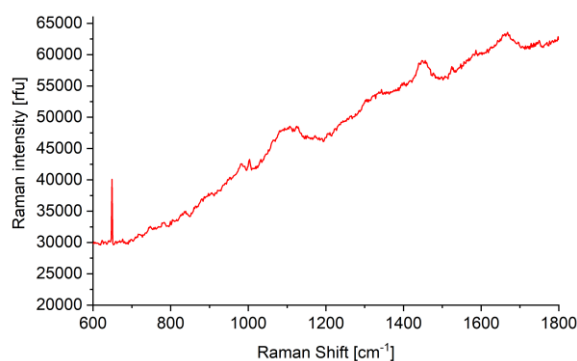


Figure 13: Spectrum after truncation.

### *Cosmic Ray removal*

In the second step, spontaneous cosmic rays were removed. Cosmic rays are sharp spikes in the spectra which are not directly related to the sample. These spikes are generated by cosmic rays (high energy particles usually coming from natural or artificial light) hitting the detector, producing a feature that is narrower than the classic Raman peaks. Removal of these peaks

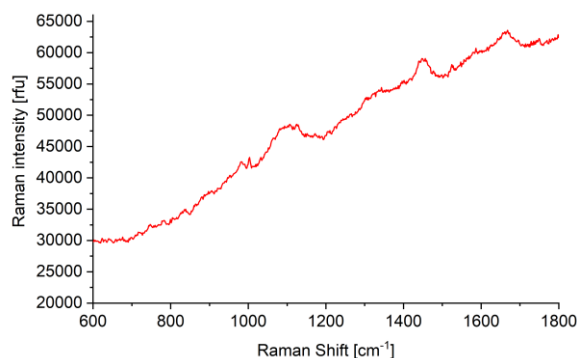


Figure 14: Spectrum after Cosmic Ray removal.

are necessary because they are not part of the spectral peaks of a sample and can result in improper multivariate statistical analysis. Cosmic rays can be removed in WiRe 5.2 after spectral acquisition using a Cosmic Ray Detection Wizard. Here, a width parameter of 3 and height parameter of 15 allowed for the detection of cosmic rays in microbiological spectra. Cosmic ray candidates were then checked manually and agreed on to be removed from the spectrum.

*Background removal*

The reference borosilicate glass slide spectrum can be found Chapter 8.5.1 in the Appendix. Borosilicate as the component of a glass slide shows two broad and one narrow band that can interfere with the spectral peaks of the microbiological samples. Here, the two most significant peaks can be found at  $572\text{ cm}^{-1}$

(broad),  $794\text{ cm}^{-1}$  (narrow) and  $1093\text{ cm}^{-1}$  (broad), whereas the last two lay in the ‘fingerprint region’ (see Chapter 8.5.1 in Appendix). In order to remove borosilicate background noise from the spectrum, specific arithmetic operations were performed. To do so, the borosilicate spectrum was subtracted from the sample spectra. This background removal was performed for every spectral group because the samples did not have the same thickness. However, for some samples the borosilicate signal could only be partially corrected for. In addition, the arithmetic operation also compensated for the background that may have come from the laser induced background fluorescence from the bacterial sample (Yakubovskaya et al., 2019) and can be seen by the general up riding of the spectrum in its raw form. The negative values that resulted after background removal were the results of the high counts of the borosilicate spectrum and were compensated for by baseline correction.

*Baseline correction*

The type of baseline correction method used to estimate or adjust a baseline of the spectrum is critical (Guo et al., 2016). It allows the emphasis on spectral peak information rather than the artefact of different heights of spectra and thus greatly improves the statistical analysis, differentiation and comparability of

different bacteria species. Mathematical methods for baseline correction, apart from first and second order deviations, are polynomial fits. WiRe 5.2 allows an intelligent polynomial baseline subtraction. After automatically excluding regions with peaks, the baseline was fitted to all remaining points. A polynomial order of 12 and noise tolerance of 1.5 was used for all spectra. This allowed for quick data processing and a tight baseline adjustment based on peak

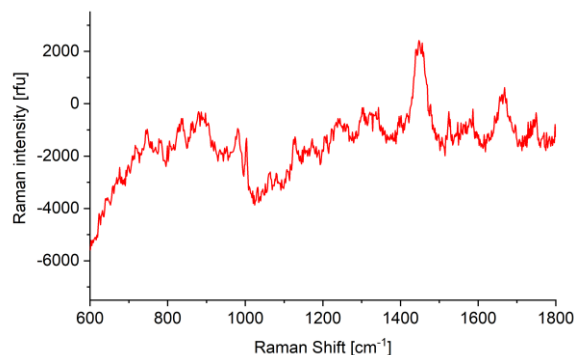


Figure 15: Spectrum after background removal.

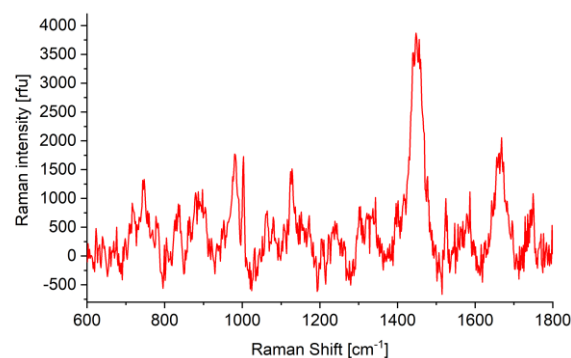


Figure 16: Spectrum after baseline correction.



behavior. Baseline corrections are spectra specific and were applied automatically to each spectrum by recalculating the baseline based on peak behavior.

### *Noise filtering*

For increased automation potential, noise was reduced using noise filtering settings. Noise is the random small peaks that do not provide information on the peak behavior but can however silence important spectral peaks. Additionally, an increase in signal to noise ratio (by reducing noise) increases the success of a multivariate analysis because weak spectral features and differences can be taken into account. WiRe 5.2 allows a PCA based noise filtering where PCs are calculated and ranked on order of decreasing significance. After doing so, the components were inspected individually and the effect on the spectra was evaluated. After the manual inspection, PCs that retain all components that contain Raman information and the samples were selected. All other peaks/noise were then automatically removed, only leaving Raman peaks deriving from the sample itself. Finally, the analysis was done per data group. Selected PCs ranged from three to five depending on the amount of noise in the sample group.

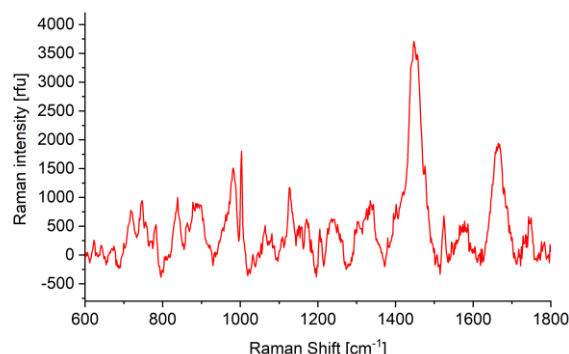


Figure 17: Spectrum after noise filtering.

### *Smoothing*

In order to improve the signal to noise ratio further, smoothing was applied. A Savitzky-Golay algorithm was used for processing (Savitzky and Golay, 1964). Savitzky-Golay smoothing uses a process known as convolution, by fitting continuous sub-sets of adjacent data points with a low-degree polynomial by the method of linear least squares. Both of these parameters can be defined before fitting. In this research, the smoothing window sub-set was set to 7 with a polynomial convolution order of 2. Due to the measurement settings, the spectrum consisted of 706 equally spaced data points where an analytical solution to the least-squares equations could be found. This then allowed the evaluation of a convolution coefficient that could be applied to all sub-sets, resulting in a specific smoothed signal. This signal was calculated for every spectra individually.

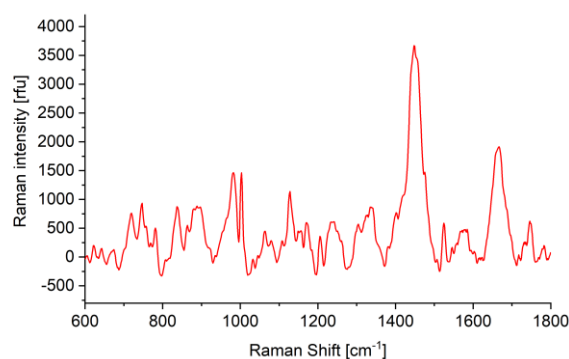


Figure 18: Spectrum after smoothing.

### Normalization

The spectral differences with regard to presence and/or absence of peaks between species are only minor, whereas there are more frequently differences in the intensities and heights of spectral peaks. These variances are a direct result of the acquisitions and the nature of samples. As differences can have an effect on the assignment of spectra to species and accuracy of calibration datasets. Therefore, it was necessary to normalize the spectra. Normalization was able to compensate for the changes in intensities. Generally the peak characteristics do not change after normalization. In this work, the minimum point of the spectrum was set to 0 while the maximum was set to 1. The normalization was calculated for every spectra individually.

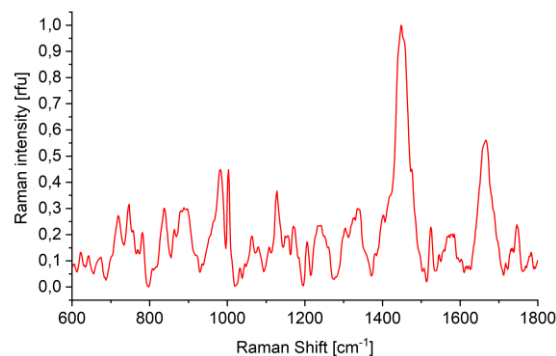


Figure 19: Spectrum after normalization.

### Differentiation

As the last step for multivariate analysis, differentiation of spectra are performed. Savitzky-Golay differentiation was applied based on the same arguments made for smoothing. The fundamental principle of the process are described in Savitzky and Golay, 1964. A window size of 9 and polynomial order of 2 was selected for a 2<sup>nd</sup> order differentiation based on the analysis performed. Differentiated spectra were selected for multivariate analysis, because the value of the peaks were increased by differentiation and therefore improved the grouping of species in multivariate statistical analysis (Rinnan, 2014). For the consideration of peak characteristics, this step was unnecessary because it reduces the visibility of peaks in the ‘fingerprint region’.

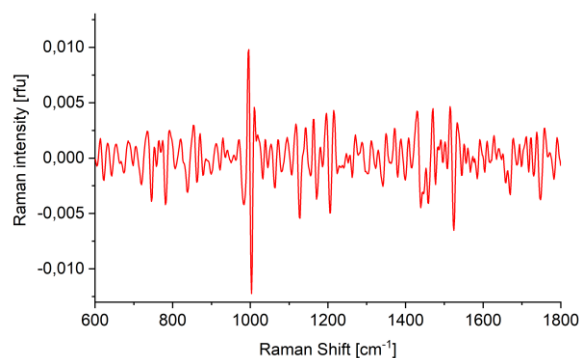


Figure 20: Spectrum after differentiation.

### 3.3.2 Statistical modelling

In general, a model is a mathematical function that allows the prediction of unknown data. An example of such mathematical functions is the use of calibration lines to quantify chemicals. Specific concentrations are plotted in a coordinate system that allow for the calculation of a regression line. Using common linear regression equations calculated from calibration lines, it is then possible to predict concentrations of an unknown sample. Qualitative analysis models

such as the grouping of multiple characteristics are not possible with such univariate mathematical functions and require the use of multivariate models that allow the consideration of different variables. The goal of such models is the extraction of information while remaining reliable for the prediction of unknown data. For the differentiation of multiple microorganisms based on their chemical spectra, these multivariate approaches were selected as the methods of choice because they could be well integrated into the mapping of biofilms. Further, they allowed for the use of the whole spectrum range and were not confined to specific areas. As a ground principle for multivariate analysis approach, each sample spectrum was taken as one observation with each data point in a spectrum representing one variable.

In this work, three different multivariate models were used for the comparison of data. Their specific analytical characteristics will be introduced further in the next chapters. Subject to the questions being asked, different statistical methods were applied accordingly.

### *Principal Component Analysis (PCA)*

Principal Component Analysis (PCA) is seen as the foundation of all latent variable projection methods and one of the simpler multivariate analysis approaches and was first invented and used by Pearson in 1901. PCA is able to reduce the dimensionality of a data set by choosing components explaining most of the variances in the data. As a result giving form of PCA, score data plots summarize the observations and are able to identify patterns, trends and clusters. Alternatively, loading data plots summarize the variables and explains the positions of observations in a score plot (Shlens, 2005). Applicability of PCA for differentiation of bacteria based on their Raman spectra was demonstrated successfully by Lu et al., 2011 in the past. For the information extraction of this work, the resulting score plot is valuable because it demonstrates the possibility of separating bacterial groups statistically based on their Raman spectra.

PCA provides a data-driven hierarchical coordinate system to capture the maximum variation in a dataset. Using PCA, the model first calculated an average for each wavenumber. In the datasets of this research, this resulted in a total of 706 average values. Next, these values were standardized in order to prevent certain variables from dominating the analysis. In the second step, a covariance matrix was computed considering the calculated averages to see if a relationship could be found between the samples. To analyze the distribution of samples in a two-dimensional score plot, eigenvectors and eigenvalues were computed to determine the principal components (PC) of the data. Principal components are sets of new variables. The system tries to put as much information in the first principal components in order to explain the

maximum possible variance with the first component. The process continued by explaining the second most information with the second component and so on.

Two chosen PCs then allowed for the definition of a model plane (in this work the first two PCs were selected but combinations of other PCs were possible to create score and loading plots but don't show improved separation of clusters). Then, all observations in the calibration dataset were able to be visualized in the score plot using PCs as the axis of the plane and the coordinate values stemming from the individual samples. In this work, known bacterial species were used in combination with their spectra and thus it was possible to color code each bacterial species individually to determine specific clusters in the score plots. For some analysis settings in the development and proof of the analysis workflow, it was necessary to determine confidence ellipses (CE) to demonstrate the accuracy and confidence of the group assignments. Here, all ellipses were based on a 95% confidence.

For this reason, PCA was mostly used for models that required differentiation of two species because it allowed for easier classification.

### *Orthogonal Two-Way Partial Least Square Analysis with Discriminant Analysis (O2PLS-DA)*

PLS-DA is a multivariate dimensionality-reduction tool that has been popular in the field of chemometrics and was applied in this thesis for that reason. In comparison to PCA being a model that corresponds to the demonstration of maximum variance, Orthogonal Two-Way Partial Least Square Analysis with Discriminant Analysis (O2PLS-DA) corresponds to maximum separation and is an extension of Partial Least Square (PLS) analysis. The model was first described by Trygg and Wold in 2002. Compared to PCA, OPLS focuses on predictive information in one component and, then in the next step, on other systematic information that can then be found in higher components. This maximum separation is performed using known class information found in the averaged spectrum for every bacterial species generated after all processing steps. Thus, the separation is performed in a so-called supervised approach. In this work, known class information represents the calibration spectra generated.

OPLS is a regression and prediction method. Additionally, the method works with discrete values therefore making it a discriminant analysis. For the classification model, two steps are necessary: 1. Training a model using representative, calibration data (here the known spectra collected to setup the calibration dataset) and 2. Testing the model by using new data (to prove the calibration dataset, more known values were collected. Using these data and calibration

values, predictions were made to evaluate how well the calibration dataset is able to predict new sample spectra by comparing it to all the datasets generated for each species).

In the first step, the model groups the variables from the collected Raman spectra into explanatory variables (X) and dependent variables (Y). For this analysis step, O2PLS-DA takes into account multiple Y-values for the model. The variables are then further decomposed into latent structures in an iterative process with scores  $t$  for X and  $u$  for Y. Using the information of explanatory and dependent variables it is then possible to display these values in a score plot.

In order to confirm the O2PLS-DA model for the differentiation of species, it was necessary to prove the model by a validation approach. Consequently, additional spectra of all species that were not part of the calibration dataset were collected and used for cross validation. Sample preparation remained the same to prevent a spectral effect based on sample preparation. Here, both types of variables were calculated and compared to the calibration O2PLS-DA model. This model then allowed for the classification of the bacteria to a specific bacterial species. This process was repeated for the classification of mono-species biofilm Raman spectra based on a calibration dataset consisting of spectra generated from planktonic bacteria.

Data was visualized in two ways: 1. Performing O2PLS-DA on the datasets and 2. Showing the prediction results and grouping of the spectra. As the identity of the sample was known before the statistical analysis, the accuracy of the calibration model was able to be determined.

### *Cluster Analysis (CA)*

Several methods of determining distributions of spectra over a specified area have been previously described. These methods include PLS-based (Trygg and Wold, 2002; Villa et al., 2019; Zhu et al., 2007) or PCA-based (Almarashi et al., 2012; Colniță et al., 2017; Jung et al., 2014) approaches. Additional methods try to cluster data based only on information found in the data that describes the objects and their specific relationships. One of these methods is Cluster Analysis (CA) (Jarvis and Goodacre, 2004; Kniggendorf et al., 2011). CA is a method that allows the grouping of a set of spectra into clusters of similar spectra. This analysis allows for the calculation of a centroid spectra for each cluster, gathered by taking the mean of all spectra in the cluster and can be correlated to previous calibration spectra. The underlying mathematical equation for the differentiation and clustering within the CA method can be found in Döring et al. (2006).

Within CA different centroid initializing methods, the selection of the number of clusters or the fuzzification rate have an influence on the success of differentiation of subgroups (Schwämmle

and Jensen, 2010). For simplicity of this work, only the selected settings that are beneficial for the mapping of biofilms are further discussed and evaluated.

K-means clustering is a common initialization method with the purpose of selecting initial centroids found across the whole dataset (Bradley and Fayyad, 1998). With this method, the first centroid of the dataset is chosen at random and the next centroids for the additional clusters are selected in a way that the spectra are furthest away from the existing centroid that have the highest probability of being selected. Thus, the amount of centroids is dependent on the number of clusters chosen. Even though K-mean clustering (also known as hard clustering) allows the assignment of spectrum to only one cluster, fuzzification clustering (also known as soft clustering) was selected. With the help of fuzzification parameters, it was possible that a spectrum could belong to multiple clusters giving the spectra values between 0 to 1, depending on how much the spectrum fits to the cluster. The cluster with the highest value is then assigned to the spectrum. Because no definite assignment needed to be made, fuzzy c-means clustering showed the best cluster differentiation in the validation of the model and was selected for that reason. In addition, background and signal-to-noise ratios have an effect on the success of the method and have been evaluated previously by Guo, 2018. Because background and signal-to-noise have been removed from the spectra as part of the workflow in the processing steps, Euclidean distance measure was able to be used, which is a standard measure of the distance between the spectrum vector and the mean spectrum vector.

The number of restarts within the cluster analysis determines new initial centroids with every restart. The result of every restart is determined by the sum of the total distance from each spectrum to its centroid. As a result, the restart with the shortest total distance is then selected as the final centroids. Increasing the number of restarts increases the chances of having optimized centroids, but requires more computing power and for that reason time for a result. The number of iterations determines how many attempts are made to align spectra closest to the centroid clusters to receive the smallest distance vector. Again, increasing the number of iterations increases the chances of having optimized alignments but increases the time for computing the results.

### *Use of the statistical methods*

PLS-DA can be seen as a “supervised” version of PCA (being an “unsupervised” version) in the sense that it achieves dimensionality reduction but with full awareness of the class labels. The terms “supervised” and “unsupervised” refers to whether the model uses a reference or not to setup the model. Ruiz-Perez et al. (2020) as well as Scott and Crone (2021) both showed that

no clear distinction can be made which model to apply for which datasets and that the analysis is specific to the data. Both statistical models were considered for the analysis of datasets. Chapter 4.1.4 compares the results of both methods for the differentiation of five oral species. The analysis of the influence of growth phase (Chapter 4.1.2) and state (Chapter 4.1.3) both required an unsupervised analysis to prevent a biased analysis and to demonstrate the similarities and interchangeability of collected spectra.

Overall, due to a maximum separation of data groups approach, O2PLS-DA will improve the visualization and interpretation of a model and is, for that reason, a better analysis model for the differentiation of multiple bacterial species while PCA can be used for the differentiation of two bacterial species (“OPLS vs PCA,” 2020) or to gain further understanding in a dataset. Additionally, O2PLS-DA allows for the prediction of bacterial species on uncorrelated information of Raman spectra based on calibration datasets. For that reason, O2PLS-DA also works well for the analysis of omics data (Bouhaddani et al., 2016). To show the differences of the two multivariate statistical models, they are compared with each other based on their score plots from an identical dataset (Chapter 4.1.4).

The comparison of models in Chapter 4.1.4 revealed that O2PLS-DA shows better differentiation of species in the score plot, which was the reason why the method was also applied for the prediction of spectra in Chapter 4.1.5. In contrary, PCA showed good differentiation for datasets of two species and were used in Chapters 4.3.2 and 4.4.2 to demonstrate that the collected spectra show sufficient differences to be applied for mapping using Raman spectra.

*Table 12: Application of different statistical methods including the used software for analysis (see Chapter 3.1.2 for more software details)*

Statistical method	Chapter	Role in biofilm	Used software
PCA	4.1.2 4.1.3	Unbiased determination if collected data is similar or different	Origin 2019b
	4.3.2 4.4.2	Differentiation of two bacterial species to generate calibration datasets	Origin 2019b
	4.1.4	Comparison of the two modelling methods for differentiation of five species	Origin 2019b and SIMCA15
PLS	4.1.5	Use of the method for the prediction and cross-validation of a calibration dataset with a supervised approach	SIMCA15
CA	4.3.3 4.3.4 4.4.3	Mapping of Raman spectra based on statistical models using an unsupervised approach	Renishaw WiRe 5.2

O2PLS-DA and PCA are both modelling methods without the consideration of dimensions of the collected data and cannot be applied for the mapping of Raman spectra in this thesis. Additionally, Jarvis and Goodacre (2004) and Kniggendorf et al. (2011) both showed the applicability of hierarchical cluster analysis for mapping of Raman spectra. For that reason and because CA is an unsupervised analysis method, this model was used for biofilm mapping in Chapters 4.3.3, 4.3.4 and 4.4.3. Table 12 gives a summary of the methods that were used to answer which question and where it was applied in this thesis.

### **3.3.3 Biofilm distribution mapping using CA**

In this work, Renishaw WiRe 5.2 allows CA through an included mapping analysis tool. As part of the tool, different parameters can be selected that are summarized and were tested beforehand (see Table 13 with all selectable parameters in WiRe 5.2 for CA). Criteria for the selection were 1. accuracy of results and 2. time for the calculation of results. As a result of preliminary mapping trials using DBIA samples, CA was performed using K++ initialization, fuzzy c-means as the clustering type with 2.0 fuzzification parameters, Euclidean distance metrics and 10 iterations and restarts. Subsampling was used and the subsampling percentage was set automatically. The centroid spectra were then compared to the calibration spectra generated from planktonic bacteria (for DBIA samples) and mono-species biofilm samples (for multi-species biofilms). Depending on the cluster affiliation, each spectral point in the same group was colored accordingly (red for *A.denticolens* and green for *S.oralis* as seen in Figure 33) and mapped.

As already stated in Chapter 3.1.1, microscopic image analysis based on morphology of *A.denticolens* and *S.oralis* was performed using morphological segmentation in the Plugin MorphoLibJ in ImageJ (Rasband, 1997). These images were then compared to the images generated through CA analysis from Raman acquisitions. Percentages of coverage for each bacterial species and analysis type was evaluated with ImageJ. Furthermore, both images were overlaid to identify areas that were not classified as the same bacterial species.

Relative coverages were evaluated based on different approaches. The types of coverage analysis are demonstrated using examples shown in Figure 21. Here, Example 1 shows two identical images of red and green areas for both Raman and morphology mapping. The difference in total coverage is 0 and there are no areas where the colors do not match. Example 2, on the other hand, still has an identical total area coverage (of 50% each) but since the shape



of the red and green area have changed there are areas where the colors are not identical anymore. Thus, the layover image shows a difference in locational coverage of 25%.

Table 13: Parameters that can be selected as part of the WiRe 5.2 that were tested and evaluated for mapping.

Parameter	Available options
Initialization type	Random K++
Clustering type	K-means Fuzzy c-means
Distance metric	Euclidean Correlation
Number of clusters	1 - $\infty$
Number of iterations	1 - $\infty$
Number of restarts	1 - $\infty$
Fuzzification parameter*	1 - $\infty$
Sampling options	Subsampling Automatically setting the subsampling percentage

\*Only available for the fuzzy c-means clustering type

Example 3 now shows changes in the total coverage and locations of the areas. Considering the morphology studies as the true method, the Raman image shows an under-representation of the red area (with 6%) while it shows an over-representation of the green area (of 6%) when compared with each other. Looking at the locational differences of the areas now the colors disagree in several areas making up for a total of 24%. Thus, it can be concluded that the difference in total coverage is not equivalent to the locational total coverage and needs to be evaluated separately because different conclusion can be made depending on the approach used.

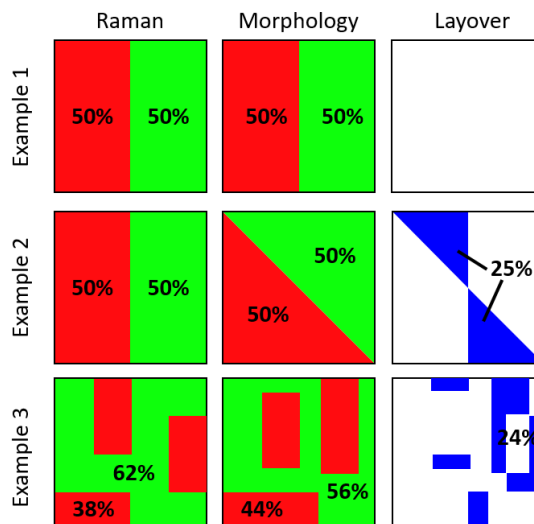


Figure 21: Examples of relative coverages and approaches of determination.

## 4 Results

This thesis aims to evaluate chemometric characteristics of bacterial species for differentiation and to provide a first workflow to map biofilms using confocal Raman microscopy. For the proof-of-concept design, multiple steps were necessary: 1. optimization of biofilm growth conditions (see Chapter 8.3.2 in the Appendix) 2. demonstration of bacterial species differentiation based on Raman spectra and 3. design of a workflow to differentiate bacteria in biofilms.

Parts of the results were already published in peer-reviewed journals (Kriem et al., 2021, 2020).

### 4.1 Differentiation of oral bacteria

#### 4.1.1 Raman spectra for five subgingival bacterial species

Spectra of five different bacterial strains were analyzed using CRM as described in Materials and Methods. The spectra are summarized in Figure 22 showing the plots of averaged Raman spectra, generated from a total of 84 spectra per strain. Overall, many vibrational peaks were similar in the acquired spectra, however, several unique peaks could be assigned to each of the individual bacterial species as displayed in Table 14. In several publications the same specific peaks were assigned to chemical compounds present within a bacterial cell (De Gelder et al., 2007; Kumar et al., 2016; Sil et al., 2017).

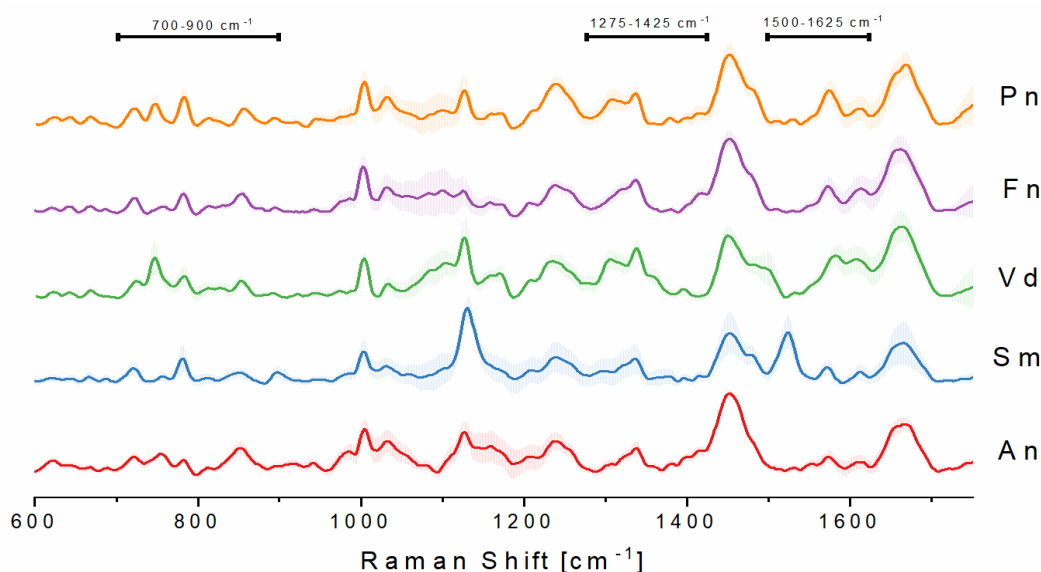


Figure 22: Averaged processed Raman signal (84 spectra total per species) from five different subgingival species of the calibration group with standard deviations. *A.naeslundii* (An), *S.mutans* (Sm), *V.dispar* (Vd), *F.nucleatum* (Fn) and *P.nigrescens* (Pn). Areas of differences in bands between species are indicated (700-900 cm<sup>-1</sup>, 1275-1425 cm<sup>-1</sup>, 1500-1625 cm<sup>-1</sup>)

## RESULTS

Some of these peaks actually can be identified by visually inspecting the spectra. By selecting the unique peak patterns of the different species, it is possible to discriminate between the individual species. Using a reference database of Raman spectra, it was previously shown that it is possible to identify predominant chemical signature patterns in spectral peaks (De Gelder et al., 2007; Kumar et al., 2016; Sil et al., 2017). Even though peak identification between different studies are almost aligned, Raman peaks, due to the nature of samples and instruments, can shift which needs to be considered according to Kuhar et al. (2018).

*Table 14: Specific peak assignments for the different species and their presence or absence compared to other species. Peak assignments are based on assignments by De Gelder et al. (2007); Kumar et al. (2016) and Sil et al. (2017).*

Raman Shift [cm <sup>-1</sup> ]					Peak Assignment of biochemical compounds
<i>A.denticolens</i>	<i>F.nucleatum</i>	<i>P.nigrescens</i>	<i>S.mutans</i>	<i>V.dispar</i>	
622	620	622	-	622	Phenylalanine
-	643	643	-	643	Tyrosine
720	722	722	720	724	Adenine
-	-	749	-	747	Thymine (ring breathing)
782	782	784	780	783	Cytosine (ring breathing)
852	853	857	852	853	Tyrosine (ring breathing)
-	894	896	898	-	$\gamma(\text{CN})$ , $\gamma(\text{CON})$ symmetric, $\delta(\text{CCH})$ aliphatic
1004	1004	1006	1004	1004	Phenylalanine ( $\gamma(\text{CC})$ aromatic ring)
1033	1033	1033	1031	1033	Phenylalanine (C-H in plane)
1127	1127	1129	1131	1127	C-C, C-N stretch of proteins
1237	1239	1239	1239	1237	Amide III (CN in plane bend)
1339	1339	1339	1337	1339	Tryptophan (C-H <sub>2</sub> twist)
1453	1451	1451	1451	1447	C-H <sub>2</sub> twist deformation (scissoring from lipids, assym. def. of amino acid side chains)
-	-	-	1523	-	C=C stretch
1573	1575	1573	1573	1581	Amide II
1665	1663	1667	1663	1665	Amide I

The presence of proteins is indicated by Amide I and Amide III peaks that are most significant at  $\sim 1250 \text{ cm}^{-1}$  (Amide III) and  $\sim 1660 \text{ cm}^{-1}$  (Amide I). Amino acids are identified as Phenylalanine at  $\sim 1003 \text{ cm}^{-1}$  and C-N and C-C stretches are found at  $\sim 1125 \text{ cm}^{-1}$ . CH<sub>2</sub> deformations at  $\sim 1450 \text{ cm}^{-1}$  are the result of lipids in the cell. The results for *Streptococci* species in this work are comparable with the results from Berger and Zhu (2003) who previously identified components in *S.mutans* and *S.sanguinis* (Amide I at  $1651 \text{ cm}^{-1}$ , C-H<sub>2</sub> deformation at  $1457 \text{ cm}^{-1}$ , C-N and C-C stretch at  $1127 \text{ cm}^{-1}$ , phenylalanine at  $1005 \text{ cm}^{-1}$ ; changes in wavenumbers come from Raman shifts of a different Raman analysis setup (Berger and Zhu, 2003)).

Differences in peak patterns between the five selected species are found mostly in the region between  $700\text{-}900 \text{ cm}^{-1}$ . This area is specific for nucleotides (DNA and RNA) due to ring breathing vibrations. Additionally, the area between  $1500 \text{ cm}^{-1}$  and  $1625 \text{ cm}^{-1}$  shows peaks that

## RESULTS

---

are the result of different amino acid compositions within bacterial species and thus can be used for differentiation of species. Minor differences can also be observed from  $1275\text{ cm}^{-1}$  and  $1425\text{ cm}^{-1}$ , revealing peaks from amino acids, fatty acids and saccharides (De Gelder et al., 2007; Kumar et al., 2016; Sil et al., 2017). Due to the nature of Raman acquisitions, different chemical compounds can have overlapping peaks (as shown in Chapter 1.3.3) that do not always allow for the specific identification of chemical groups.

For this work, identification of specific peaks for chemical compounds is not the goal, rather it is the use of differences in peaks for species differentiation based on multivariate methods. Nevertheless, identification of specific peaks for individual species is beneficial for discrimination. Major peaks such as Amides and nucleobases can be found in all species as being part of every bacteria. While the precise peak locations for proteins is difficult to determine due to overlaps of peaks from other compounds, Amide I and III peaks can especially be used for the detection and quantification of proteins. Amide II peaks are often inactive or very weak (Kuhar et al., 2021), but are visible in oral bacteria samples. Nucleic acids (Thymine, Cytosine, Adenine and Guanine) as the main components of DNA structures can be found at different positions within the spectra for all species, which applies to every microbiological sample. Lastly, different amino acids such as phenylalanine, tyrosine and tryptophan also show several compound specific peaks within the ‘fingerprint region.’ Theoretically, all amino acids can be found within the spectra, but due to overlap of peaks based on similar rotations, however, they cannot be differentiated (Socrates, 2001).

The analysis shows that there are spectral differences between the five analyzed oral species, which is due to the chemical composition of the bacteria. The specific peak assignment of signals in the ‘fingerprint region’ is important and helps with bacterial species differentiation. For the development of a workflow to map biofilms based on their Raman spectra and the underlying statistical methods, it is important that the spectra are different, not why they are different. Understanding why spectra are different will help to explain the differences between species though and should be considered for the analysis. The primary focus is thus on the evaluation of differences of peaks in the whole spectra and secondary, the specific peak assignment. Specific peak assignments may be helpful to understand the different chemical composition of bacteria.

Because the chemical composition of cells is a key factor in correctly identifying species based on their Raman spectra, conditions that can have an influence on cellular composition need to be considered. These include 1. the chemical changes and resulting Raman spectra based on a

bacteria's growth phase and 2. the influence of the state of bacteria whether they are analyzed in a hydrated or dehydrated state.

#### 4.1.2 Influence of the growth phase of bacteria on the Raman spectra

With their research, Stroala et al. (2014) indicated that Raman spectra can detect biochemical changes of metabolic states in bacterial species based on their specific growth phases using *Escherichia coli* and *Bacillus subtilis*. In order to generate a stable calibration dataset for the five selected bacterial species, the impact of the growth phase of the bacteria had to be evaluated. Results of the growth phase studies for the five species of interest and their equivalent PCA analysis are shown in Figure 23. Mean spectra are shown.

All spectra show the major peaks described earlier independent of growth phases and also don't change in their specific signal counts (equivalent to the height of peaks). Notably, peaks at  $\sim 782\text{ cm}^{-1}$ ,  $\sim 1004\text{ cm}^{-1}$ ,  $\sim 1451\text{ cm}^{-1}$ ,  $\sim 1575\text{ cm}^{-1}$  and  $\sim 1665\text{ cm}^{-1}$  remain consistent throughout the growth phases of all five species. Changes in signal counts (and thus height) appear between  $1000 - 1250\text{ cm}^{-1}$ . Overall, spectra after 24 h differ the most from the other evaluated time points. One explanation for the change could be that metabolic changes appear in the first 48h and then remain consistent throughout the considered time points. Indeed it was shown that the bacterial species have reached the stationary growth phase within the first 48h (growth experiments were performed by Stöhrer (2020) and showed that stationary growth phases were reached after 23 h for *S.oralis*, 39 h for *V.dispar* and 39 h for *A.denticolens*, data not shown).

In order to evaluate whether spectral differences based on metabolic changes and growth phase can have an influence on the calibration datasets, PCA was performed. The goal of PCA analysis was to determine whether the described changes in the spectral profiles were significant enough to generate spectra changes. This would imply that growth phases need to be taken into account resulting in growth phase dependent calibration sets.

Analyzing the PCA score plots of each species, PC1 and PC2 *F.nucleatum* and *P.nigrescens* explain 72.4 % of the variance of the data while the score plot for *S.mutans* shows 70.5 %, *A.naeslundii* shows 61.5 % of the variance and *V.dispar* explaining the lowest variance of data with 53.3 %. Overall, none of the species analyzed show a clear clustering at one time point that can be visually separated from any other time points. Only spectra at 96 h for *A.naeslundii* shows a dense region but cannot be identified as a cluster because of overlap with spectra from other time points appear as well.

For the growth phases of planktonic bacteria it can be concluded that spectra used for the evaluation and the resulting PCA analyses at different time points do not show significant differences. For all five evaluated species, spectra after 24h show different signal counts but not significant enough to have an effect on the PCA. Spectra after 48 h, 72 h and 96 h remain very similar. For setting up the calibration database, samples after 72 h were selected for two reasons: 1. Biofilms grown in ‘Zürich model’ were cultivated over a similar time period and 2. they align with the majority of the analyzed spectra at different time points (48 h and 96 h).

### 4.1.3 Influence of sample preparation on the Raman spectra

Nocker et al. (2012) previously showed that air-drying has an effect on the viability of bacteria cells. Additionally, Li et al. (2019) demonstrated that changes in the Raman spectra appear based on their viability, indicating that the influence of the state of the analyzed bacteria on Raman spectra need to be evaluated. An advantage of Raman spectroscopy is that water is not showing specific peaks within the spectrum, unlike techniques such as FT-IR. This potentially allows the use of Raman spectroscopy for bacterial and biofilm detection in liquid media or hydrated biofilms. In order to confirm this theory, dehydrated and hydrated samples (sample preparation described in Chapter 3.2.1) were compared and are shown in Figure 24 including PCA analysis for each species of interest. Mean spectra with standard deviation are shown.

Indeed, the presence of water doesn’t have an effect on the spectra in the ‘fingerprint region.’ Therefore, the spectra between the hydrated and dehydrated state do not show additional or missing peaks. Major peaks remain present for both states. However, areas show differences in the height of peaks, albeit minor. When visually investigating spectra it can be concluded that both datasets show increased standard deviations in some areas and therefore the variance within the datasets are increased. While the variance in peaks are small for all the major peaks, increased variance appears in the area between  $1000 - 1250 \text{ cm}^{-1}$ . Because these height differences are present both in the growth phase and hydration studies, it may be possible that these height differences do not impact the datasets.

In order to evaluate whether the effect of a liquid environment could have an influence on the calibration datasets, spectra were compared similarly to the growth phase analysis. When analyzing the PCA score plots of each species (hydrated vs. dehydrated spectra), PC1 and PC2 show less variance of data as for the growth phase study thus indicating a bigger variance of the spectra. Nonetheless, *A.naeslundii* shows 58 % of variance of the dataset, *F.nucleatum* 61.8 %, *P.nigrescens* 54.1 %, *S.mutans* 67.8 % and *V.dispar* 43%. *P.nigrescens* is the only species

## RESULTS

---

that shows two dense areas of data points of either hydrated or dehydrated samples within the score plot (dehydrated sample data points predominantly in the first and second quadrant, dehydrated sample data points predominantly in the first and second quadrant), while overlaps of the other four species do not allow any differentiation. Nevertheless, for *P.nigrescens*, there is no clearly defined cluster also indicating that the state of samples has no significant influence on spectral peaks.

These results demonstrate that differences between recorded spectra in a dehydrated and hydrated state, resulting from an air-drying process, are not significant in Raman spectra. Nevertheless, all sample acquisitions were done on dehydrated samples, due to easier handling procedures.

# RESULTS

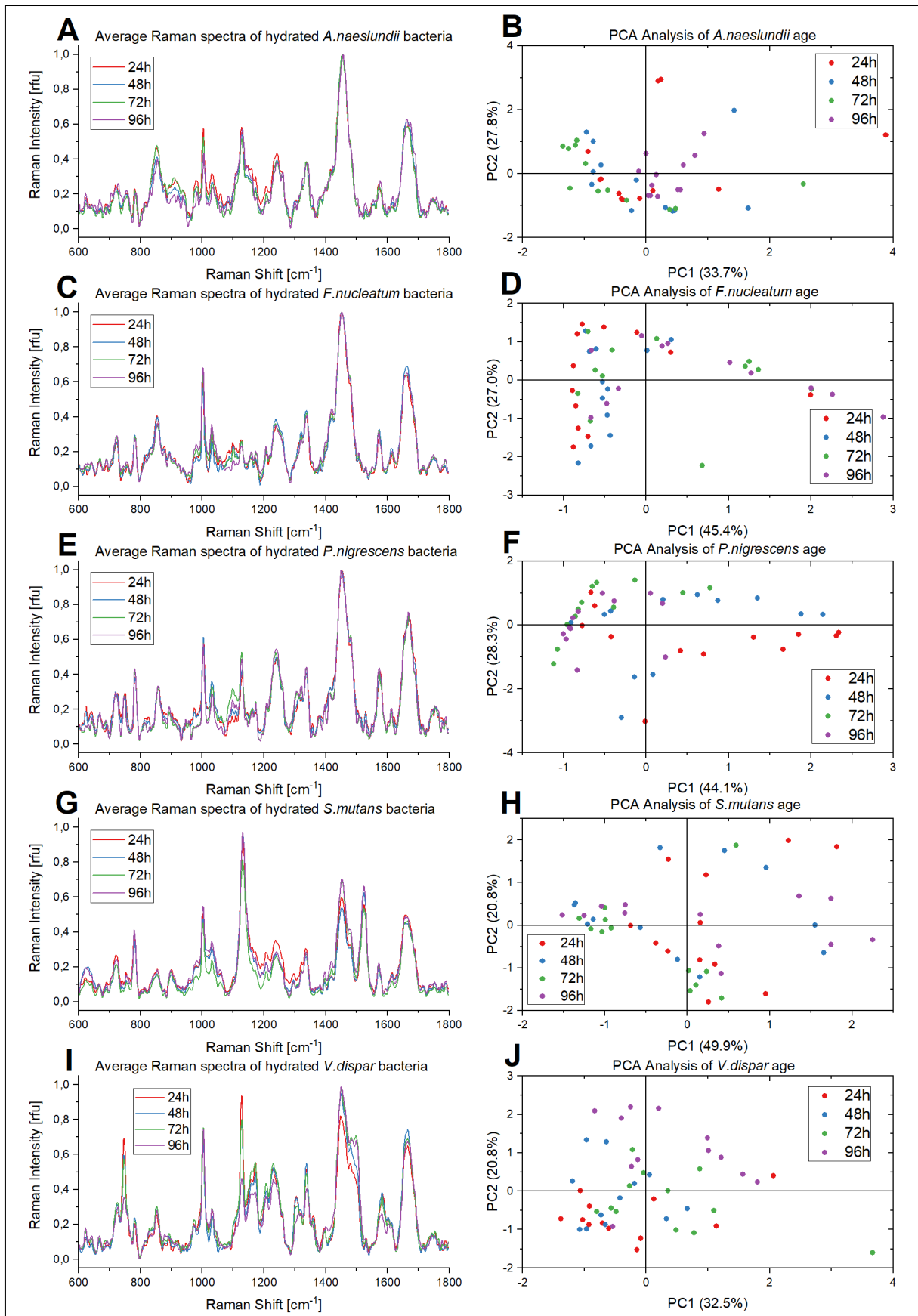


Figure 23: Average spectra for five different species at four different growth phases (24h in red, 48h in blue, 72h in green, 96h in purple) (A, C, E, G, I) and their PCA analysis of recorded spectra accordingly (B, D, F, H, J).



## RESULTS

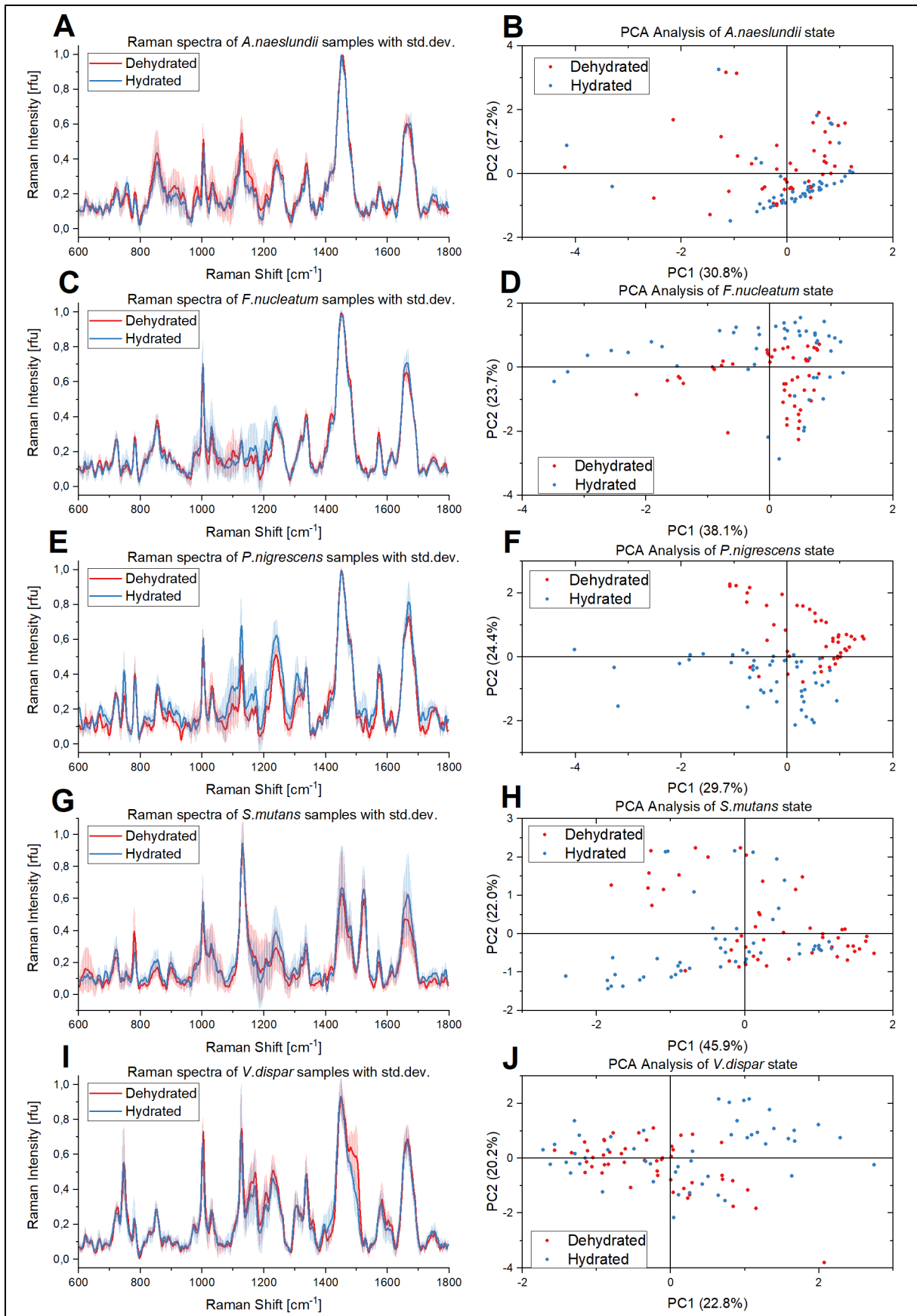


Figure 24: Average spectra for five different species in a hydrated and dehydrated state including the standard deviation (blue = hydrated, red = dehydrated) (A, C, E, G, I) and their PCA analysis of recorded spectra accordingly (B, D, F, H, J).

#### 4.1.4 Multivariate analysis of species

Within this thesis, two different multivariate models, O2PLS-DA and PCA, were used and applied depending on the questions that had to be answered. Both methods had their advantages and disadvantages. PCA, for example, considers all spectra in a dataset equally and maps spectra in a score plot based on differences to each other without pre-grouping. While the method works well for samples with well-defined boundary conditions, they have limited success with the analysis and differentiation of large datasets with many variables and groups that are similar. This may reduce the predictability for models. PCA showed good results for the differentiation of datasets containing two groups of species (Almarashi et al., 2012; Colniță et al., 2017; Samek et al., 2015). Instead, PLS models have pre-defined groups with the purpose of maximizing separation of group clusters within a score plot based on variables of interest. At the same time, some applications do not require a maximized separation, but rather, a differentiation of a dataset without the pre-grouping of the Raman spectra of selected bacterial species.

When considering the differentiation of five different subgingival oral species in this work (*A.naeslundii*, *F.nucleatum*, *S.mutans*, *P.nigrescens* and *V.dispar*), the same dataset was used for both multivariate models to determine which method allowed for the best differentiation and therefore species assignment to new spectra. Score plot results for PCA analysis and O2PLS-DA analysis are shown in Figure 25. Parts of the multivariate analysis were published before (Kriem et al., 2020).

Figure 25A shows score plots of the two greatest variations (PC1 and PC2) in the datasets and were plotted as X and Y using PCA as the multivariate method. According to the first two PCs, dense areas of spectra can be seen. Except for *A.naeslundii*, all species clusters were spread over at least two quadrants. Due to the overlaps of spectra, no clear clusters could be identified but tendencies can be seen. Clusters are spread more over the whole score plot, not allowing for clear differentiation. Since variance of samples are based on the variables of all species, it indicates that spectral differences are not major, resulting in an inconclusive score plot and incomplete separation of the score plots. *A.naeslundii*, *S.mutans* and *V.dispar*, however, shows the best separation in the five species score plot (Figure 25A, first row) and for that reason, were also considered independently in a PCA analysis of these three species (Figure 25A, second row) to attempt to improve separation of the three selected species in the score plot.

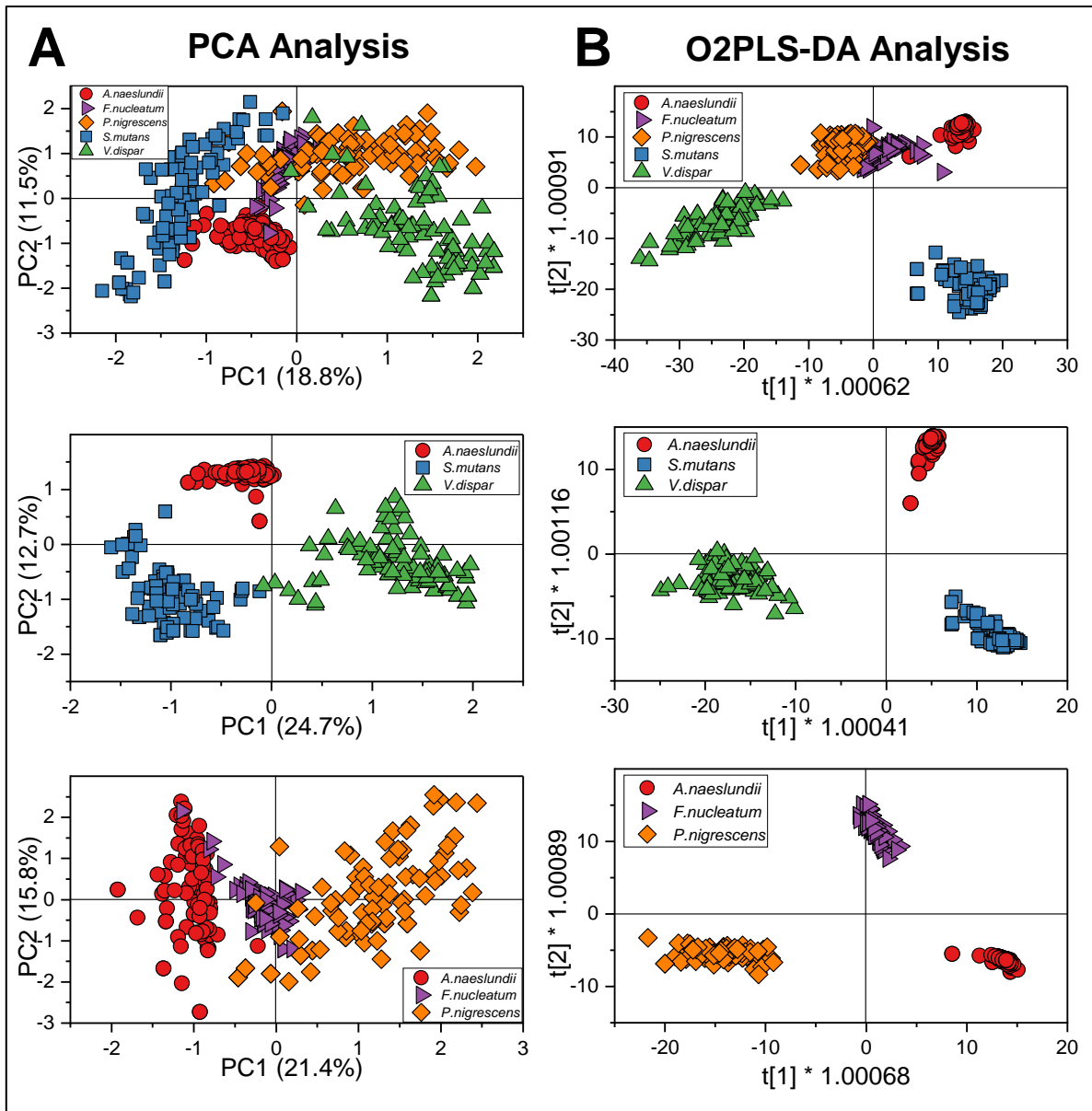


Figure 25: Multivariate analysis of selected oral bacteria show the distribution of the same set of spectra (84 spectral samples for each strain) for A. PCA Analysis and B. O2PLS-DA Analysis that have been both used in this work. First row: T-score plot of five species: *A.naeslundii* (red circles), *S.mutans* (blue square), *V.dispar* (green triangle), *F.nucleatum* (purple triangle) and *P.nigrescens* (orange diamond). Second Row: T-score plot of three species that showed clusters in the five species score plot: *A.naeslundii* (red circles), *S.mutans* (blue square) and *V.dispar* (green triangle). Third row: T-score plot of three species that didn't show clear cluster differentiation in the five species score plot: *A.naeslundii* (red circles), *F.nucleatum* (purple triangle) and *P.nigrescens* (orange diamond).

When analyzing the three species model, PCA analysis allows sufficient analytical evidence for the differentiation and clustering of the three species in the score plot. Therefore, these three species can be differentiated due to sufficient peak characteristics that are species-specific. When looking at *A.naeslundii*, *F.nucleatum* and *P.nigrescens*, which show substantial overlap in the five species analysis, the three species model separation still remains partial. Clusters are still spread over multiple quadrants with overlapping areas of spectra from the three species. It

## RESULTS

---

can be concluded that PCA analysis is not able to differentiate these three species, because their peak features are too similar. Additionally, the spectra for *P.nigrescens* show big variances. Spectra are spread across three quadrants, being the main reason why the species cannot be differentiated. PCA of datasets containing spectra of four species were not considered in this thesis.

Figure 25B shows T-score plots of different scenarios using the two greatest variations in the datasets and plotted as X and Y using O2PLS-DA as the multivariate method of five species. Based on the O2PLS-DA algorithm, every data point shown represents a Raman spectra and also contains information of all measured species. Based on the selection of the two greatest variances, three clearly distinct clusters can be identified, as well as one cluster showing an overlap of all three species (*A.naeslundii*, *F.nucleatum* and *P.nigrescens*). Spectra for *V.dispar* can be found exclusively in the third quadrant while *S.mutans* are found in the fourth. Looking at the third cluster, *P.nigrescens* is found only in the second quadrant and *A.naeslundii* in the first quadrant. Only *F.nucleatum* shows distributions in two quadrants (first and second). Since variance of samples are based on the average of a specific dataset, Figure 25B, first row uses all five species to build the averages. This process results in the insufficient separation of *A.naeslundii*, *F.nucleatum* and *P.nigrescens*, because their calculated variances, and therefore their Raman spectra are too similar.

In order to further analyze the available datasets, some species have been excluded from the multivariate analysis to determine whether this allows separation the same way as for the PCA analysis. The second row of Figure 25B uses *A.naeslundii*, *S.mutans* and *V.dispar* for analysis. These three species previously showed strong differentiation within the five species model. For that reason, it is no surprise that the calculated variances also shows three clearly separated clusters.

The third row focused on the three species that previously showed overlaps in the five species model. The O2PLS-DA T-score plot of the three species was generated from the three species (*A.naeslundii*, *F.nucleatum* and *P.nigrescens*) that could not be differentiated in the initial five species T-score plot. By solely using an O2PLS-DA model for the three species, it was possible to clearly discriminate species. This analysis employs the average of the spectra of *A.naeslundii*, *F.nucleatum* and *P.nigrescens* (pre-defined cluster) for the calculation of variation. This change allows the separation of species due to the recalculation of averages based on the available data. Because data from *S.mutans* and *V.dispar* are omitted here, the average are more defined and separated because the model doesn't have to consider data from the other two species. While

spreading of the data points remains similar to the other three species model and less compared to the five species model, it can be concluded that O2PLS-DA was able to differentiate the three species (*A.denticolens*, *S.oralis*, *V.dispar*) in this multivariate setup (Kriem et al., 2020).

Comparing the two selected multivariate analysis methods they were both successful in differentiating *A.naeslundii*, *S.mutans* and *V.dispar* in a model exclusively considering these three species. Due to the nature of the model, O2PLS-DA shows increased separation compared to PCA because of the underlying mathematical calculation and O2PLS-DA using the maximum separation of clusters based on a supervised approach. The differentiation of *A.naeslundii*, *F.nucleatum* and *P.nigrescens* was only successful when using O2PLS-DA.

Overall, when looking at the five species models, separation and differentiation of species is more present for O2PLS-DA rather than PCA. This is due to dense clusters because O2PLS-DA achieves separation when species data is used separately (see Figure 25B second and third row). In conclusion, for the analysis and prediction of multiple species O2PLS-DA should be the model of choice. When using a two-step approach, unknown species spectra should be able to be classified correctly. If a prediction of a species is inconclusive in the five species model because the spectra falls into the overlapping area of *A.naeslundii*, *F.nucleatum* and *P.nigrescens*, the specific three species model should then be able to predict species correctly. This approach however is not possible when using PCA modelling (Kriem et al., 2020).

For simplicity and the proof-of-concept design, the three species consisting of *A.naeslundii*, *S.mutans* and *V.dispar* were used for prediction of species because peak characteristics of the species were unique enough to be differentiated using both models. Additionally, O2PLS-DA was selected for the prediction of species in a planktonic and biofilm state due to the dense and well separated clusters in the dataset model.

### **4.1.5 Identification of bacteria with Raman**

In order to test the robustness of the O2PLS-DA multivariate analysis using Raman spectra for bacteria differentiation model, the calibration datasets consisting of *A.naeslundii*, *S.mutans* and *V.dispar* was selected (each species dataset consisting of 84 spectra). These datasets were then used to predict species for which new sets of spectra were generated (36 spectra for planktonic bacteria samples and 30 spectra for mono-species biofilm spectra). Two sets of predictive analyses were carried out using this training data method: 1. predict the identity of planktonically grown organisms and 2. predict the identity of biofilm grown organisms.

## RESULTS

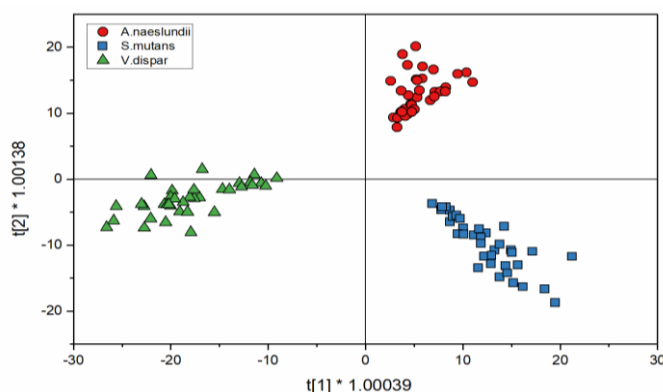


Figure 26: O2PLS-DA analysis of planktonic cell spectra for three species shows the distribution of spectra (36 spectra for each strain) after discriminant analysis in a 2D sphere; *A.naeslundii* (red circles), *S.mutans* (blue squares) and *V.dispar* (green triangle).

Figure 26 shows the score plot for spectra from unknown planktonic bacteria cells for three species when analyzed with O2PLS-DA. The distribution in each of the quadrants is the same as the calibration spectra (Figure 25B), but the spectra are more spread in the score plot indicating a larger variance between the spectra. After the spectra were collected for prediction, they were compared to the model that has been set up with calibration spectra (Figure 25B, second row) for cross validation. Table 15 shows the comparison of predicting planktonic cells using the O2PLS-DA model. The diagonal, bold values show the spectra that agree with the calibration spectra while the other values represent the errors of classification. Here, none of the spectra were misclassified by the model, resulting in a prediction accuracy of 100% for a total of 36 spectra for each strain (Kriem et al., 2020). This demonstrated that the developed model is able to successfully differentiate planktonic subgingival oral bacteria based on their chemometric Raman spectra.

Table 15: Comparison of the performance of species identification using the O2PLS-DA model for planktonic cells. The columns indicate the known/calibration species; the rows indicate the prevalence of predicted species using the O2PLS-DA model of the known/calibrated species spectra.

	Known Species		
	<i>A.naeslundii</i>	<i>S.mutans</i>	<i>V.dispar</i>
Predicted			
<i>A.naeslundii</i>	<b>36 (100%)</b>	0	0
<i>S.mutans</i>	0	<b>36 (100%)</b>	0
<i>V.dispar</i>	0	0	<b>36 (100%)</b>
Total Successful Prediction:	108 (100%)		

In a second step, the same calibration set was tested to determine whether it also allows the prediction of species grown as mono-species biofilms. Figure 27 shows the score plot for mono-species biofilm cell spectra for three species (30 spectra for each strain) when analyzed with O2PLS-DA. The distribution into quadrants is the same as for the calibration spectra. In Figure

## RESULTS

27, the *V.dispar* cluster was distributed between the second and third quadrant. In comparison to the O2PLS-DA plot from the planktonic spectra (Figure 26), clusters are more defined and closer together, indicating less variance between the individual spectra of each species dataset. For the prediction of species, spectra were also compared to the model that was set up with calibration spectra consisting of spectra from planktonic bacteria (Figure 25B, second row) for cross validation of the model. Table 16 shows the comparison of predicting mono-species biofilm cells using the O2PLS-DA model generated from planktonic bacteria. The training set of data enabled the correct identification of more than 76% of *S.mutans*, more than 90% of *V.dispar* and 100% of *A.naeslundii* (Kriem et al., 2020). In summary, the model was still able to predict 90% of all spectra in the dataset successfully with *A.naeslundii* showing the best prediction rate and *S.mutans* showing the least prediction rate.

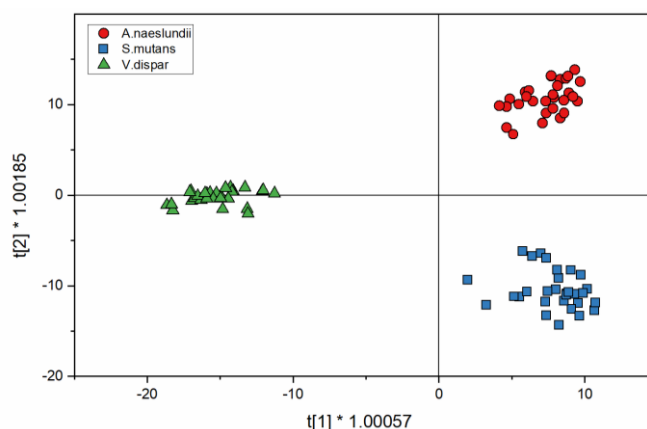


Figure 27: O2PLS-DA analysis of mono-species biofilm spectra (30 spectra for each strain) for three species shows the distribution of spectra after discriminant analysis in a 2D sphere; *A.naeslundii* (red circles), *S.mutans* (blue squares) and *V.dispar* (green triangle).

Table 16: Comparison of the performance of species identification using the O2PLS-DA model for mono-species biofilm spectra. The columns indicate the known/calibration species; the rows indicate the prevalence of predicted species using the O2PLS-DA model of the known/calibrated species spectra.

	Known Species		
	<i>A.naeslundii</i>	<i>S.mutans</i>	<i>V.dispar</i>
Predicted			
<i>A.naeslundii</i>	<b>30 (100%)</b>	0	0
<i>S.mutans</i>	2 (6.6%)	<b>23 (76.7%)</b>	5 (16.7%)
<i>V.dispar</i>	0	2 (6.7%)	<b>28 (93.3%)</b>
Total Successful Prediction:	81 (90%)		

In summary, the prediction of species for both oral planktonic and mono-species biofilm spectra demonstrated that acquired Raman spectra can be used to differentiate species based on their chemometric profile.

## 4.2 Analysis of biofilm structure

The next step was the use of multivariate analysis models based on Raman spectra in the differentiation of multi-species biofilms. Biofilms consisting of two bacterial species were generated and a workflow for mapping biofilms based on Raman spectra was developed. *A.denticolens* and *S.oralis* are seen as key players in the initial formation of subgingival biofilms (early colonizers) (Ammann et al., 2013; Kolenbrander and London, 1993). The analysis of biofilm structures with Raman mapping was therefore performed with these two species. Since hydroxyapatite surfaces, imitating a tooth surface, showed large Raman peaks in the ‘fingerprint region’ of bacterial samples (Chapter 8.5.2 in the Appendix) they were replaced by borosilicate glass to reduce background noise.

The biofilms were analyzed using FISH and CLSM as a control. A qualitative characterization of dual-species biofilms was performed (see Chapter 3.2.4 for the methods used) and is shown in Figure 28 as a stack of 16 individual images (individual images before the stack are found in Chapter 8.7 in the Appendix). Biofilms were stained with two species-specific oligonucleotides (6-FAM for *S.oralis* and Cy3 for *A.denticolens*) according to the protocol described in Chapter 3.2.4. A quantification of species distribution was not performed in this work. Figure 28 shows an exemplary image of a total of 15 analyzed samples with similar distribution patterns.

The CLSM image shows that dual-species biofilms were formed successfully using the modified ‘Zürich model’. Because labeled oligonucleotides were designed for the staining of bacterial RNA and DNA, they were able to stain the whole cell. Due to that characteristic it was possible to correlate morphology of bacterial cells with staining by FISH with *S.oralis* being cocci shaped (green stain) and *A.denticolens* being rod shaped (red stain) (Figure 28).

*S.oralis* (green color) was more prevalent in the biofilm than *A.denticolens* (red color). Distribution patterns in the biofilm also showed cluster formation in areas that were predominantly *S.oralis* and other areas that were predominantly *A.denticolens*. Due to the layering of multiple images, some areas appear in a yellow/orange color. These yellow/orange colors range from having both bacterial species present in the same point but in different layers and can mostly be observed in transition areas of two clusters (Kriem et al., 2021). These areas can be especially interesting for the mapping of dual-species biofilms and can be the source of possible artefacts due to both species being present at a specific location.



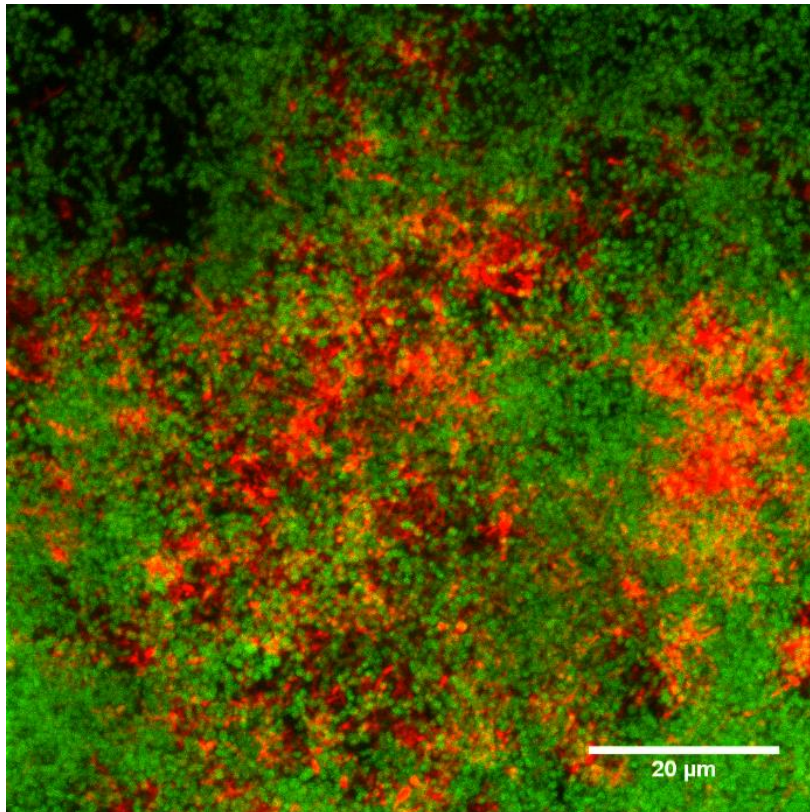


Figure 28: CLSM image of the FISH-stained dual-species biofilm. 16 individual images with a z-step size of 1.018  $\mu\text{m}$  of the biofilm stained with species-specific 16S rRNA FISH probes for *S.oralis* (MIT447, green) and *A.denticolens* (ACT476, red) were overlaid to one image using ImageJ. The 16 individual images before they were combined to a Z-stack are found in Chapter 8.7 (Appendix).

### 4.3 Model development for spatial mapping of biofilms

It has been demonstrated that CRM is able to differentiate oral subgingival species based on their chemometric profile (Chapter 4.1). In a second step this information was used to establish a workflow and multivariate model for two-dimensional mapping of bacteria in a dual-species biofilm which includes the acquisition and processing steps necessary before modelling as described in Chapter 3.3.1. This first approach serves as a proof-of-concept design for the evaluation of biofilms using Raman spectra. While this work only focuses on subgingival biofilms and biofilms composed of *C.albicans* and *P.aeruginosa*, this workflow can be applied to mapping of biofilms of interest in general, when species specific calibration datasets are available.

In order to perform biofilm mapping using Raman spectra, a Renishaw inVia™ Qontor was used due to the higher sensitivity of the instrument (see Chapter 3.1.1). Since Raman spectra from complex samples like microorganisms are instrument specific to some extent, new calibration datasets had to be generated to develop a model for the spatial differentiation of bacteria in a biofilm.

## RESULTS

For the differentiation and mapping of biofilms using CRM with the Renishaw inVia™ Qontor CA was used. O2PLS-DA and PCA are both modelling methods without the consideration of area dimensions of the collected data and cannot be applied for the mapping of Raman spectra. To develop a method for spatial mapping of biofilms, different datasets, samples, and analysis technologies were used to confirm: 1. species clustering in the *in-vitro* grown subgingival dual-species biofilm model 2. the use of a multivariate analysis model for spatial differentiation of bacteria and 3. the use of chemometric information from Raman spectra collected from *in-vitro* dual-species biofilm models to achieve two-dimensional mapping. This analysis was compared to-state-of-the-art methods like FISH/CLSM and morphology of samples. An overview of the different calibration datasets, analyzed samples and the technologies used for the workflow is shown in Figure 29.

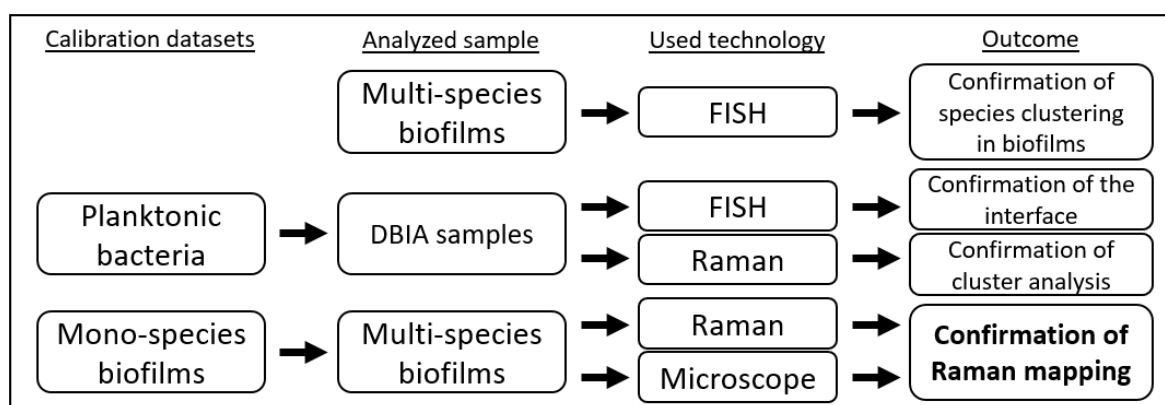


Figure 29: Experimental design setup for the differentiation and confirmation of Raman mapping in a dual-species biofilm model.

### 4.3.1 Calibration of planktonic bacteria and mono-species biofilms using Renishaw inVia™ Qontor

In a first step, calibration datasets were acquired for three species (*A.denticolens*, *S.oralis* and *V.dispar*). *S.oralis* and *V.dispar* are both cocci shaped and therefore, morphological differentiation is difficult. For the proof-of-concept, their shape makes it difficult to compare morphology and Raman maps. As seen in Figure 4B and C, *Streptococcus sp.* and *Actinomyces sp.* make up the majority of species present while *Veillonella sp.* are only present in small concentrations. Additionally, Figure 42 suggests that *Streptococcus sp.* and *Actinomyces sp.* have the highest concentration when grown *in-vitro* with the ‘Zürich model’, making up more than 97% of the total cell count. Because *Streptococcus spp.* play a key role in the early colonization of a surface and also have high concentrations in a subgingival biofilm, *S.oralis* (cocci shaped) was selected together with *A.denticolens* (rod shaped) for the analysis of dual-species biofilms while *V.dispar* was not used further for the proof-of-concept experiments.

## RESULTS

Calibration datasets were generated for the two organisms, *S.oralis* and *A.denticolens* to enable accurate mapping using Raman spectra. The two calibration datasets were created from mono-species biofilms and planktonic bacteria for *A.denticolens* and *S.oralis*. The confirmation of the CA as the multivariate model of choice required the use of planktonic bacteria to identify species for DBIA samples. Even though differences between biofilm and planktonic bacteria spectra are only minor, they may still be sufficient to give inconclusive results for the CA and should not be used interchangeably (see Figure 30C and F).

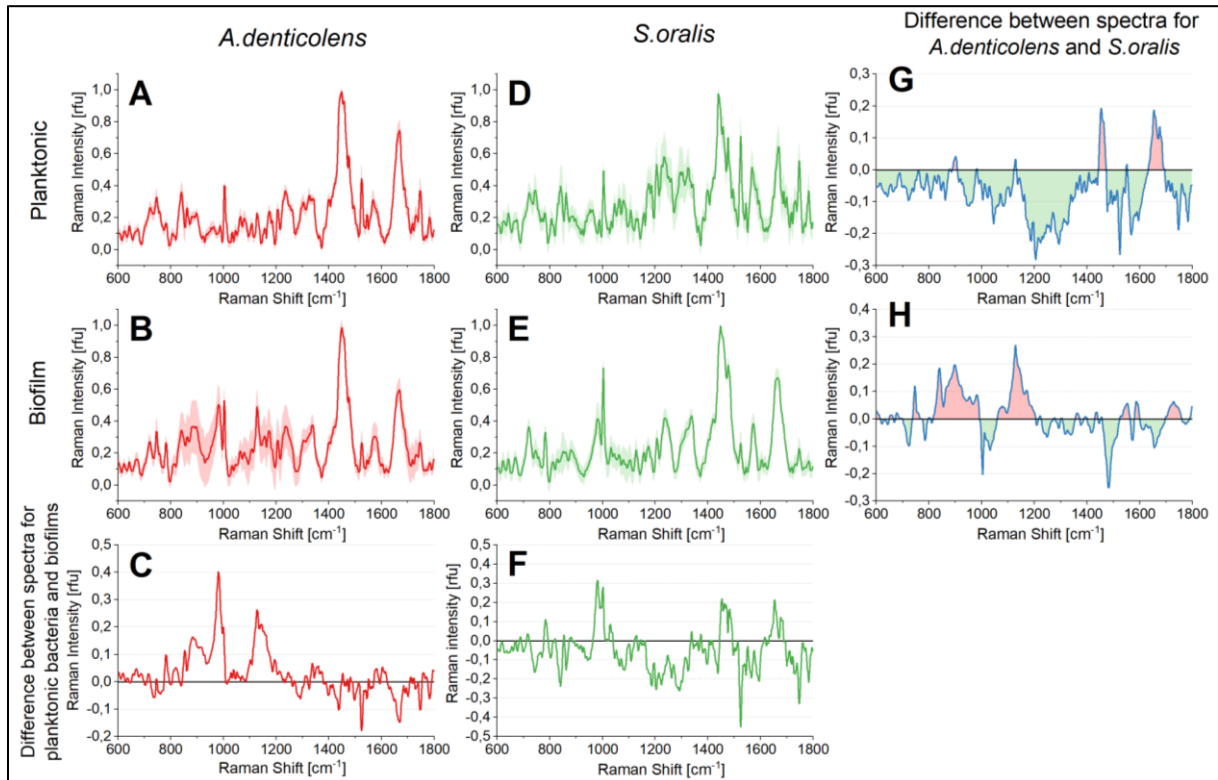


Figure 30: Averaged processed Raman signals (300 spectra for each dataset) before Savitsky-Golay differentiation for *S.oralis* and *A.denticolens* and their standard deviations. (A) and (B) shows the spectra for *A.denticolens* with (A) for planktonic bacteria and (B) for mono-species biofilms. (C) shows the spectral difference between planktonic bacteria and mono-species biofilm spectra. A negative number indicates a higher count in the planktonic spectra while a positive count indicates a higher count in the biofilm spectra (D) and (E) shows the spectra for *S.oralis* with (D) for planktonic bacteria and (E) for mono-species biofilms. (F) shows the spectral difference between planktonic bacteria and mono-species biofilm spectra. A negative number indicates a higher count in the planktonic spectra while a positive count indicates a higher count in the biofilm spectra. (G) and (H) shows the spectral difference between *A.denticolens* and *S.oralis* for (G) planktonic bacteria and (H) mono-species biofilms. Negative numbers indicate a higher count for *S.oralis* spectra while positive counts indicate higher counts *A.denticolens*.

Spectra of *A.denticolens* and *S.oralis* were analyzed using CRM as described in Materials and Methods. Figure 30 shows the plots of averaged Raman spectra with 300 spectra acquired per strain and either as planktonic or biofilm bacteria with the Renishaw inVia™ Qontor. In comparison to the dataset acquisition described in previous chapters, the number of spectra in

## RESULTS

---

the dataset have been increased to reduce the variance and increase the robustness of the dataset as suggested by Guo (2018). This should improve predictability of species in biofilm settings. Reference databases in previous works demonstrated that it is possible to identify dominant chemical signature patterns in microorganisms that can be found and differentiated in a Raman spectra (De Gelder et al., 2007; Kumar et al., 2016; Sil et al., 2017) as data already showed in Chapter 4.1.1. As for the data generated with the ThermoFisher DXRxi instrument (Chapter 4.1), major common peaks in microbiological samples such as Amide I and Amide III, which can be identified at  $\sim 1250\text{ cm}^{-1}$  (Amide III) and  $\sim 1660\text{ cm}^{-1}$  (Amide I), were also found using the Renishaw inVia™ Qontor. Amino acids can be seen at multiple wavenumbers. In this study, oral bacteria mostly identified as Phenylalanine and are seen at  $\sim 1000\text{ cm}^{-1}$  and C-N and C-C stretches (specific for proteins) at  $\sim 1125\text{ cm}^{-1}$ . Additionally, the presence of lipids can be seen as  $\text{CH}_2$  deformations at  $\sim 1450\text{ cm}^{-1}$ . These described peak patterns were found across both oral bacteria species in planktonic and biofilm conditions (Figure 30).

*A.denticolens* only showed small peak differences between planktonic and biofilm bacteria. The biggest differences appeared at  $\sim 982\text{ cm}^{-1}$  (Polysaccharides) and  $\sim 1129\text{ cm}^{-1}$  (C-N, C-C stretch Protein) (Figure 30C) with an increase in counts for the mono-species biofilm spectra. *S.oralis* however showed a change of peaks in multiple regions, with an increase of counts at  $\sim 982\text{ cm}^{-1}$  (Polysaccharides),  $\sim 1003\text{ cm}^{-1}$  (phenylalanine) and  $\sim 1452\text{ cm}^{-1}$  (C-H<sub>2</sub> deformation) while there is a reduction of signal counts predominantly between  $900\text{ cm}^{-1}$  to  $1350\text{ cm}^{-1}$  and at  $\sim 1524\text{ cm}^{-1}$  (C=C stretch) and  $\sim 1746\text{ cm}^{-1}$  (C=O stretch) (Figure 30F).

The differences observed, however, were not due to the presence or absence of peaks, but mostly, the height and signal counts of these peaks (Figure 30C and F). This indicates an up or down regulation of processes within the cell due to the planktonic or biofilm growth phase. This was also seen when comparing species. Most peaks are present for both *A.denticolens* and *S.oralis*, while heights of these peaks differ. No reoccurring pattern of height increases or decreases of certain peaks can be identified for planktonic and biofilm bacteria when comparing *A.denticolens* and *S.oralis*. Overall, considering the absolute differences between the two species of planktonic bacteria and mono-species biofilm spectra, the differences typically ranged between 0 to 0.2 on a normalized scale between  $600 - 1800\text{ cm}^{-1}$  with few peaks showing differences greater than 0.2 (Figure 30G and H) (Kriem et al., 2021). This indicates that *A.denticolens* and *S.oralis* show similar chemical compositions with differences in counts of peaks. These differences may, however, be substantial enough to be differentiated statistically.

## RESULTS

---

As seen in the spectral differences between the two species in Figure 30G, the amount of peak differences of up to about 0.3 allows the use of planktonic bacteria for DBIA samples. Especially the counts throughout the spectra between 600 – 1800  $\text{cm}^{-1}$  for *S.oralis* are increased (seen by the negative numbers) while only three peaks show significant higher counts for *A.denticolens* ( $\sim 1454 \text{ cm}^{-1}$ ,  $\sim 1654 \text{ cm}^{-1}$ ,  $\sim 1678 \text{ cm}^{-1}$ ). Using DBIA samples is well suited to validate differentiation of bacteria using CRM in biofilms on a system where the investigated areas are already defined.

The same assumption can be made for the use of mono-species biofilm bacteria for differentiation in a dual-species biofilm then because several peaks show differences as seen in Figure 30H. Here, counts larger than 0.1 on a normalized scale are increased for *A.denticolens* mono-species biofilm spectra at  $\sim 747 \text{ cm}^{-1}$ ,  $\sim 840 \text{ cm}^{-1}$ ,  $\sim 901 \text{ cm}^{-1}$  and  $\sim 1130 \text{ cm}^{-1}$  when compared to *S.oralis* mono-species biofilm spectra. On the other hand, spectral counts are increased for *S.oralis* at  $\sim 1003 \text{ cm}^{-1}$ ,  $\sim 1033 \text{ cm}^{-1}$ ,  $\sim 1482 \text{ cm}^{-1}$ ,  $\sim 1656 \text{ cm}^{-1}$ . Hence, there are different peaks in *A.denticolens* and *S.oralis* mono-species biofilm spectra allowing differentiation.

Showing visual spectral changes based on presence, absence and height of spectral peaks is not sufficient enough to analyze biofilm identities in depth. In order to evaluate the spectra generated for the calibration datasets, statistical analyses were performed to demonstrate that the collected Raman spectra are: 1. able to be used for the differentiation in general and 2. able to be used for mapping.

### 4.3.2 Multivariate analysis of calibration datasets

In order show that bacterial spectra for *A.denticolens* and *S.oralis* can be used for differentiation, PCA analysis was performed on the collected and processed Raman data (individual processing steps are described in Chapter 3.3.1) for both planktonic and mono-species biofilm spectra (Figure 31). PCA was selected as the statistical analysis of choice because it works well for systems that only considers two groups.

Figure 31 shows the score plots of the first two principal components (PC1 and PC2). From the visual inspection of the score plots, it can be concluded that the chemometric profile of *A.denticolens* and *S.oralis* could be used to differentiate the two species in both conditions. For planktonic bacteria spectra the two PCs explained 41.7% (the summary of both PCs) of the overall variance present in the dataset (Figure 31A), while only 26.2% of the variance of the mono-species biofilms was explained (Figure 31B). The PCA analysis demonstrated that two

## RESULTS

distinguishing clusters were shown, allowing a cluster analysis for the distribution analysis of multi-species biofilms.

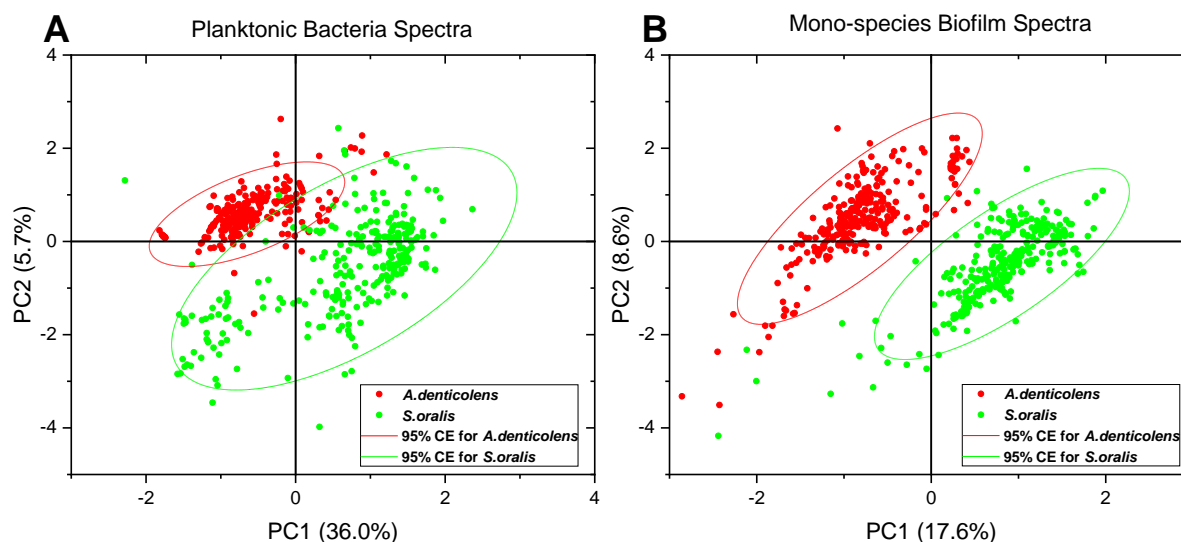


Figure 31: PCA Analysis of selected oral bacteria show the distribution of the 2nd order derivative of spectra (300 spectral samples for each strain) in a score plot. *A.denticolens* is marked in red while *S.oralis* is marked in green. A) Score plot for planktonic bacteria spectra with a 95% confidence ellipse. B) Score plot for mono-species biofilm spectra with a 95% confidence ellipse.

Planktonic *S.oralis* showed a larger variance in the dataset, resulting in a broader spreading of data points within the cluster, while spectra clusters for *A.denticolens* were more narrow. High variance can additionally be seen in the size of the confidence ellipse (CE). Due to the size of the CE for planktonic *S.oralis* bacteria, increased variance is present in the calibration dataset. This is represented by the spread of data points over three quadrants. Additionally, the distribution of spectra also displays one larger group of spectra and one smaller group, thus indicating variation in the dataset within the spectra groups. Nevertheless, a clear difference between the two clusters can be determined (Figure 31A) and allows for the use in the differentiation of bacteria for DBIA samples.

PCA analysis of the mono-species biofilm samples show stronger differentiation of the groups. Even though less variance is described by the two PCs in biofilm conditions with 26.2 %, the clusters show more defined separation of the species. Additionally, both clusters visually show a similar CE size, suggesting that the variance of the spectra within the clusters is comparable (Figure 31B) (Kriem et al., 2021). Moreover, the clusters are uniformly spread without multiple groups within the cluster suggesting sufficient confidence for the application in referencing bacteria in biofilm mapping experiments.

### 4.3.3 Evaluation of mapping analysis model

One key element of this work is the evaluation whether Raman spectra can be used for the analysis and differentiation of bacteria within a biofilm consisting of different bacterial species. In order to implement the gathered information from previous chapters, it is now necessary to connect these results with methods that are able to link Raman spectra to the locations in which the spectra were taken and put it in relation to other spectra. Previous research (Harz et al., 2005; Kniggendorf et al., 2011) displayed a convincing potential of CA for the differentiation of bacteria in multi-species biofilms and was thus evaluated in this thesis. Details of the method can be found in Chapter 3.3.2 and 3.3.3.

After demonstrating that the generated datasets, derived from *S.oralis* and *A.denticolens*, allow differentiation of the species (Chapter 4.3.2), the next step was to select an appropriate analysis model to demonstrate spatial differentiation based on chemometric profiles acquired by CRM. To this day, there is no method available that allows the growth of mono-species biofilms on one specific surface with a spatial separation of less than 10  $\mu\text{m}$  (which is needed for successful CRM acquisitions). In order to be able to validate the selected multivariate method, mapping of known species in a defined area is necessary. As evaluated previously, the spectra of planktonic bacteria may be used for the analysis because they show similar chemometric features to biofilm grown bacteria (Chapter 4.3.1). Planktonic bacteria allow easier sample handling and the preparation of an artificial interface of known species necessary to evaluate the performance of the method. Sample preparation is described in detail in Chapter 3.2.1. Using this method allows for the manual construction of a 'biofilm-like' structure where species and their location are known and a spatial separation of less than 10  $\mu\text{m}$  is possible. The used samples were hence labeled as DBIA samples to show a clear distinction between biofilm samples and manually constructed 'biofilm-like' structures.

By using cocci (*S.oralis*) and rod shaped (*A.denticolens*) bacteria for the validation of the method, the shape of bacteria can be used to validate mapping results from CRM with morphology. To further add to the comparison of species, FISH/CLSM, the standard method for subgingival biofilm mapping, was also used to verify the mapping (see Chapter 4.2). Due to the nature of the method and sample preparation, FISH/CLSM analysis is not possible to be performed on the same sample area as for CRM and morphology. Hence, two samples from the same batch of experiments were used for the evaluation. Details on the sample preparation are described in Chapter 3.2.2.



## RESULTS

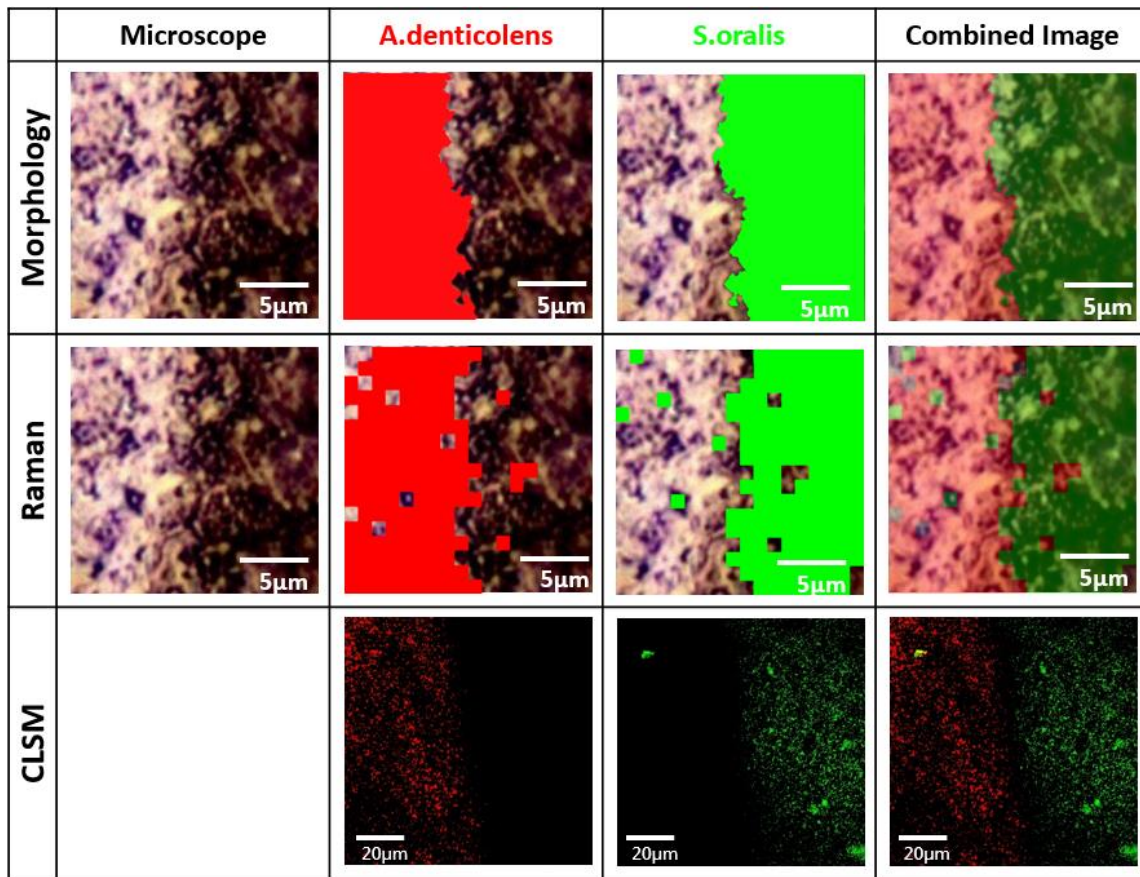


Figure 32: Distribution of *A.denticolens* and *S.oralis* in a DBIA sample. Morphological and Raman analysis was performed using the identical random area in a sample. Morphological analysis was done using ImageJ. Raman analysis was performed using cluster analysis with WiRE 5.2. FISH analysis was performed on a new sample from the same experimental batch the image of one layer is shown.

Raman distribution images from CA were compared to morphological distribution and FISH distribution in Figure 32. Overall, all three images show two clusters of distribution in the transition area between *A.denticolens* and *S.oralis* while some methods were more successful in differentiating than others. Morphology images showed a defined edge between the two areas. Separation details are more clear in morphology analysis because of its ability to differentiate small areas ( $<1 \mu\text{m}$ ) better than Raman mapping. CLSM is able to reach similar results but due to the limitation of the instrument (available objectives) a close analysis of a zoomed view was not possible.

FISH/CLSM confirmed morphology imaging by indicating the same edge. It needs to be noted, however, that FISH imaging was taken over an image area of  $100 \mu\text{m} \times 100 \mu\text{m}$  (due to the instrument limitations and availability of objectives) while Raman and morphology imaging was done over an image area of  $18 \mu\text{m} \times 18 \mu\text{m}$ . In this example, FISH/CLSM was successfully used to analyze larger areas with reduced resolution. It also showed a clear interface between



the two bacteria species, therefore confirming what can be seen in detail for the morphology analysis.

Raman imaging also showed a similar biofilm boundary as determined by morphology analysis. Due to the technical limitation of the Raman imaging process (1  $\mu\text{m}$  steps), the edge at the transition area is not as specifically assigned, as in morphology imaging. Additionally, some areas that were defined as *A.denticolens* in the morphology image have been classified as *S.oralis* (five 1  $\mu\text{m}^2$  points) in the Raman images and vice versa (five 1  $\mu\text{m}^2$  points) while eight 1  $\mu\text{m}^2$  points were unable to be classified as either bacteria. When compared to all acquired points (324 point in total), these misidentified points only make up a total of 5.56 % and can therefore be seen as minimal.

Overall, visually all three images demonstrate a clear boundary between the two species. When comparing all three mapping methods, it can be concluded that CA was confirmed as a method for distribution evaluation of multi-species biofilms using spectral Raman mapping based on the analysis using DBIA samples (Kriem et al., 2021). Besides the test of different variations of CA as described in Chapter 3.3.3, CA was the only method tested for biofilm mapping using Raman spectra.

### **4.3.4 Mapping of dual-species biofilms**

The previous chapter showed that bacteria can be differentiated using DBIA samples in a 'biofilm-like' setting with planktonic bacteria as a calibration dataset. This demonstrated the possible applicability of CA for the analysis of biofilms. In order to confirm the results from the DBIA analysis in Chapter 4.3.3, CA was now applied to *in-vitro* dual-species biofilms using mono-species biofilm spectra as the calibration dataset. The map acquisition of dual-species was done according to procedures described in Chapter 3.2.2. For the analysis and validation of the use of Raman distribution mapping, 15 random areas (18  $\mu\text{m}$  x 18  $\mu\text{m}$ ) of 15 *in-vitro* biofilm clustered bacteria samples were selected and analyzed based on their morphology and Raman spectra in combination with CA. Here, the same settings and approach was used as in Chapter 4.3.3 that were determined in Chapter 3.3.3. The spatial distribution of *A.denticolens* and *S.oralis* in dual-species biofilms are demonstrated in Figure 33. Additionally, spatial maps from morphology and Raman spectra analysis are compared with each other and shown as layer images.

## RESULTS

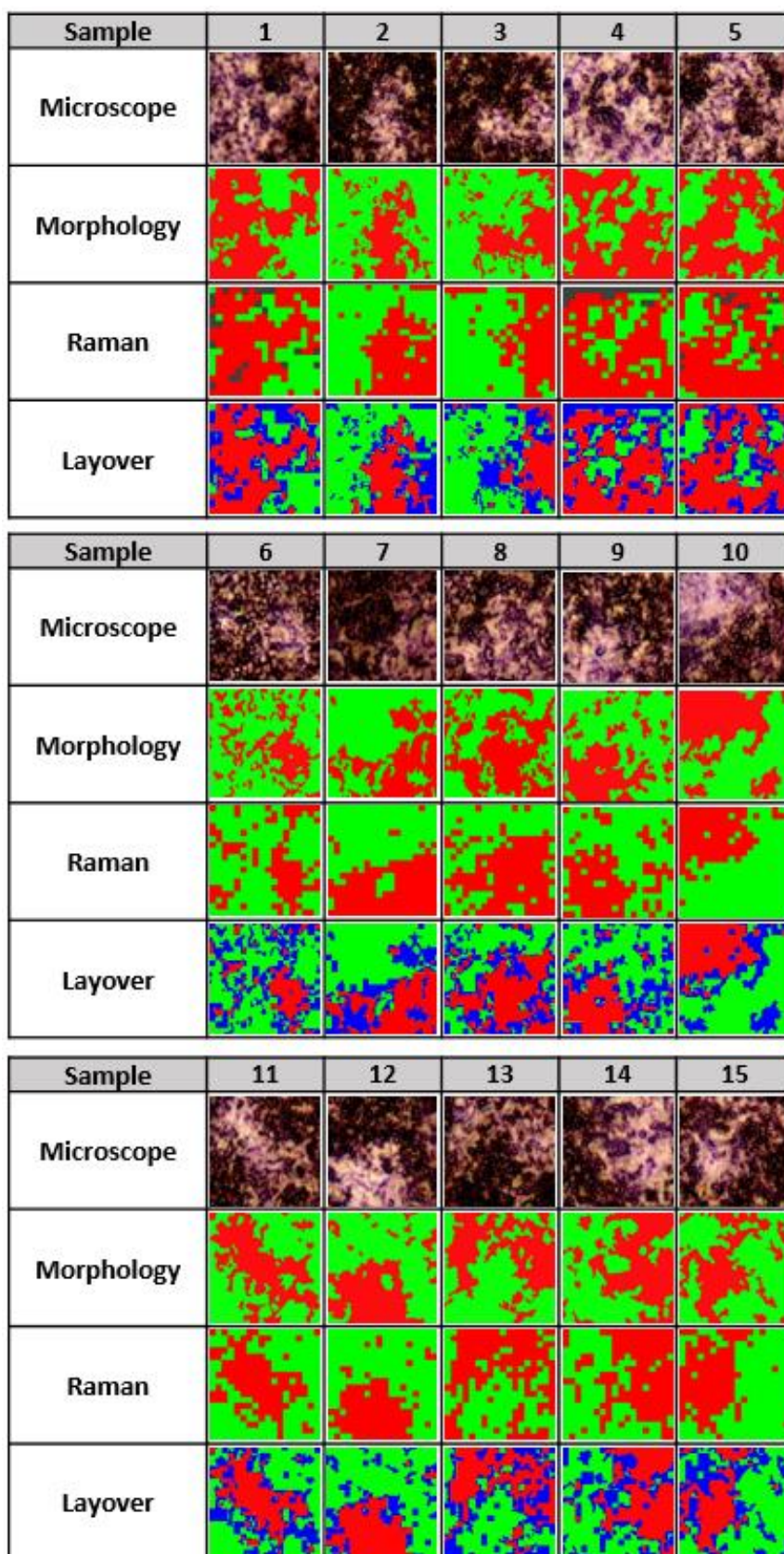


Figure 33: Distribution of *A.denticolens* (red areas) and *S.oralis* (green areas) in 15 dual-species biofilms. Image window is  $18\ \mu\text{m} \times 18\ \mu\text{m}$ . Morphological and Raman analysis was performed using the identical random area in a sample. Morphological analysis was done using MorphoLibJ in ImageJ. Raman analysis was performed using PCA based cluster analysis with WiRE 5.2. Grey areas show unidentified areas. Morphology and Raman images were layovered to show areas that were not classified as the same species and were labeled blue (values in Chapter 8.8 of the Appendix).

## RESULTS

---

The analysis of bacteria based on their morphology using MorphoLibJ in ImageJ generated detailed information and enabled detection and differentiation of individual organisms within a biofilm. Especially small clusters with low amounts of bacteria are detected here. Additionally, morphology analysis confirms clusters identified using FISH/CLSM that was already shown in Figure 28.

Unlike morphology, CA using Raman spectra was not always able to make a distinct classification of bacteria for some sample areas. If Raman spectra were unable to be classified as either *S.oralis* or *A.denticolens*, the specific areas were color coded in grey. Each acquired Raman spectra accounts for an area of  $1 \mu\text{m}^2$ . The number of squares that are not accounted to one species are counted and put into relation to the total analyzed area of  $324 \mu\text{m}^2$ . Inability to classify bacteria based on their Raman spectra can be seen in samples 1, 4 and 5 totaling for  $23 \mu\text{m}^2$ ,  $23 \mu\text{m}^2$ ,  $17 \mu\text{m}^2$  or 6.98%, 6.76% and 3.18% of total analyzed area per sample respectively (see the distribution based on Raman; all coverage values are shown in Chapter 8.8 of the Appendix). The other 12 samples showed 100% classification of either *A.denticolens* or *S.oralis*.

To further evaluate the bacteria assignment, centroid spectra of the clusters from CA were compared to the mono-species biofilm calibration spectra created previously (Figure 30B and E). Depending on the assignment, clusters were then colored in either red (for *A.denticolens*) or green (for *S.oralis*). Comparing location of clusters from Raman and CA with morphology showed, that the assigned clusters were similar, thus also confirming results from Figure 28.

In order to validate the clustering from Raman spectra, the maps were compared to morphology analysis. The morphology maps were generated over the same area, and layover images were created (Layover images in Figure 33). Here, areas that we classified as identical bacterial species remained in their code color (red for *A.denticolens* and green for *S.oralis*). Areas that were classified as *A.denticolens* by morphology and *S.oralis* by Raman spectra and vice versa were labeled in a blue color in the layover image (also see Chapter 3.3.3 for further details on labeling).

When looking at the layover images in Figure 33 all major clusters have been identified correctly in all 15 analyzed samples. Grey areas in the Raman images in samples 1, 4 and 5 were classified as incorrect cluster assignment. Additionally, CA missed the detection and assignment of small clusters and individual bacteria. Besides the insufficient classification of small clusters, transition areas of two clusters also show increased misclassification (Kriem et

## RESULTS

al., 2021). The calculated relative total coverage distribution of each sample and mapping type are shown in Figure 34 (see Chapter 8.8 (Appendix) for values).

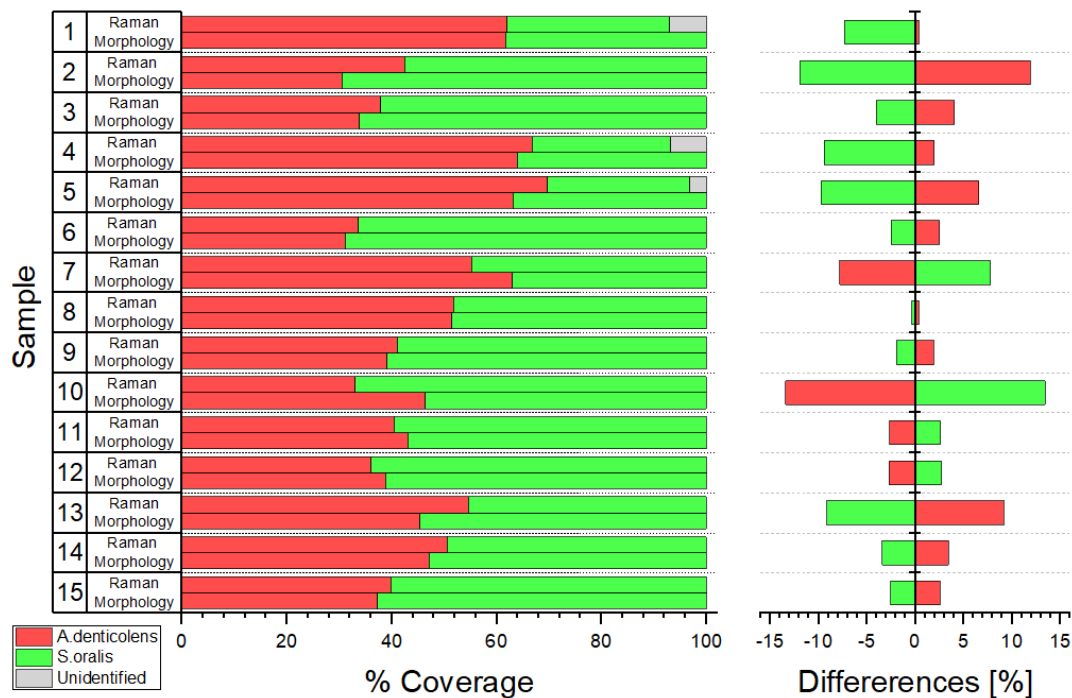


Figure 34: Coverage distribution was calculated from samples shown in Figure 33 for morphology and Raman analysis using ImageJ. Percent difference of total coverage between the two analysis methods was compared considering morphology analysis as the true distribution. Negative values in differences indicate reduced identification of the species in Raman analysis compared to morphology analysis while a positive value indicates increased identification. Specific values are found in Chapter 8.8 of the Appendix.

When looking at the coverage of the two bacteria in the selected areas, they agree well with each other. Highest differences appear for sample 10 with 13.42% incorrect identification and as low as 0.35% in sample 8. On average, the difference of classification between morphology and Raman analysis for *A.denticolens* was 4.75% and for *S.oralis* 5.93% (average difference derives from unidentified areas that were also identified by Raman analysis). There is no trend whether *A.denticolens* or *S.oralis* were over-identified in Raman samples compared to morphological analysis. Eleven samples showed an over-identification of *A.denticolens* while four samples showed an over-identification of *S.oralis* when compared to morphology analysis (Kriem et al., 2021).

Blue areas of the layover images range between 17.66% (sample 12) and 31.54% (sample 4) with an averaged area of 26.71% (see Figure 33). Blue areas are equivalent to the results that are indicated in Chapter 8.8 (Appendix) as different classification of morphology vs. Raman. While Figure 34 shows the overall total relative quantities of the two species from the evaluated area, it lacks the evaluation how well the areas from optical microscopy and CRM agree with

## RESULTS

each other. Thus, Figure 35 looks at the agreement of identified areas as seen in the layover maps in Figure 33 over two dimensions. As a result, areas that were identified differently and labeled in blue color, to show the differences between the two mapping methods related to the 2D dimension, were quantified (for details how the evaluation was done, see Chapter 3.3.3).

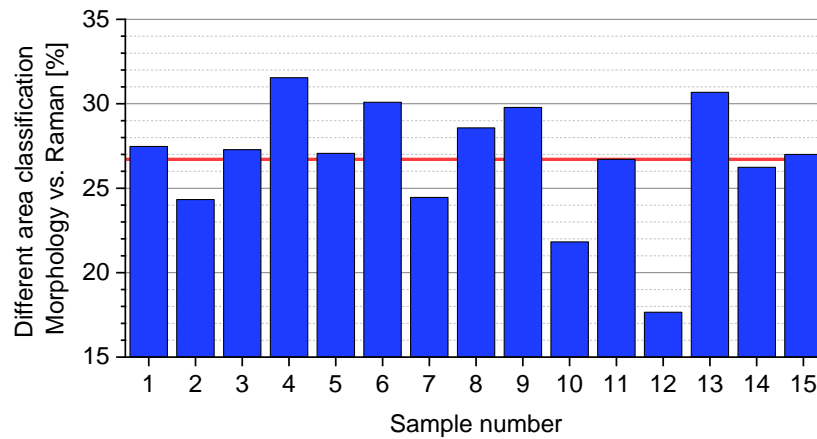


*Figure 35: Specific Coverage distribution based on the blue areas in Figure 33 that were calculated based on the specific differences at each location using ImageJ. The red line indicates the average difference of the 15 samples with 26.71 %.*

This shows that while overall relative total distributions of bacteria in biofilms using Raman mapping are comparable to morphology mapping (Figure 34), the dimensional differences of the two mapping methods related to the 2D dimensions are larger in distribution as seen in Figure 35. Here, sample 4 shows the highest dimensional differences of 31.55 % while sample 12 shows the lowest dimensional differences with 17.66%. The average dimensional difference for all 15 analyzed samples was 26.71 %.

### 4.3.5 Comparison of different mapping technologies to CRM

After successfully demonstrating that subgingival dual-species biofilms can be differentiated using CRM, the method was compared to other mapping technologies that are commonly used for the analysis of biofilm architecture and are summarized in Table 17. This analysis showed that: 1. compared to the other methods, CRM mapping allows the continuous analysis of biofilm mapping of one specific spot and 2. analysis is possible when the biofilm sample is in a hydrated state. Particularly the non-destructive nature of the methods is a key advantage. Conversely, low resolution doesn't allow for a detailed analysis, especially when only small areas are of interest. Additionally, because the method relies on the chemometric profile of bacteria, changes in the profile due to changing environmental conditions may result in failure of correct classification. Because the other methods are not dependent on the chemometric information of

## RESULTS

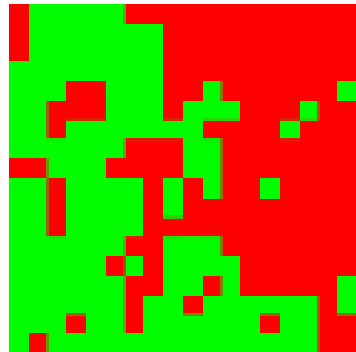
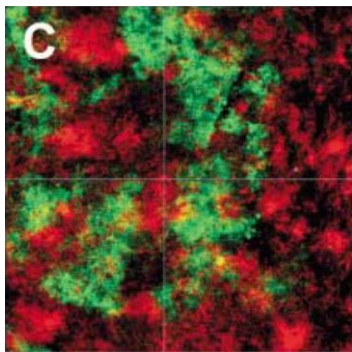
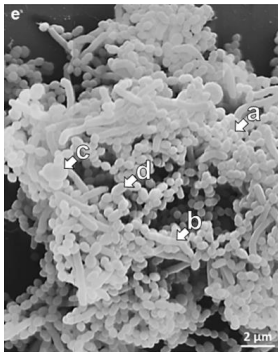
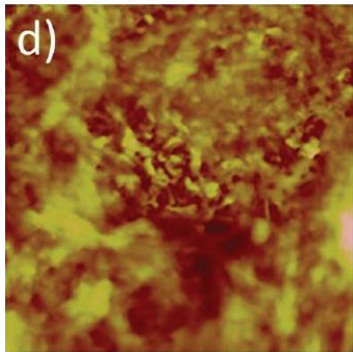
---

a biofilm this has not proven to be problematic for the other mapping techniques. The comparison of methods to CRM are further discussed in Chapter 5.3.



## RESULTS

Table 17: Comparison of relevant imaging techniques that consider the mapping of multi-species biofilms. Results from this work are compared to data that have been previously published.

Technology	Confocal Raman Microscopy	Confocal Laser Scanning Microscopy and Fluorescent <i>in-situ</i> hybridization CLSM/FISH	Scanning Electron Microscopy	Atomic Force Microscopy
Acronym	CRM	CLSM/FISH	SEM	AFM
Reference	This work	(Guggenheim et al., 2004)	(Kommerein et al., 2017)	(James et al., 2016)
Organisms	<i>A.denticolens</i> , <i>S.oralis</i>	<i>F.nucleatum</i> , <i>S.oralis</i>	<i>S.oralis</i> , <i>A.naeslundii</i> , <i>V.dispar</i> , <i>P.gingivalis</i>	Unknown species
Images from the named references				
Image size	18 $\mu\text{m}$ x 18 $\mu\text{m}$	100 $\mu\text{m}$ x 100 $\mu\text{m}$	16 $\mu\text{m}$ x 20 $\mu\text{m}$	10 $\mu\text{m}^2$
Advantages	Continuous study of sample, measurement in hydrated state	Reconstruction of 3-D images, high specificity, differentiation of species with same morphology	High resolution imaging, good morphological differentiation	Continuous study of sample, reconstruction of 3-D images
Limitation	Low resolution, time consuming, chemometric profile dependent	Low axial resolution, limited laser penetration, complex sample preparation, no continuous study	Complex sample preparation, dehydrated samples only, prone to artefacts due to sample preparation	Small scanning area, sample damage, fragile probe, time consuming, visual differentiation difficult
Sample preparation and environment	No sample preparation	Cell lysis, fluorescence label	Destructive, conductive or gold/platinum coating of sample	No sample preparation

## 4.4 Application of the used model for other biofilms

Chapter 4.3 successfully demonstrated the use of acquired chemometric profiles by CRM for differentiation of bacteria in a dual-species biofilm. The developed workflow of 1. data acquisition 2. data processing and 3. spatial mapping coupled with multivariate analysis can be used as an alternative to other mapping technologies like FISH/CLSM. This method was implemented using oral biofilms. This workflow was transferred to another biofilm relevant for medical applications. *In-vitro* biofilm models consisting of *P.aeruginosa* and *C.albicans* also show pathogenicity in medical settings and in the oral cavity. With *P.aeruginosa* being a prokaryote and *C.albicans* being a eukaryote, this expands the analysis using CRM to biofilms with organisms of different kingdoms. The selected biofilm furthermore allows fast morphological differentiation (typical *P.aeruginosa* size: 2-4  $\mu\text{m}$ , typical *C.albicans* size: 4-10  $\mu\text{m}$ ). Cultivation methods were used based on techniques developed at Fraunhofer IGB and have been described in Purschke (2012).

### 4.4.1 Formation of calibration datasets for *C.albicans* and *P.aeruginosa*

In a first step, spectra from *C.albicans* and *P.aeruginosa* had to be collected for calibration datasets. A total of 300 mono-species biofilm spectra were acquired for each, *P.aeruginosa* and *C.albicans*. Both mono-species biofilms were cultivated under identical conditions. Averaged spectra are shown in Figure 36. Specific peak assignments for biochemical compounds are found in Chapter 8.5.3 in the Appendix.

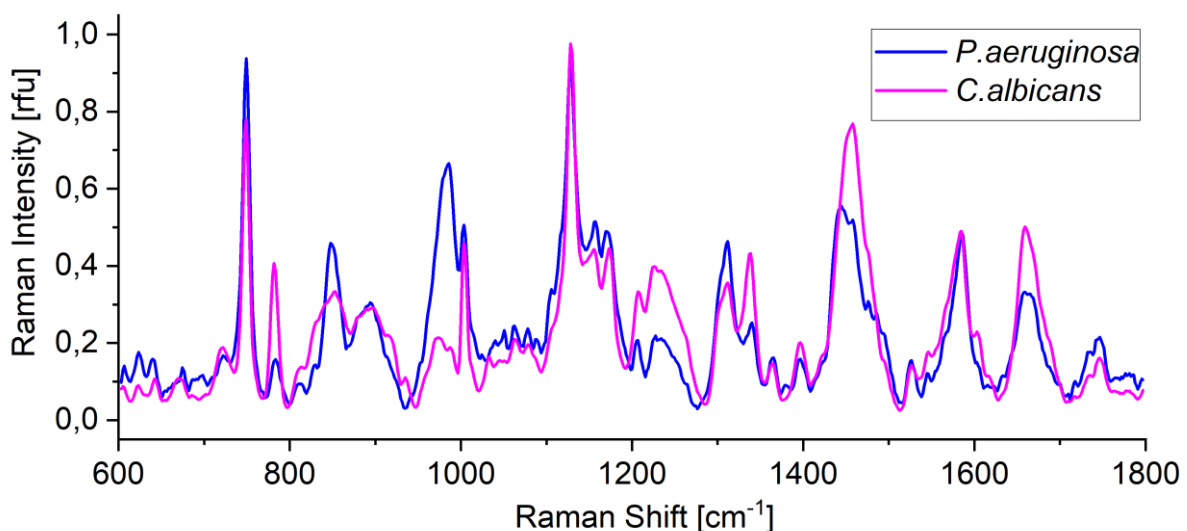


Figure 36: Averaged processed Raman signal (300 spectra total) for *P.aeruginosa* and *C.albicans* mono-species biofilms after processing without differentiation.



## RESULTS

When visually evaluating the biochemical assignments almost all peaks present for *P.aeruginosa* are also present for *C.albicans*. Specifically, Thymine peaks ( $749\text{ cm}^{-1}$ ), protein stretches ( $1128\text{ cm}^{-1}$ ),  $\text{COO}^-$  symmetric/ $\text{CH}_2$  asymmetric deformations ( $1397\text{ cm}^{-1}$ ) or Amide II peaks ( $1585\text{ cm}^{-1}$ ) are present at almost the same height. Nevertheless, there are many peaks that are present in both species where the heights or signal counts of the peaks are significantly different under the conditions used. In comparison, these height differences are more frequent and more prominent than the height differences seen between different oral bacterial species. Examples of these peaks can be seen for Cytosine ring breathing ( $\sim 782\text{ cm}^{-1}$ ), proteins ( $\sim 850\text{ cm}^{-1}$ ), polysaccharides ( $986\text{ cm}^{-1}$ ), tryptophane C-H<sub>2</sub> twist or Amide I peaks ( $1659\text{ cm}^{-1}$ ).

Overall, visual inspection of the chemometric profiles of the two organisms showed that peak differences present should allow for differentiation of these species based on Raman spectra. As shown for oral dual-species biofilms, CA was used for the mapping of the two species in a dual-species biofilm model (see Chapter 4.3.4). Multivariate analysis was performed using PCA as it was already used for the analysis of oral biofilms.

### 4.4.2 Multivariate analysis of biofilm calibration datasets

PCA analysis was used to demonstrate that processed mono-species biofilm Raman spectra of both species show significant spectral variances to be used for biofilm mapping (Figure 37).

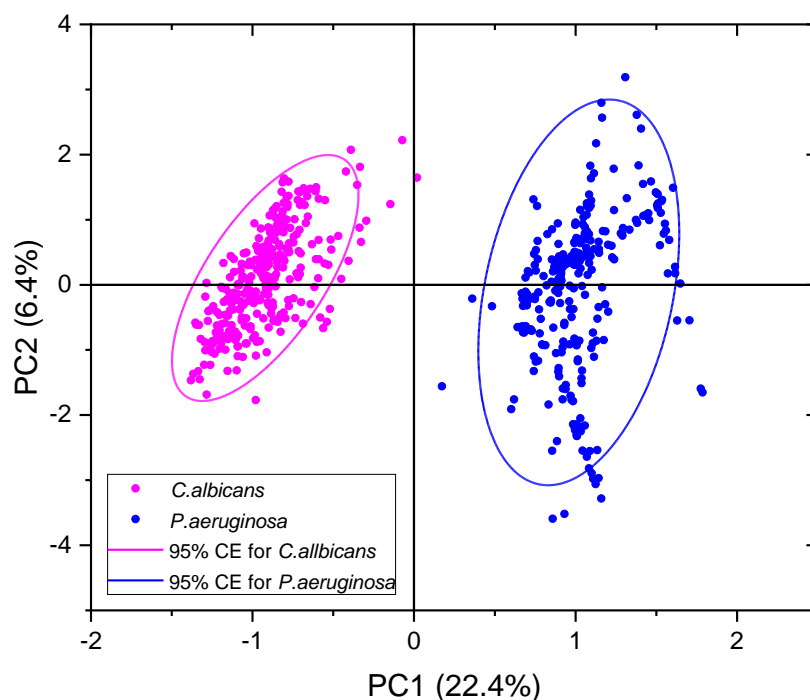


Figure 37: PCA Analysis in the form of a score plot of two selected medically relevant bacteria show the distribution of the 2nd order derivative of spectra from mono-species biofilms (300 spectral samples for each strain) in a score plot. *C.albicans* is marked in pink while *P.aeruginosa* is marked in blue. 95 % confidence ellipses are shown for both species.

Figure 37 shows the score plots of the first two principal components (PC1 and PC2). From the visual inspection of the score plots, it is evident that the chemometric profiles of *C.albicans* and *P.aeruginosa* show enough variance in the spectra to be clearly differentiated. The two PCs were able to explain 28.8% of the overall variance present in the dataset. When comparing the observed variance to the analysis of oral biofilms (Figure 31), this model was able to include slightly more variance whereas the difference of 1.6% between the two explained variances are minor. This means that for the evaluation of *C.albicans* and *P.aeruginosa* slightly more data point were used than for *A.denticolens* and *S.oralis*. The small differences indicate that similar amounts of the spectral areas were considered for PCA analysis, therefore additionally indicating that the areas with differing spectral features (*A.denticolens* vs. *S.oralis* and *C.albicans* vs. *P.aeruginosa*) are also comparable. However, it was not possible to determine, whether the same areas and peaks were used in the PCA model. The comparable variance of the two models confirms, that PCA can be used to evaluate whether selected species can be used for differentiation. For *C.albicans* and *P.aeruginosa*, the PCA analysis in Figure 37 shows two clearly separated clusters, providing a good basis for cluster analysis for the distribution analysis of multi-species biofilms, confirming the variance of peaks in spectra observed in Figure 36.

*P.aeruginosa* showed a larger variance in the dataset, resulting in a broader spreading of data points within the cluster, while spectra clusters for *C.albicans* were narrower. Increased variance within the individual datasets can additionally be seen in the size of the CE. The size of the CE for *P.aeruginosa*, indicates that variance is increased within the dataset compared to *C.albicans*.

#### 4.4.3 Mapping of dual-species biofilms

A total of five biofilms were cultivated according to the procedure described in Chapter 3.2.2. The map acquisition of dual-species was done according to procedures described in Chapter 3.1.1 with the difference that for *C.albicans* and *P.aeruginosa* biofilms an area of 35  $\mu\text{m}$  x 35  $\mu\text{m}$  was evaluated. 1.5  $\mu\text{m}$  scanning steps were chosen due to the large size differences between *C.albicans* (4-10  $\mu\text{m}$ ) and *P.aeruginosa* (2-4  $\mu\text{m}$ ). Figure 38 shows an exemplary image of the analyzed samples. To compare generated maps from Raman spectra coupled with CA, morphology differentiation was also analyzed using MorphoLibJ. The spatial distribution of *C.albicans* and *P.aeruginosa* in dual-species biofilms was demonstrated in Figure 38B for the morphological analysis and Figure 38D for the analysis based on Raman spectra. Due to the large size differences between the considered species, the analysis of bacteria based on their

## RESULTS

morphology shows very detailed information and is able to detect and differentiate individual organisms within the cultured biofilm.

In order to determine the bacteria and fungi assignment from the two clusters generated by CA, centroid spectra of the clusters were compared to the calibration spectra created previously (Figure 36). Depending on the assignment, clusters were then colored in either pink (for *C.albicans*) or blue (for *P.aeruginosa*) according to their cluster belonging. Figure 38 visualizes that some *C.albicans* cells were detected and, to some extent, were also represented as spherical shapes using CRM.

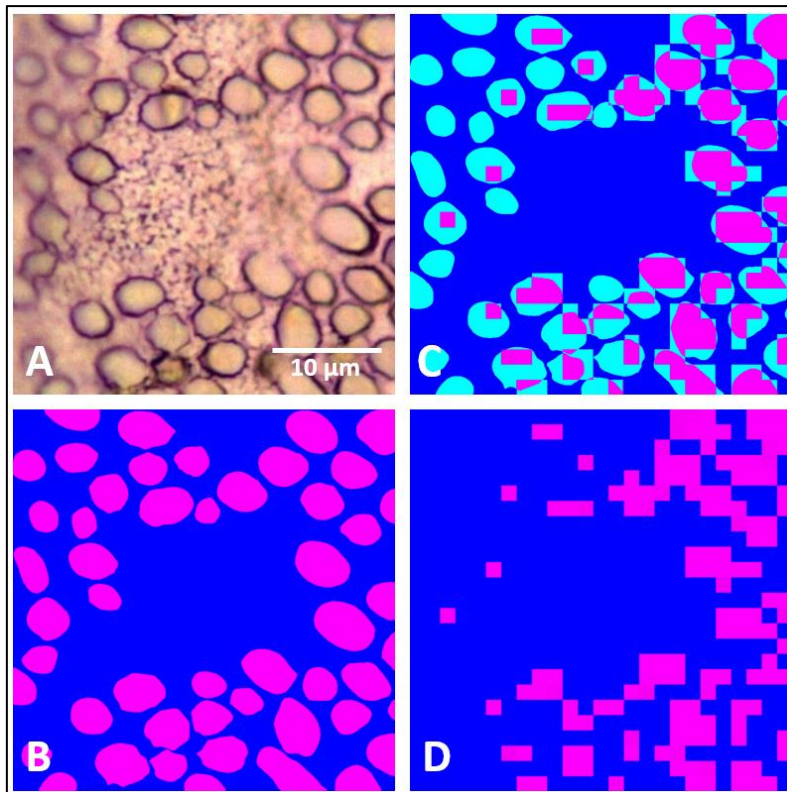


Figure 38: Distribution of *C.albicans* and *P.aeruginosa* in a biofilm. Image window is  $35\ \mu\text{m} \times 35\ \mu\text{m}$ . (A) Shows the microscopic image of the analyzed area. (B) Morphological and (D) Raman analysis was performed using the identical random area in a sample. Morphological analysis was done using ImageJ. Raman analysis was performed using PCA based cluster analysis with WiRE 5.4. Morphology and Raman images were layered (C) to show areas that were not classified as the same species and were labeled cyan.

After Raman spectra based mapping, the map was compared to morphology analysis. The maps were generated over the same area and a layover image was created (Figure 38C). Areas that were classified with the same species in Raman and morphology mapping remained in their specific color (pink for *C.albicans* and blue for *P.aeruginosa*). Areas that were classified as *C.albicans* by morphology and *P.aeruginosa* by Raman spectra and vice versa were labeled in a cyan color in the layover image.

## RESULTS

The overlay image shows that many *C.albicans* cells were detected and mapped by CRM, however, not all. Because Raman spectra were only taken every 1.5  $\mu\text{m}$ , it was also not possible to determine the complete shape of *C.albicans* from CRM spectra acquisition and CA due to the use of the area and scanning steps. This was already observed in the Raman mapping for oral dual-species biofilms (see Figure 33). Additionally, while all *C.albicans* structures were successfully identified on the right side of the image, most *C.albicans* organisms were not detected on the left side. These areas were instead identified as *P.aeruginosa*, thus resulting in misclassification. Morphological analysis determined these structures as *C.albicans*.

To further compare coverage distributions of bacteria and fungi, coverage ratios for morphology and Raman spectra analysis were compared with each other (Table 18). Additionally, areas of same as well as differing classifications between morphology and CRM were shown. When looking at the coverage of the two methods it can be seen that the results quantitatively agree with the visual analysis thus demonstrating that *C.albicans* coverage was lower in CRM than in morphology while coverage of *P.aeruginosa* was higher. In addition to the direct comparison of the two methods, the layered image (Figure 38C) shows 17.22 % of the same classification (for Raman and morphology analysis) for *C.albicans* and 58.24 % of *P.aeruginosa*. 24.54 % of the image was classified differently.

*Table 18: Quantitative results of bacterial and fungal coverage for the sample analyzed in Figure 38 (letter in brackets behind method technology indicates which image it is referred to in Figure 38). Values for the layered image shows the areas that were identified as the same organism by both methods and quantifies the cyan area of Figure 38 of differently classified species.*

Mapping Method	Classification of organism in %		Area of different classification Morphology vs. Raman in %
	<i>C.albicans</i>	<i>P.aeruginosa</i>	
<b>Morphology (B)</b>	37.79	62.21	-
<b>Raman (D)</b>	22.73	77.27	-
<b>Layover Image (C)</b>	17.22	58.24	24.54

Looking at the left side of the microscopic image in Figure 38A, the area is out of focus. Because of this, the focal point of the laser is not focused on the sample anymore, exciting surrounding areas of the identification point. The consequences of this out of focus acquisition may result in misclassification.

## 5 Discussion

Microbiological studies nowadays focus more and more on the research of biofilms. However, methods to study biofilms are scarce. Natural biofilms typically don't exist as single species biofilms, but are rather an assortment of different microbial species. Oral biofilms, specifically subgingival biofilms, represent a typical example of such biofilms consisting of multiple species. Because of their impact on oral health, oral biofilms have been studied intensively and vast progress has been made in understanding the metabolics and architecture of such biofilms, as outlined in Chapter 1. Nevertheless, there is little knowledge on the architecture analysis of biofilms over time using non-destructive techniques. In this thesis, CRM methods that lay the groundwork for the use of this technique for future biofilm growth studies were developed and were also applied to other medically relevant biofilms outside of the field of oral research. Throughout the progression of this project, it became apparent that in order to have a reproducible *in-vitro* biofilm model that allows the acquisition of consistent results, certain growth conditions and multivariate methods had to be optimized to be able to ensure analysis results.

### 5.1 CRM method development

The key element of this thesis was the development of Raman methods for mapping biofilms using CRM by first establishing a proof-of-concept approach using oral biofilms and then demonstrate the applicability of the approach on other medically relevant biofilms. In a first step, it was necessary to enable the differentiation of oral bacteria based on their spectral fingerprint peaks. Overall, the collected spectral data for the five species of interest all showed similar peaks in the fingerprint region and agree with the peak assignment shown in previous publications (Kumar et al., 2016; Sil et al., 2017; Tewes, 2019). The Raman spectra information for oral bacteria (Beier et al., 2012, 2011) showed strong agreement between *Streptococci* bacteria analyzed in this thesis and Beier (2011). This confirms that the used data collection procedures and resulting calibration datasets are reproducible between laboratories and able to identify species-specific peaks for oral bacteria. The same conclusion can be drawn when comparing *P.aeruginosa* and *C.albicans* to Jung et al. (2014) (for *P.aeruginosa*) and Maquelin et al. (2002) (for *C.albicans*).

As part of the evaluation process, the maturation and state of bacteria and biofilms were evaluated as well. Strola et al. (2014) demonstrated previously that chemical changes could be

## DISCUSSION

---

observed overtime. However, their analysis only considered growth spectra over a 10 h time window of planktonic bacteria (*E.coli* and *B.subtilis*), whereas this thesis looked at 96 h and oral bacteria as well as *C.albicans* and *P.aeruginosa*. Strola et al. (2014) were able to demonstrate that Raman spectra in the exponential growth phase of bacteria show some differences during growth. However, within the stationary growth phase the Raman spectra don't change anymore. Consequently, oral bacteria spectra recorded after 24h only show minor changes in the following recorded time steps, because the bacteria had already reached the stationary phase. However, in the PCA analysis, the differences between the exponential and static growth phases of oral bacteria weren't significant enough to generate separate clusters. This allows for the use of both data from exponentially growing cells as well as stationary growing cells as one calibration dataset. This additionally increases the robustness of the data because more time points were included in the dataset. For the matured biofilms that were analyzed in this work, the timely evaluation of change in Raman spectra in the initial biofilm growth phase within the first 24h (similar to Strola et al. (2014)) is not critical for this work. The differentiation on growth phases should, however, be evaluated in future research.

While the presence of water in a sample analyzed by CRM is not problematic for spectra interpretation (in contrast to FT-IR), chemical changes between a hydrated and dehydrated sample may still appear. For example, DNA conformation changes in *Lactobacillus rhamnosus* depending on their hydration stage were demonstrated previously by Myintzu Hlaing et al. (2017) and for that reason had to be considered in this thesis. Changes in the DNA backbone (especially the areas 1243–1223  $\text{cm}^{-1}$  and 1093–1084  $\text{cm}^{-1}$ ) can also be seen in all oral bacterial species similar to Myintzu Hlaing et al. (2017), but because the whole spectrum is used in this thesis these changes don't impact the overall analysis of the spectrum and thus did not result in a clear differentiation between hydrated and dehydrated samples in the PCA analysis.

In this work, it was demonstrated that statistically there are not sufficient differences between the growths phases and hydrated vs. dehydrated state of bacteria in terms of chemometric profile changes. Therefore, they were used as one uniform dataset. In fact, because minor changes in the chemometric profile are now included in the calibration dataset, they result in broader data clusters in multivariate analysis models and also increase the robustness of the dataset with regard to minor differences in the mapping data.

Comparisons of two multivariate analysis models that were used in combination with Raman spectra from oral bacteria showed good applicability in this thesis. In this work, PCA was used to answer questions that usually involved two different Raman datasets, while O2PLS-DA was

## DISCUSSION

---

used to answer questions that involved multiple datasets, requiring a more complex statistical model. CA, as a third multivariate analysis tool, was used for the multivariate dimensional mapping of dual-species biofilms because it is able to include the location where the spectra was taken, while the other two multivariate methods lack the ability to consider the location within a sample. Due to their similar genetic and metabolic characteristics, the chemical composition in a bacterial cell between the evaluated subgingival oral bacteria showed limited, but unique differences in their Raman spectra.

PCA as one multivariate analysis option was inconclusive when used for the differentiation of five species because of significant overlaps of the species clusters (Figure 25A, first row). When analyzing a three species model using spectra from *A.naeslundii*, *S.mutans* and *V.dispar* separation was achieved (Figure 25A, second row). For *A.naeslundii*, *F.nucleatum* and *P.nigrescens* a clear differentiation was not achieved using PCA even if only the three species are analyzed. *P.nigrescens* and *F.nucleatum* can be found within the same Socransky complex, indicating a close relationship. Consequently, they show substantial overlap in Raman spectra in the PCA analysis. Thus, PCA is unable to differentiate these three species (Figure 25A, third row).

By using O2PLS-DA, it was possible to distinguish several species. Similar results were obtained for *Uncaria* species in a different application as described in Feng et al. (2019) when O2PLS-DA was applied. Furthermore, it was possible to distinguish and predict *S.mutans* and *V.dispar* and *A.naeslundii* grown in suspension (Figure 26) and in mono-species biofilms (Figure 27) after establishing a calibration set of spectra generated from planktonically grown cells (Figure 25B, second row). As already observed for PCA analysis, the three species examined (*A.naeslundii*, *S.mutans* and *V.dispar*) were found to coincide within the different complex groups described by Socransky, indicating significant chemotypic differences between these species. When performing O2PLS-DA with three selected species from three different Socransky complexes, it was possible to reliably identify spectral differences enabling species differentiation (Figure 25B). Additionally, *A.naeslundii*, *S.mutans* and *V.dispar* could already be distinguished within the pool of five species (Figure 25A, first row). Thus, these three species were chosen for prediction of planktonic and mono-species biofilm cells. Unlike PCA, O2PLS-DA is further able to differentiate *A.naeslundii*, *P.nigrescens* and *F.nucleatum* when considered in a three species model (Figure 25A, third row) but was unable to do it in a five species model also including *S.oralis* and *V.dispar*.

## DISCUSSION

---

Both types of cells grown as planktonic cells and as biofilms cells (Socransky et al., 1998) could be identified and differentiated successfully using O2PLS-DA analysis. Comparing the prediction score plots for both, planktonic and biofilm spectra, it could be observed that the clusters generated from planktonic cells are more spread out while the clusters for biofilm spectra remain compact with little distribution in the plot. This could be the result of bigger variance in the planktonic cells, resulting in a higher variance in signals between spectra. This explains the broadening of the cluster. Biofilm spectra, on the other hand, show less variance, indicating that the collected mono-species biofilm cells have a more uniform appearance in Raman spectra which can be beneficial for the application as calibration datasets. This allows the use of calibration datasets from planktonic cells for the mapping analysis of DBIA samples (where planktonic cells were used for establishing an 'artificial' biofilm) and the use of calibration datasets from mono-species biofilm cells for the mapping analysis of dual-species biofilms.

*A.naeslundii*, *S.mutans* and *V.dispar* were able to be predicted with an accuracy of 100%, if grown planktonically using O2PLS-DA. For biofilm cells, an accuracy of 90% was achieved. As mentioned above, biofilm cells show changes in spectra if compared to planktonic cells. Thus, prediction of biofilm cells using data from planktonic cells for calibration might generate incorrect assignments due to these differences. The spectral changes between planktonic and mono-species biofilm spectra are demonstrated for *A.denticolens* and *S.oralis*. These species were used for the evaluation of mapping. Changing spectral profiles and peaks can also be expected for *A.naeslundii*, *S.mutans* and *V.dispar*. The reason for increased misclassification of biofilm cells might be the use of planktonic bacteria as the calibration dataset for the prediction of mono-species biofilms spectra. This indicates the need for a biofilm based dataset for calibration, in addition to the databases generated from planktonic cells, despite their high similarity. This was later considered for the mapping of dual-species biofilms. The change in Raman signal for biofilm cells is likely the result of a change in metabolism when transitioning from a planktonic to a biofilm growth state (Huang et al., 2011).

Specifically, *S.mutans* showed low predictions accuracy (76.7%) compared to *A.naeslundii* (100%) and *V.dispar* (93.3%) which performed much better. *S.mutans* is known to be a key contributor in the production of EPS while *A.naeslundii* and *V.dispar* lack the ability to form EPS when grown as mono-species biofilms. Hence, low prediction accuracy could be the result of spectral interferences from EPS in the data acquisition of *S.mutans* mono-species biofilm spectra (Koo et al., 2010; McCabe and Donkersloot, 1977; Vacca-Smith and Bowen, 1998).



One of the most significant changes in the spectra was the difference of the 1525 cm<sup>-1</sup> peak in *S.mutans*. Due to the large difference of this specific peak, differences between *V.dispar* and *S.mutans* became much smaller and led to several misclassifications of these biofilm spectra. As a result, new calibration datasets derived from biofilm grown cell were generated for the mapping of dual-species biofilms using the Renishaw inVia™ Qontor to prevent the misclassifications based on the setup of the calibration dataset from planktonically grown cells.

## 5.2 Use of CRM for mapping of dual-species biofilms

With confidence in the acquired biofilm based datasets and the statistical analysis of the spectra, the last step was the study of mixed biofilms (specifically dual-species biofilms) to determine the applicability of the developed workflow. In oral biofilm research, CLSM is seen as the state-of-the-art technique to analyze the architecture of multi-species biofilms (Abdullah et al., 2019). As seen in previous chapters, CRM can serve as an alternative technique with specific and unique advantages, making it possible to analyze the composition of biofilms. In this thesis, CRM methods were developed that were able to visualize the distribution of two bacterial species in a dual-species biofilm model. CRM has established the spatial discrimination between species in cultivated multi-species biofilms without sample preparation to keep the biofilm structure unaltered. CA as the multivariate statistical tool was able to use chemometric information from Raman spectra to distinguish *A.denticolens* and *S.oralis* in a dual-species biofilm. Mapping biofilms by CRM was confirmed through a morphology analysis of the same area and FISH/CLSM. PCA and O2PLS-DA were not used as mapping techniques as the methods don't allow for a direct correlation of Raman spectra to the acquisition location.

By comparing information of planktonic and biofilm spectra of one species (for *A.denticolens* and *S.oralis*), it could be seen that both show similar chemometric profiles (see Figure 30C and F). The biggest differences appear in the height and thus signal counts of individual peaks. These differences can be explained by metabolic changes and up or down regulation of processes when bacteria are forming a biofilm (Marsh, 2004; Svensäter et al., 2001; Wan et al., 2018). Additionally, the formation of EPS in the cultivation of biofilms may explain the change in the chemometric signals in the spectra (Sandt et al., 2007), especially the peak at ~982 cm<sup>-1</sup> associated to polysaccharides and is increased in *A.denticolens* and *S.oralis* mono-species biofilm spectra. This may also explain the reduced number of correct predictions for mono-species biofilm spectra of *S.mutans* in Chapter 4.1.5.

## DISCUSSION

---

Nevertheless, it was possible to demonstrate that PCA is able to differentiate the selected two species in a planktonic and biofilm setup although, PCA for planktonic species showed an overlap of the two clusters. While *A.denticolens* showed a dense clustering of the spectra, *S.oralis* was spread broader suggesting an increased variance within the dataset, causing the overlap of clusters.

Even though sample preparation for analysis remained consistent throughout the experiments, bacteria that were analyzed at random spots may be in different metabolic phases. While the phases may not have a detectable influence on the chemometric profile for *A.denticolens*, they may be significant enough for *S.oralis* to show variance of the analysis (Strola et al., 2014), resulting in a broader range in the score plot (Figure 31A). Here, PCA analysis shows a larger distribution of spectra, especially for planktonic *S.oralis* samples, suggesting larger variance, which also explains the increased standard deviations of every spectral point for *S.oralis*.

Using the averaged planktonic and mono-species biofilm Raman spectra of *A.denticolens* and *S.oralis*, as well as the resulting PCA analysis of this data, the analysis indicates that *S.oralis* has a lot of differing peaks compared to *A.denticolens* (Figure 30 and Figure 31). Additionally, the amount of peak differences for planktonic and mono-species biofilms for *A.denticolens* appear to be only minor except for a few peaks as described in Chapter 4.3.1 (Figure 30C). The same observation can be made for mono-species biofilms samples for *A.denticolens* and *S.oralis* (Figure 30H). However, peak differences appear to be increased when planktonic and mono-species biofilms of *S.oralis* were compared (Figure 30F), as well as planktonic spectra for *A.denticolens* and *S.oralis* (Figure 30G). Because counts are generally increased for planktonic *S.oralis* except for two areas, this suggests that the data collection of planktonic *S.oralis* samples may have had insufficient baseline correction (Guo et al., 2016) for some spectral samples resulting in larger variance within the dataset that can also be seen in the PCA analysis Figure 31. In detail, the spectral counts in the region of 1200-1400  $\text{cm}^{-1}$  and the peak at 1525  $\text{cm}^{-1}$  are increased for planktonic *S.oralis* samples. Spectral peaks in this area are however also present in the other collected datasets (planktonic and mono-species biofilm spectra for *A.denticolens* and *S.oralis*). Thus, the increased count for planktonic *S.oralis* underlines a possible issue in the data processing of the planktonic bacteria dataset of *S.oralis*.

The peak at 1525  $\text{cm}^{-1}$  has been identified the first time in the analysis of oral bacteria. This specific peak doesn't only appear for planktonic *S.oralis* bacteria but is also present in *A.denticolens* samples and *S.oralis* biofilm spectra (Figure 39). *S.oralis* mono-species biofilm spectra show a reduction of 63.38% (see Figure 30F) compared to planktonic spectra while the

## DISCUSSION

reduction in count is lower with 40.29% for *A.denticolens* mono-species biofilms (see Figure 30C) when compared to planktonic bacteria. Component assignments based on other bacterial species (Dhankhar et al., 2021; Kumar et al., 2015; Scholtes-Timmerman et al., 2009) assigned this specific peak as a C=C symmetric stretching coming from carotenoids within a bacterial cell. The metabolic pathways of oral bacteria however don't allow the synthesis of carotenoids. Because Amide II, Adenine and Cytosine are also showing spectral peaks in this area (Cepeda-Pérez et al., 2016; Gieroba et al., 2020; Seredin et al., 2019), it is possible that they could be the reason for the peak height in the analyzed samples and could be shifted due to the complexity of the samples composed of various chemical components. However, further investigation of the assignment of this peak is necessary and how this peak influences multivariate models.

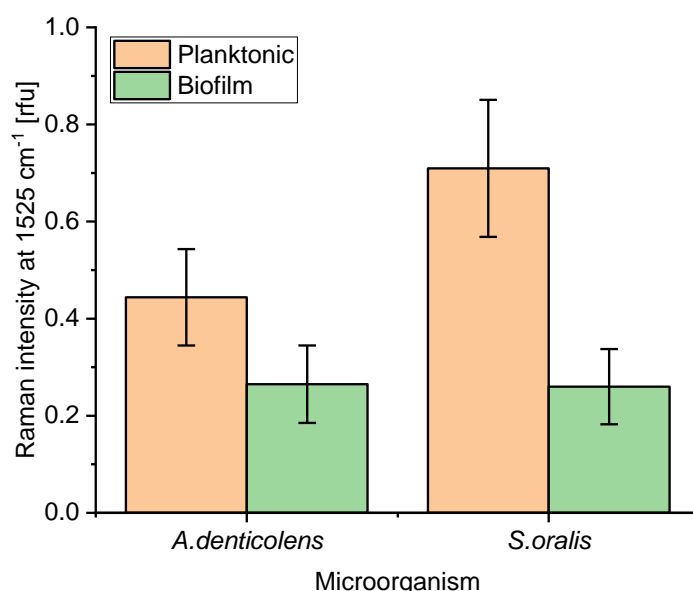


Figure 39: Peak intensity at  $1525\text{ cm}^{-1}$  using CRM with standard deviation.

Conversely, the spectral peak at  $982\text{ cm}^{-1}$  is increased in biofilms for both, *A.denticolens* and *S.oralis* (Figure 40). While both bacteria show a similar signal for planktonic bacteria, Raman counts are increased by 304% for *S.oralis* mono-species biofilm samples and increased by 373% for *A.denticolens* mono-species biofilm samples. This peak is specifically interesting, because very little literature identified this peak. Beier et al. (2010) showed spectra that flagged the  $982\text{ cm}^{-1}$  peak by linear regression. While that peak was identified, they did not assign it to a specific compound. Assignments from different spectra were made previously though. For instance, Paret et al. (2010) identified the peak around  $982\text{ cm}^{-1}$  as a C-C stretch of proteins and =CH bending of lipids in different Gram-positive and Gram-negative plant bacteria. On the other hand, Kahraman et al. (2009) assigned the same peak (present as a weak peak) as a C-N stretch in *E.coli* bacteria samples using SERS.

## DISCUSSION

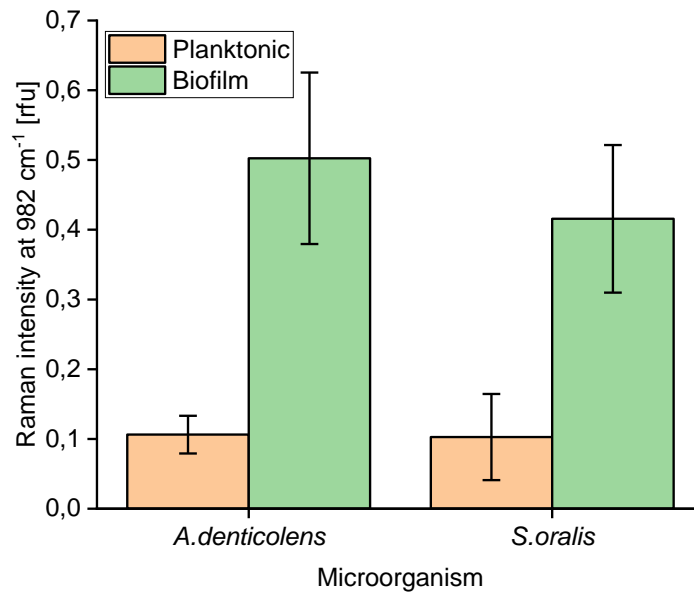


Figure 40: Peak intensity at 982 cm<sup>-1</sup> using CRM with standard deviation.

The more likely explanation of this peak increase could be the increase in polysaccharide concentration due to EPS formation. This increase has been shown by Ramirez-Mora et al. (2019) where peaks observed at 880-980 cm<sup>-1</sup>, 1055 cm<sup>-1</sup> and 1075 cm<sup>-1</sup> were tentatively assigned to rhamnose, galactose and glucose which were further associated to *Actinomyces spp.* by Rosan and Hammond (1974). Since C-C stretches are also present in saccharides, this could explain the increase of signal for mono-species biofilm spectra. However, further investigation of this peak is necessary to make a clear determination.

Because a robust dataset is essential for the success of CA and biofilm mapping, calibration dataset differentiation may improve by increasing the number of spectra in the dataset to better represent the complete data distribution, which then leads to more accurate predictability of species (Guo, 2018) and reduces the variance within the datasets. For this thesis, the statistical analysis of biofilm spectra showed two defined clusters with only minor outliers, which suggests less variance within the cluster and thus allows for a more specific analysis model compared to planktonic species (Figure 31). The analysis using PCA demonstrated sufficient evidence of differentiation of the two species and allows to be used for species classification when performing Raman mapping using CA.

It needs to be noted that the implemented amounts of variants for the individual PCs of all PCA analyses are not a representation of the quality of collected data. For PCA analysis, a total of 706 spectral points were used. Not all of these spectral points show enough differences to be considered for differentiation by PCA. Instead, it can be said that reduced variance is the result of similar datasets and only small amounts of peaks that can be differentiated from each other.

## DISCUSSION

---

For planktonic bacteria spectra calibration of *A.denticolens* and *S.oralis*, the two PCs explained 41.7% of the overall variance present in the dataset (Figure 31A), while for mono-species biofilms, 26.2% of variance was explained (Figure 31B). Especially when looking at the total variances, this indicates that in order to achieve two distinct clusters using PCA, less variance was necessary to differentiate mono-species biofilm spectra. This indicates that the data points used were distinct enough, resulting in low variance (Figure 31), while more data points were used for planktonic bacteria spectra differentiation. The same conclusions can be made for the analysis of *C.albicans* and *P.aeruginosa* mono-species biofilm spectra where 28.8% of the variance was explained (Figure 37).

The analysis of DBIA samples confirmed the use of CA for the analysis of multi-species biofilms. It was shown that cluster mapping based on Raman spectra was comparable with the morphology analysis and it was able to determine two areas of predominantly one species. While morphology showed only two distinct areas, CA also classified a few areas with the other species not detected by morphology. The more likely explanation, however, is that due to the overlap of statistical clusters in the PCA analysis, the CA model was not as species-specific, thus causing misclassification (Ben-Hur and Guyon, 2003). Overall, CA coupled with Raman analysis confirmed that CA could be used as a method to differentiate species in a DBIA biofilm with only minor differences between morphology and Raman analysis.

For dual-species biofilm models, CA was able to successfully map species of a focused layer. Additionally, determination of coverages between morphology and Raman mapping was comparable indicating that similar amounts of *S.oralis* and *A.denticolens* were detected in selected areas. This confirms that the differences in the chemometric profile is significant enough to allow the mapping of the two species in a multi-species biofilm model. Nevertheless, the Raman analysis showed some limitations mostly visible in the transition areas of clusters where bacteria were classified differently when compared to morphology. An explanation of different classifications could be that signals from layers below the focused layer were not the same species (Gieroba et al., 2020; Ramirez-Mora et al., 2019). This effect causes the detection of both species and generates a mixed chemometric profile of both species. When comparing these areas to the FISH/CLSM image (Figure 28), yellow/orange areas in the transition areas confirmed both species to be present. This suggests that indeed the Raman spectra in the transition areas carry chemometric information from both species that may result in the difference in classifications.

Quantifications of the misclassified areas (blue areas in Figure 33) are summarized in Chapter 8.8 in the Appendix as ‘Different classification morphology vs. Raman’ and are shown in Figure 35. The differences can be compared to the overall quantifications of the individual methods (difference in % in Chapter 8.8 (Appendix)). Here, the numbers are lower compared to the blue areas (Figure 35). The reduced numbers indicate that the amounts of over- and under-representation of *A.denticolens* and *S.oralis* from CRM within the blue areas are similar (see description of method in Chapter 3.3.3), therefore confirming that there is no trend that one species is over- or under-represented. Only the direct comparison of the two methods (‘Difference in %’ in Figure 34) showed samples in which species are over- and/or under-represented within the biofilms as a result of relative quantification. However, it was not possible to specifically indicate the areas within the biofilm where *A.denticolens* and *S.oralis* were over- and under-represented compared to light microscopic determination.

Being able to improve the resolution of the laser (below the measurable 1  $\mu\text{m}$ ) may further reduce the differences between light microscopy and CRM and thus the discrepancy of bacteria as seen in Figure 35. Especially, the transition areas of two clusters (where misclassification appears a lot) may then be assigned, more precisely small clusters may also be identified more accurately. Furthermore, because a high laser power was used for the spectra acquisition, the surrounding area of the sample point was also excited. Especially in the transition areas of two clusters it may then be possible that compounds of both microorganisms are excited and emit photons that are then detected. The same accounts for the excitation of layers below the focus. If the layers below the focused area are different than the focused species, this may also result in excitation of unwanted areas and misclassification. These conditions need to be considered for future experiments by optimizing the resolution of sample acquisition as well as sampling laser power.

The application of the generated workflow to dual-species biofilms consisting of fungi and bacteria was also successful. In agreement with the results from oral biofilm mapping, it was possible to differentiate these microorganisms and the area of coverage. A requirement for identification is, that the areas observed are in focus for the differentiation of spectra. The area in the top left corner of the shown image (Figure 38A) is out of focus and coincides with the area that is misclassified as *P.aeruginosa*, as shown in Table 18. Everall (2008) was already able to demonstrate the effect of out-of-focus acquisitions on Raman spectra. Therefore, to have a successful differentiation of species, it is essential that areas are in focus (Figure 38).

Biofilms consisting of more than two different species were not analyzed in this work. However, the statistical analysis of the five oral bacterial species suggest that biofilms consisting of more than two species can be differentiated. This complicates the differentiation of species based on their morphology, because the majority of oral bacteria species are either cocci or rod shaped. In order to be able to compare results from CRM it is necessary to establish a different method for mapping comparisons. One option is FISH/CLSM. A method needs to be established that allows the analysis of the same area with CRM and CLSM. After CRM measurements, staining of biofilms needs to be achieved without a dislocation of the sample to be able to locate the identical area to analyze. Alternatively, staining can be done before Raman analysis. Because fluorescence signals of stained cells are high, coherent anti-Raman Stokes (CARS) measurements are required as they do not detect fluorescent signals. Nevertheless, this method is very complex and requires substantial knowledge of the instrument as well as signals may not be comparable to CRM measurements anymore. Thus, in order to be able to measure multi-species biofilms consisting of three species or more, these challenges need to be overcome.

### **5.3 Comparison of Raman mapping to other methods**

There are multiple techniques that enable the mapping of biofilms and each of these techniques have their own unique advantages and disadvantages in comparison to CRM used in this work. These differences are discussed within the next chapters, focusing on the differences to CRM.

Overall, there is no superior technique that allows the optimal structural mapping and differentiation of biofilms yet - not even CRM. For that reason, strategies to combine the discussed techniques may show the greatest success. The discussed techniques below showcase only a selection of methods suitable for the architectural analysis of biofilms based on their underlying analysis principles and are not intended to be complete.

#### **5.3.1 Fluorescent and morphological mapping techniques**

A first comparison of different methods to spatially map biofilms was displayed in Chapter 4.3.5 and can also be seen in Table 17, where CRM mapping was compared to mapping methods such as CLSM coupled with FISH, SEM and AFM. These methods have previously been established as alternatives to CRM (Huang et al., 2020). This analysis showed as advantages for CRM that 1. CRM mapping allows the continuous consideration of biofilm mapping of one specific spot and 2. analysis is possible when the biofilm sample is in a hydrated state without

sample destruction. One key disadvantage of using CRM for mapping, however, is the low resolution of the analysis methods. As previously addressed, specific advancements in CRM with regard to laser techniques may allow improved resolution of this method in the future.

CLSM coupled with FISH remains to be the primary technique to reconstruct the structure of biofilms due to its good resolution, reliable results and relatively high throughput of samples. However, the technique cannot be applied to *in-vivo* studies. In contrast, *in-vivo* studies are possible using CRM (Malik et al., 2017). Additionally, FISH/CLSM relies on the need to know about the compounds of the biofilm to be analyzed in order to select correct primer stains for FISH. Because CRM uses chemometric information, this method remains unbiased as long as calibration datasets are established and allow the differentiation of species. This remains an important task for CRM measurements.

Classic AFM sample measurements require the coating of the sample with conductive or gold materials. As a result, this led to the use of another technique commonly known as ESEM, where no special sample treatment is needed and as such retains the natural state of the sample while it reduces the resolution compared to classical SEM (Alhede et al., 2012). ESEM allows the observation of hydrated biofilms under low pressure (Fernández-Delgado et al., 2015). In theory, ESEM can be applied for *in-vivo* biofilm analysis but has not been done yet. Thus, ESEM remains a technique that only allows differentiation of cells based on morphology and is limiting for that reason. The same issues apply for AFM measurements, which is based on morphological differentiation as well. Due to the complexity of the required instrument, only *in-vitro* measurements of biofilms have been demonstrated successfully (James et al., 2016) and it is unlikely that it will be used as an *in-vivo* biofilms analysis tool in the future.

### **5.3.2 Laser-induced vibrational mapping technique**

Another emerging method that utilizes the biochemical composition of a biofilm by measuring the vibrational changes from sample excitation, similar to CRM, is IR spectroscopy. In IR spectroscopy, an infrared beam is directed onto the sample similar to CRM, but here, the radiation that is absorbed by the sample at different frequencies is measured. It therefore relies on the absorbance, transmittance or reflectance of infrared light where the different amounts of absorbed light are being acquired. The most common technique is FTIR, a technique which adheres to the described principles above. The two major disadvantages of FTIR are the detection OH stretching in water, limiting the success of analyzing hydrated samples, as well as its constraints on sample thickness and uniformity. On the contrary, FTIR measurement



## DISCUSSION

---

doesn't show interference that comes from sample fluorescence, a factor that can be beneficial when compared to CRM. Because the technique is based on the same key fundamental of laser-induced vibrational measurements, the technique needs to be discussed in detail. Especially so as only a few publications have compared FT-IR and Raman Spectroscopies in biofilm research before (Gieroba et al., 2020; Sharma and Prakash, 2014).

The existing research demonstrated that both techniques are able to be used successfully in a biological context. Sharma and Prakash (2014) concluded that FTIR showed higher intensities for polysaccharides, amide I, amide II vibrational mode of ester and carboxylate group, while higher intensities were found for Raman peaks assigned to tyrosine, amide III, carbohydrates, carotenoids, DNA and lipids (analysis was done on *Cronobacter sakazakii* biofilms). Additionally, Gieroba et al. (2020) concluded that based on the measurements of different cariogenic *streptococci spp.*, the two spectroscopies should be seen complementary because they can offer a more comprehensive approach for the analysis of biofilm samples on account of different sensitivities detecting particular chemical groups.

To the best of my knowledge, only a few publications looked at FTIR for mapping (Cheeseman et al., 2021; Gieroba et al., 2020; Holman et al., 2009; Probst et al., 2013). These publications, however, focused on the localization of specific chemical compounds in mono-species biofilms and not the use of the complete spectra to predict species in a multi-species biofilm. It was rather shown in this research, that spatial areas that show an increased amount of certain chemical components can be identified.

Interestingly, Cheeseman et al. (2021) used a very similar experimental designs as the ones exhibited in this work. For the analysis of pathogenic bacterial and yeast biofilms, he used a combination of Synchrotron macro attenuated total reflectance-Fourier transform infrared (ATR-FTIR) Microspectroscopy, which is a specific modification of FTIR. Similar to this work here, Cheeseman et al. demonstrated the presence of biofilms using CLSM and SEM imaging. *P.aeruginosa* and *C.albicans* (and *S.aureus*) were also used for the experiments. Further, Cheeseman et al. performed CA for the localization of a specific Amide I peak, which was then used to differentiate the species by cluster formation using PCA. Due to similarities in experimental setup and analysis, a good comparison to this work is allowed.

Cheeseman et al. (2021) successfully showed that ATR-FTIR can be used for the differentiation of microbial species. He also demonstrated the use of CA for mapping. While they only used a specific Amide I peak for mapping, this work considered the full chemometric profile for the

mapping of bacteria. Additionally, they also used PCA analysis to demonstrate differentiation based on chemometric information. Their experiments came to similar conclusions as in this work. Since it was shown that ATR-FTIR is able to differentiate biofilms based on their spectra, it will be interesting to see whether the spatial mapping of multi-species biofilm models is also possible. This possibility would further help to compare CRM with other techniques and establish vibrational spectroscopy as a complementary technique to established methods.

The application of ATR-FTIR for *in-vivo* biofilm studies, to the best of my knowledge, has not yet been demonstrated. The analyzed samples by Cheeseman et al. (2021) were fixed using formaldehyde/glutaraldehyde and were not in a living and hydrated state.

### **5.3.3 Mapping techniques based on chemometric profiles**

Another technique that acquires chemometric profiles is MALDI-TOF, a type of mass spectrometry that allows the measurement of biomolecules like peptides, lipids, saccharides or other organic macromolecules through laser ionization. Because bacteria have unique molecular compositions, specific bacterial assignments can be achieved based on the chemical profiles. In theory, these assignments can be used for the differentiation of bacteria in biofilms. Indeed, MALDI-TOF has been used in the past to analyze biofilms (Caputo et al., 2018; Pereira et al., 2015; Stîngu et al., 2008).

Known as mass spectrometry imaging, the spatial analysis of samples was demonstrated when coupled with MALDI, mostly on tissue samples (Aichler and Walch, 2015; Smith et al., 2018) and biofilms (“Re-discovering Bacterial Biofilm Heterogeneity with MALDI Mass Spectrometry Imaging,” n.d.). However, low spatial resolution similar to CRM do not allow sufficient differentiation. While it is now possible to achieve a resolution below 1.5  $\mu\text{m}$  or lower in some cases (Kompauer et al., 2017), the ion yields are very low and require the development of more sensitive detectors and increased computing power (McDonnell and Heeren, 2007; Ščupáková et al., 2020).

Besides the currently insufficient resolution of MALDI mass spectrometry imaging, the analysis also requires destructive sample preparation, a process entailing different chemical steps. This destructive sample preparation makes the method insufficient for the analysis of *in-vivo* and continuous analysis of *in-vitro* biofilms. With that being said, however, the use of MALDI-TOF as a mapping tool was successfully demonstrated, although it is not as developed as CRM to determine the architecture of biofilms yet.

### **5.3.4 Combination of techniques for mapping with CRM**

As demonstrated in this work, the combination of microscopy methods and chemometric methods will allow a good understanding of dual-species biofilms. This specific combination may be improved by using a higher resolution camera, as well as laser improvements. To improve the use of CRM as a competitive method for biofilm architecture research, it may need to be considered complementary to other techniques. Several methods have showed good success when multiple techniques were used for the analysis of biofilms including CRM.

As already introduced in this work, the combination of Raman techniques with CLSM could improve the application greatly and can help to establish CRM as an alternative technique to the state-of-the-art CLSM. One option could be bacterial staining without any dislocation of the sample. The other option for performing the simultaneous measurement is the switch to use CARS as the Raman spectroscopy technique in order to prevent signals from the fluorescent staining process. While this could serve as the improved proof for the use of Raman spectroscopy for biofilm mapping compared to the evidence displayed in this work, this method can also serve as a complementary technique to analyze the chemical composition of bacteria, depending on the research topic.

One other combination would be the use of Raman technologies with infrared methods because they both exploit laser-induced vibrations. Specifically, coupling CRM and ATR-FTIR to perform cluster analysis may improve the success of the clustering or may open the door to new multivariate statistical models. However, this would require the spectral analysis of the same spot to enable comparison. Because biofilms require a resolution of at least 1  $\mu\text{m}$  or below to perform biofilm mapping, this could be difficult. Additionally, ATR-FTIR can also be used as a comparative method to evaluate CRM mapping. Because spectra are expected to be similar, processing methods and statistical analysis, as introduced in this work, can be applied. However, analyzing the same spots and location is required in order to perform this comparison. The analysis of hydrated samples will remain challenging for ATR-FTIR analysis.

Lastly, the combination of Raman spectroscopy with AFM represents a great opportunity to improve biofilm mapping using Raman. As introduced in Chapter 1.3.4, TERS is a modification of Raman spectroscopy that uses a tip of a conductive metal such as gold or silver particles for spectral acquisition. This method results in a theoretical Raman signal enhancement of up to  $10^8$  counts (Kurouski, 2017) and thus improves the spectral peak counts and reduces background noise. The same tip can be used for TERS and AFM analysis giving the opportunity

## DISCUSSION

---

to measure morphology and chemical composition on a nanoscale level simultaneously. To the best of my knowledge, the use of TERS for mapping in a biological context has only been used twice (Böhme et al., 2010; Rusciano et al., 2014). Using TERS as a mapping technique of biofilms, though, has not yet been demonstrated. As much as the measurements on a nanoscale level improve the resolution, it also reduces the fast mapping ability over a bigger area.

This thesis has laid the groundwork in demonstrating that mapping and differentiation of bacteria in biofilms is possible. Using TERS with AFM may be a next step in demonstrating the applicability of this work's developed workflow in differentiating bacterial species. If proven successful, TERS would be able to improve differentiation due to increased resolution, therefore allowing the mapping of multi-species biofilm of more than two species and comparing the results to CRM mapping from this work. Additionally, the combination will allow high resolution morphology imaging.

It needs to be noted however, that the biggest disadvantage of the method is the difficulty of fabricating the required tips, as they have a poor reliability and lifetime. Being able to overcome the low quality of tips and improving the reliability of the method will greatly improve the research of biofilm mapping using Raman spectroscopy in the future. Furthermore, the application of *in-vitro* research is questionable. For that reason, it can be concluded that the application of TERS for multi-species biofilm mapping needs to be evaluated in future experiments, but it shows promising advantages over the CRM used in this work.

## 6 Conclusion and Outlook

In this thesis, the potential of using CRM for mapping of microbial biofilms was evaluated on *in-vitro* subgingival oral biofilms and was further assessed analyzing biofilms often found on catheters or other medical devices. Figure 33 and Figure 38 illustrate the final results of the workflow development for the analysis of the selected biofilms.

The purpose of this thesis was to lay the groundwork for whether differentiation of subgingival bacteria was possible using CRM and to determine if this technique can be applied for mapping biofilm models. CRM coupled with two-way orthogonal Partial Least Square with Discriminant Analysis was applied to 1. discriminate three oral bacterial species in score plots and 2. develop a prediction model to successfully identify microbial species both from planktonic cells and cells in a mono-species biofilm model. Here, it was possible to correctly identify 100 % of planktonic spectra and 90 % of mono-species biofilm spectra belonging to three different Socransky clusters. Additionally, PCA also demonstrated species discrimination when only two species were analyzed and could be used as a valuable analysis tool for different inquiries instead of O2PLS-DA. O2PLS-DA in general is more prone to overfitting of data because the analysis is done with lesser variables than for PCA. This overfitting can be problematic because the model then doesn't perform an unbiased analysis anymore. For that reason, PCA is an alternative for future biofilm analysis due to easier applicability and unbiased evaluations. However, PCA should not be used for two-species models per se but should rather be evaluated for every biofilm analysis especially for biofilms consisting of more than two species as described before (Chapter 3.3.2).

The experiments showed the discrimination of planktonic bacteria and the prediction of mono-species biofilms, therefore, the presented method can also be used to build a spectral Raman library for bacteria discrimination. This can make it easier to assess and determine spatial distribution of multi-species biofilm models in the future. For the analysis of mono-species biofilm models, the established method was successfully able to predict species, indicating the applicability of the method for inquiries asked in a biofilm setting. Due to the nature of Raman spectroscopy *in-vivo* and *ex-vivo*, studies can be directed and have a wide range of applications (Paraskevaidi et al., 2021). Specifically, *in-vivo* studies showing the evaluation and mapping of oral cancerous tissue using Raman spectroscopy have been conducted (Malik et al., 2017). Using the information from this study it can be concluded that it may be possible to differentiate biofilms from periodontal healthy patients and patients with periodontitis *in-vivo* because

differentiation is possible using a similar instrumental setup as described by Malik et al. (2017) for clinical application.

It was furthermore possible to show that it is feasible to differentiate two species in a multi-species biofilm model of a two-dimensional area using CRM by comparing the results to morphology of the biofilms and FISH/CLSM as the state-of-the-art technique. Specifically the comparison between morphology and CRM analysis showed the potential of using CRM for biofilm mapping, because the major bacterial clusters were spatially correctly identified for two different species in biofilms. This is the first time that the use of CRM in a dimensional mapping setting has been used. Future steps may include the transfer of the findings to a clinical application *ex-vivo* (through the collection of samples) and *in-vivo* (directly in a patient's mouth). While the *ex-vivo* studies can be conducted already with the equipment (such as mobile Raman probes or micro-Raman setups) and statistical results already available, *in-vivo* studies would require the reduction of acquisition times to a few minutes or seconds.

A key finding of this thesis was foremost that in order to perform spatial predictions (in two or three dimensions) it is necessary to combine batch spectra processing with the developed multivariate analysis technique in a workflow to use multivariate analysis for multi-species biofilm imaging. Additionally, it was demonstrated that oral species can be differentiated based on their chemometric profile without specific sample preparation. Because oral bacteria inhabit similar environments, spectral differences are only minor but significant enough to allow differentiation. Biofilms composed of substantially different organisms may allow an easier differentiation as seen with the analysis of a biofilm from *C.albicans* and *P.aeruginosa*. Lastly, it is possible to apply CRM for bacterial differentiation based on their chemometric profiles and for that reason confirms the hypothesis that this technology is able to map biofilms when combined with statistical models.

This thesis indicates the possibility of bacterial cluster differentiation with different prevalence in oral diseases like periodontitis and gingivitis because they both have high concentrations of *A.denticolens* and *S.oralis* (Ximenez-Fyvie et al., 2000). In future research, it will be pivotal to apply this model not only to mono-species and dual-species biofilm models, but to also extend the analysis to multi-species biofilm models. Consequently, next steps of establishing CRM for biofilm mapping should be 1. extending the database to more oral species as well as determine and show statistical differentiation 2. the analysis of more than two species in a biofilm and 3. Evaluating the potential for three-dimensional views of biofilms. Even though CRM was successfully used, questions remain unanswered in order to make it a competitive technique to

FISH/CLSM. Nevertheless, with the results of this study, it is possible to consider and establish Raman mapping as a complementary technique to CLSM, because it is able to give information on the chemometrics of species in biofilms. With the advancements of the technique in the future, it may be possible to use Raman as an alternative and competitive method for biofilm mapping.

In a multi-species setup it will be necessary to validate and evaluate results from CRM with other methods like qPCR or CLSM. The morphology differentiation used in this thesis may not be sufficient to achieve differentiation of cells of similar shape. Due to the nature of sample preparation for CLSM and the fluorescent signal, it will be essential to use CARS to omit the signal from FISH in the spectral analysis. As part of this development, it will be necessary to evaluate the limitations of the technique. While it may not be possible to differentiate all species present, species with higher abundances may be differentiated in a 3D structure successfully.

For applications, it will be pivotal to determine the limits of this analysis technique. One major downfall of this technique is the technical limitation of only receiving spectral information in 1  $\mu\text{m}$  steps. With advancements in laser technology, it may be possible to reduce the resolution limitation and move towards the possibility of implementing nanoRaman Scattering Microscopy (allowing a spatial resolution of 65 – 114 nm) (Kawata et al., 2017) in microbiological settings such as biofilm mapping.

This limitation results in the lack of detection of small sized clusters. This can be specifically difficult in multi-species biofilms when species are only present in small amounts. The second great downfall of CRM was that spectral acquisitions required around 60 min for an area of 324  $\mu\text{m}^2$ , due to numbers of accumulations and long exposure times. It will be important to determine how far accumulations and exposure times can be reduced and optimized while still being able to receive differentiation of species in a multi-species biofilm and keeping the same resolution.

For the applicability of this technique, especially in an industrial setting such as biofilm mapping in the food processing or potable and wastewater distribution system industry, results need to be delivered quickly. While CRM is still faster than CLSM when the whole sample preparation and analysis time is put into consideration, CLSM allows the sample preparation of multiple samples at the same time. CRM technique can be improved by reducing laser power in order to minimize the possible artifact from chemometric spectral information from layers below the focused layer, thereby improving the quality of spectra.

The implemented CRM technique used an approach that didn't require sample preparation (such as staining or nanoparticles) or a specific surface (such as silver coated surfaces) for analysis. With the advancements in CRM related technologies such as resonance Raman, SERS, TERS or CARS, it could improve the quality of spectra as well as reduce the acquisition time when combined with the developed workflow from this thesis. TERS especially demonstrates a good opportunity for the use of CRM in the field of biofilm architecture mapping. As discussed, sufficient and exact differentiation is dependent on the quality of the calibration dataset as well as the acquisition of the spectra at a specified location. Using the above mentioned Raman-based methods may improve both aspects of making the prediction more robust.

Future directions of research applying the developed workflow and taking into account the non-destructive characteristic of CRM, are the study on topics that include the variations in biomass composition which depend on: 1. the microorganisms present and their metabolic activity 2. the available nutrients and the environmental conditions and 3. the development phase of the biofilm on a single sample over time. For a reliable analysis, these parameters must be taken into account. With this knowledge, a direct link to biofilm functions can be achieved, which in return leads to a better understanding of these very complex and challenging systems and allows the development of more effective treatment approaches to inhibit the growth of unwanted microorganisms within a biofilm.

In conclusion, it can be said that CRM shows a high potential for the characterization of bacteria and mapping of biofilms in the field of oral and medical biofilm research. Specifically, the use of CA in combination with CRM shows a promising approach of differentiating microbial clusters within a biofilm and helps the understanding of the requirements for successful mapping. The applications of sample non-destructive biofilm mapping technologies based on metabolic and chemometric methods for the analysis of samples *in-situ* and *in-vivo* are fast growing topics in research, industry and medicine. To improve the method of biofilm mapping using CRM in the future, different challenges need to be overcome: 1. increase the understanding of obtained data 2. improvement of reproducibility of analysis 3. establishment, improvement and extension of databases for the analysis of microbial samples 4. increased detection strength from technical developments such as CCD cameras or above described Raman-based technologies 5. improvement of statistical analysis of spectra and 6. reduction of analysis time and thus higher sample throughput. Finally, in terms of biofilm research, it will



## CONCLUSION AND OUTLOOK

---

be pivotal to improve comparison with other established biofilm mapping technologies either as a competitive or complementary technology.

## 7 References

- Abdullah, N., Al-Marzooq, F., Mohamad, S., Abd Rahman, N., Chi Ngo, H., Perera Samaranyake, L., 2019. Intraoral appliances for in situ oral biofilm growth: a systematic review. *J. Oral Microbiol.* 11, 1647757. <https://doi.org/10.1080/20002297.2019.1647757>
- Abusleme, L., Dupuy, A.K., Dutzan, N., Silva, N., Burleson, J.A., Strausbaugh, L.D., Gamonal, J., Diaz, P.I., 2013. The subgingival microbiome in health and periodontitis and its relationship with community biomass and inflammation. *ISME J.* 7, 1016–1025. <https://doi.org/10.1038/ismej.2012.174>
- Aichler, M., Walch, A., 2015. MALDI Imaging mass spectrometry: current frontiers and perspectives in pathology research and practice. *Lab. Invest.* 95, 422–431. <https://doi.org/10.1038/labinvest.2014.156>
- Alhede, M., Qvortrup, K., Liebrechts, R., Høiby, N., Givskov, M., Bjarnsholt, T., 2012. Combination of microscopic techniques reveals a comprehensive visual impression of biofilm structure and composition. *FEMS Immunol. Med. Microbiol.* 65, 335–342. <https://doi.org/10.1111/j.1574-695X.2012.00956.x>
- Almarashi, J.F.M., Kapel, N., Wilkinson, T.S., Telle, H.H., 2012. Raman Spectroscopy of Bacterial Species and Strains Cultivated under Reproducible Conditions. *Spectrosc. Int. J.* 27, 361–365. <https://doi.org/10.1155/2012/540490>
- Ammann, T.W., Bostanci, N., Belibasakis, G.N., Thurnheer, T., 2013. Validation of a quantitative real-time PCR assay and comparison with fluorescence microscopy and selective agar plate counting for species-specific quantification of an in vitro subgingival biofilm model. *J. Periodontal Res.* 48, 517–526. <https://doi.org/10.1111/jre.12034>
- Aruni, A.W., Dou, Y., Mishra, A., Fletcher, H.M., 2015. The Biofilm Community: Rebels with a Cause. *Curr. Oral Health Rep.* 2, 48–56. <https://doi.org/10.1007/s40496-014-0044-5>
- Bandara, H.M.H.N., K Cheung, B.P., Watt, R.M., Jin, L.J., Samaranyake, L.P., 2013. *Pseudomonas aeruginosa* lipopolysaccharide inhibits *Candida albicans* hyphae formation and alters gene expression during biofilm development. *Mol. Oral Microbiol.* 28, 54–69. <https://doi.org/10.1111/omi.12006>
- Barranguet, C., van Beusekom, S., Veuger, B., Neu, T., Manders, E., Sinke, J., Admiraal, W., 2004. Studying undisturbed autotrophic biofilms: still a technical challenge. *Aquat. Microb. Ecol.* 34, 1–9. <https://doi.org/10.3354/ame034001>
- Beier, B.D., 2011. Confocal Raman Microspectroscopy of Oral Streptococci. University of Rochester, Rochester, New York, USA.
- Beier, B.D., Quivey, R.G., Berger, A.J., 2012. Raman microspectroscopy for species identification and mapping within bacterial biofilms. *AMB Express* 2, 35. <https://doi.org/10.1186/2191-0855-2-35>
- Beier, B.D., Quivey, R.G., Berger, A.J., 2011. Confocal Raman microscopy for identification of bacterial species in biofilms, in: Miller, B.L., Fauchet, P.M. (Eds.), . Presented at the SPIE BiOS, San Francisco, California, USA, p. 78880D. <https://doi.org/10.1117/12.871819>
- Beier, B.D., Quivey, R.G., Berger, A.J., 2010. Identification of different bacterial species in biofilms using confocal Raman microscopy. *J. Biomed. Opt.* 15, 066001. <https://doi.org/10.1117/1.3505010>
- Ben-Hur, A., Guyon, I., 2003. Detecting Stable Clusters Using Principal Component Analysis, in: *Functional Genomics*. Humana Press, New Jersey, pp. 159–182. <https://doi.org/10.1385/1-59259-364-X:159>

## REFERENCES

---

- Berger, A.J., Zhu, Q., 2003. Identification of oral bacteria by raman microspectroscopy. *J. Mod. Opt.* 50, 2375–2380. <https://doi.org/10.1080/09500340308233569>
- Bocklitz, T., Walter, A., Hartmann, K., Rösch, P., Popp, J., 2011. How to pre-process Raman spectra for reliable and stable models? *Anal. Chim. Acta* 704, 47–56. <https://doi.org/10.1016/j.aca.2011.06.043>
- Böhme, R., Cialla, D., Richter, M., Rösch, P., Popp, J., Deckert, V., 2010. Biochemical imaging below the diffraction limit - probing cellular membrane related structures by tip-enhanced Raman spectroscopy (TERS). *J. Biophotonics* 3, 455–461. <https://doi.org/10.1002/jbio.201000030>
- Bonifacio, A., Beleites, C., Vittur, F., Marsich, E., Semeraro, S., Paoletti, S., Sergo, V., 2010. Chemical imaging of articular cartilage sections with Raman mapping, employing uni- and multi-variate methods for data analysis. *The Analyst* 135, 3193. <https://doi.org/10.1039/c0an00459f>
- Bouhaddani, S. el, Houwing-Duistermaat, J., Salo, P., Perola, M., Jongbloed, G., Uh, H.-W., 2016. Evaluation of O2PLS in Omics data integration. *BMC Bioinformatics* 17, S11. <https://doi.org/10.1186/s12859-015-0854-z>
- Bradley, P.S., Fayyad, U.M., 1998. Refining Initial Points for K-Means Clustering. *Microsoft Res.* 10.
- Branda, S.S., Vik, Å., Friedman, L., Kolter, R., 2005. Biofilms: the matrix revisited. *Trends Microbiol.* 13, 20–26. <https://doi.org/10.1016/j.tim.2004.11.006>
- Bridier, A., Piard, J.-C., Pandin, C., Labarthe, S., Dubois-Brissonnet, F., Briandet, R., 2017. Spatial Organization Plasticity as an Adaptive Driver of Surface Microbial Communities. *Front. Microbiol.* 8, 1364. <https://doi.org/10.3389/fmicb.2017.01364>
- Brooijmans, R.J.W., Pastink, M.I., Siezen, R.J., 2009. Hydrocarbon-degrading bacteria: the oil-spill clean-up crew. *Microb. Biotechnol.* 2, 587–594. <https://doi.org/10.1111/j.1751-7915.2009.00151.x>
- Bruun, S., 2013. Raman spectroscopy on microbial rhodopsins. Technische Universität Berlin.
- Bryers, J.D., 2008. Medical biofilms. *Biotechnol. Bioeng.* 100, 1–18. <https://doi.org/10.1002/bit.21838>
- Cals, F.L.J., Bakker Schut, T.C., Caspers, P.J., Baatenburg de Jong, R.J., Koljenović, S., Puppels, G.J., 2018. Raman spectroscopic analysis of the molecular composition of oral cavity squamous cell carcinoma and healthy tongue tissue. *The Analyst* 143, 4090–4102. <https://doi.org/10.1039/C7AN02106B>
- Caputo, P., Di Martino, M., Perfetto, B., Iovino, F., Donnarumma, G., 2018. Use of MALDI-TOF MS to Discriminate between Biofilm-Producer and Non-Producer Strains of *Staphylococcus epidermidis*. *Int. J. Environ. Res. Public Health* 15, 1695. <https://doi.org/10.3390/ijerph15081695>
- Carey, P.R., Gibson, B.R., Gibson, J.F., Greenberg, M.E., Heidari-Torkabadi, H., Pusztai-Carey, M., Weaver, S.T., Whitmer, G.R., 2017. Defining Molecular Details of the Chemistry of Biofilm Formation by Raman Microspectroscopy. *Biochemistry* 56, 2247–2250. <https://doi.org/10.1021/acs.biochem.7b00116>
- Cepeda-Pérez, E., Moreno-Hernández, C., López-Luke, T., Monzón-Hernández, D., de la Rosa, E., 2016. Evaluation of bacterial presence in the root canal by Raman spectroscopy: a preliminary study. *Biomed. Phys. Eng. Express* 2, 065006. <https://doi.org/10.1088/2057-1976/2/6/065006>
- Chao, Y., Zhang, T., 2012. Surface-enhanced Raman scattering (SERS) revealing chemical variation during biofilm formation: from initial attachment to mature biofilm. *Anal. Bioanal. Chem.* 404, 1465–1475. <https://doi.org/10.1007/s00216-012-6225-y>
- Cheeseman, S., Shaw, Z.L., Vongsvivut, J., Crawford, R.J., Dupont, M.F., Boyce, K.J., Gangadoo, S., Bryant, S.J., Bryant, G., Cozzolino, D., Chapman, J., Elbourne, A.,

## REFERENCES

---

- Truong, V.K., 2021. Analysis of Pathogenic Bacterial and Yeast Biofilms Using the Combination of Synchrotron ATR-FTIR Microspectroscopy and Chemometric Approaches. *Molecules* 26, 3890. <https://doi.org/10.3390/molecules26133890>
- Colnița, A., Dina, N., Leopold, N., Vodnar, D., Bogdan, D., Porav, S., David, L., 2017. Characterization and Discrimination of Gram-Positive Bacteria Using Raman Spectroscopy with the Aid of Principal Component Analysis. *Nanomaterials* 7, 248. <https://doi.org/10.3390/nano7090248>
- Costerton, J.W., 1999. Bacterial Biofilms: A Common Cause of Persistent Infections. *Science* 284, 1318–1322. <https://doi.org/10.1126/science.284.5418.1318>
- Daood, U., Burrow, M.F., Yiu, C.K.Y., 2020. Effect of a novel quaternary ammonium silane cavity disinfectant on cariogenic biofilm formation. *Clin. Oral Investig.* 24, 649–661. <https://doi.org/10.1007/s00784-019-02928-7>
- Darrene, L.-N., Cecile, B., 2016. Experimental Models of Oral Biofilms Developed on Inert Substrates: A Review of the Literature. *BioMed Res. Int.* 2016, 1–8. <https://doi.org/10.1155/2016/7461047>
- De Gelder, J., 2008. Raman spectroscopy as a tool for studying bacterial cell compounds (dissertation). Ghent University.
- De Gelder, J., De Gussem, K., Vandenabeele, P., Moens, L., 2007. Reference database of Raman spectra of biological molecules. *J. Raman Spectrosc.* 38, 1133–1147. <https://doi.org/10.1002/jrs.1734>
- Dhankhar, D., Nagpal, A., Li, R., Chen, J., Cesario, T.C., Rentzepis, P.M., 2021. Resonance Raman Spectra for the In Situ Identification of Bacteria Strains and Their Inactivation Mechanism. *Appl. Spectrosc.* 000370282199283. <https://doi.org/10.1177/0003702821992834>
- Diaz, P.I., Chalmers, N.I., Rickard, A.H., Kong, C., Milburn, C.L., Palmer, R.J., Kolenbrander, P.E., 2006. Molecular Characterization of Subject-Specific Oral Microflora during Initial Colonization of Enamel. *Appl. Environ. Microbiol.* 72, 2837–2848. <https://doi.org/10.1128/AEM.72.4.2837-2848.2006>
- Dillon, W.R., Goldstein, M., 1984. *Multivariate Analysis: Methods and Applications* | Wiley, 1st ed, Wiley Series in Probability and Statistics. John Wiley & Sons Inc, New York, USA.
- Di Pippo, F., Di Gregorio, L., Congestri, R., Tandoi, V., Rossetti, S., 2018. Biofilm growth and control in cooling water industrial systems. *FEMS Microbiol. Ecol.* 94, fiy044. <https://doi.org/10.1093/femsec/fiy044>
- Döring, C., Lesot, M.-J., Kruse, R., 2006. Data analysis with fuzzy clustering methods. *Comput. Stat. Data Anal.* 51, 192–214. <https://doi.org/10.1016/j.csda.2006.04.030>
- El Senousy, A.S., Farag, M.A., Al-Mahdy, D.A., Wessjohann, L.A., 2014. Developmental changes in leaf phenolics composition from three artichoke cvs. (*Cynara scolymus*) as determined via UHPLC–MS and chemometrics. *Phytochemistry* 108, 67–76. <https://doi.org/10.1016/j.phytochem.2014.09.004>
- Everall, N., 2008. The Influence of Out-of-Focus Sample Regions on the Surface Specificity of Confocal Raman Microscopy. *Appl. Spectrosc.* 62, 591–598. <https://doi.org/10.1366/000370208784658057>
- Fanesi, A., Zegeye, A., Mustin, C., Cébron, A., 2018. Soil Particles and Phenanthrene Interact in Defining the Metabolic Profile of *Pseudomonas putida* G7: A Vibrational Spectroscopy Approach. *Front. Microbiol.* 9, 2999. <https://doi.org/10.3389/fmicb.2018.02999>
- Feng, Z., Hou, J., Yu, Y., Wu, Wenyong, Deng, Y., Wang, X., Zhi, H., Zhang, L., Wu, Wanying, Guo, D., 2019. Dissecting the Metabolic Phenotype of the Antihypertensive Effects of Five *Uncaria* Species on Spontaneously Hypertensive Rats. *Front. Pharmacol.* 10, 845. <https://doi.org/10.3389/fphar.2019.00845>

## REFERENCES

---

- Fernández-Delgado, M., Duque, Z., Rojas, H., Suárez, P., Contreras, M., García-Amado, M.A., Alciaturi, C., 2015. Environmental scanning electron microscopy analysis of *Proteus mirabilis* biofilms grown on chitin and stainless steel. *Ann. Microbiol.* 65, 1401–1409. <https://doi.org/10.1007/s13213-014-0978-9>
- Fleischmann, M., Hendra, P.J., McQUILLAN, A.J., 1974. Raman Spectra of Pyridine Adsorbed at a Silver Electrode. *Chem. Phys. Lett.* 26, 4.
- Flemming, H.-C., 2011. The perfect slime. *Colloids Surf. B Biointerfaces* 86, 251–259. <https://doi.org/10.1016/j.colsurfb.2011.04.025>
- Flemming, H.-C., Neu, T.R., Wozniak, D.J., 2007. The EPS Matrix: The “House of Biofilm Cells.” *J. Bacteriol.* 189, 7945–7947. <https://doi.org/10.1128/JB.00858-07>
- Flemming, H.-C., Wingender, J., 2010. The biofilm matrix. *Nat. Rev. Microbiol.* 8, 623–633. <https://doi.org/10.1038/nrmicro2415>
- Gieroba, B., Krysa, M., Wojtowicz, K., Wiater, A., Pleszczyńska, M., Tomczyk, M., Sroka-Bartnicka, A., 2020. The FT-IR and Raman Spectroscopies as Tools for Biofilm Characterization Created by Cariogenic Streptococci. *Int. J. Mol. Sci.* 21, 3811. <https://doi.org/10.3390/ijms21113811>
- Gmür, R., Guggenheim, B., 1983. Antigenic heterogeneity of *Bacteroides intermedius* as recognized by monoclonal antibodies. *Infect. Immun.* 42, 459–470. <https://doi.org/10.1128/IAI.42.2.459-470.1983>
- Gmür, R., Lüthi-Schaller, H., 2007. A combined immunofluorescence and fluorescent in situ hybridization assay for single cell analyses of dental plaque microorganisms. *J. Microbiol. Methods* 69, 402–405. <https://doi.org/10.1016/j.mimet.2006.12.012>
- Grainha, T., Jorge, P., Alves, D., Lopes, S.P., Pereira, M.O., 2020. Unraveling *Pseudomonas aeruginosa* and *Candida albicans* Communication in Coinfection Scenarios: Insights Through Network Analysis. *Front. Cell. Infect. Microbiol.* 10, 550505. <https://doi.org/10.3389/fcimb.2020.550505>
- Gualerzi, A., Niada, S., Giannasi, C., Picciolini, S., Morasso, C., Vanna, R., Rossella, V., Masserini, M., Bedoni, M., Ciceri, F., Bernardo, M.E., Brini, A.T., Gramatica, F., 2017. Raman spectroscopy uncovers biochemical tissue-related features of extracellular vesicles from mesenchymal stromal cells. *Sci. Rep.* 7, 9820. <https://doi.org/10.1038/s41598-017-10448-1>
- Guggenheim, B., Gmür, R., Galicia, J.C., Stathopoulou, P.G., Benakanakere, M.R., Meier, A., Thurnheer, T., Kinane, D.F., 2009. In vitro modeling of host-parasite interactions: the “subgingival” biofilm challenge of primary human epithelial cells. *BMC Microbiol.* 9, 280. <https://doi.org/10.1186/1471-2180-9-280>
- Guggenheim, B., Guggenheim, M., Gmür, R., Giertsen, E., Thurnheer, T., 2004. Application of the Zürich Biofilm Model to Problems of Cariology. *Caries Res.* 38, 212–222. <https://doi.org/10.1159/000077757>
- Guo, S., 2018. Chemometrics and statistical analysis in raman spectroscopy-based biological investigations. Friedrich-Schiller-Universität Jena, Chemisch-Geowissenschaftliche Fakultät, Jena.
- Guo, S., Bocklitz, T., Popp, J., 2016. Optimization of Raman-spectrum baseline correction in biological application. *The Analyst* 141, 2396–2404. <https://doi.org/10.1039/C6AN00041J>
- Hahnel, S., 2007. Die Eignung von Proteinmischungen als Speichelersatz für die bakterielle in vivo Adhäsion. Universität Regensburg.
- Hall-Stoodley, L., Costerton, J.W., Stoodley, P., 2004. Bacterial biofilms: from the Natural environment to infectious diseases. *Nat. Rev. Microbiol.* 2, 95–108. <https://doi.org/10.1038/nrmicro821>

## REFERENCES

---

- Hamasha, K.M., 2011. Raman spectroscopy for the microbiological characterization and identification of medically relevant bacteria. Wayne State University, Detroit, Michigan, USA.
- Hannig, M., Joiner, A., 2006. The Structure, Function and Properties of the Acquired Pellicle. *elsevier* 2, 1599–1607. <https://doi.org/10.1159/000090585>
- Harris, D.C., Bertolucci, M.D., 1978. Symmetry and spectroscopy: an introduction to vibrational and electronic spectroscopy. Oxford University Press.
- Harz, M., Rösch, P., Peschke, K.-D., Ronneberger, O., Burkhardt, H., Popp, J., 2005. Micro-Raman spectroscopic identification of bacterial cells of the genus *Staphylococcus* and dependence on their cultivation conditions. *The Analyst* 130, 1543. <https://doi.org/10.1039/b507715j>
- Hermann, C., Hermann, J., Munzel, U., Ruchel, R., 1999. Bacterial flora accompanying *Candida* yeasts in clinical specimens. *Mycoses* 42, 619–627. <https://doi.org/10.1046/j.1439-0507.1999.00519.x>
- Hogan, D.A., Kolter, R., 2002. Pseudomonas-Candida Interactions: An Ecological Role for Virulence Factors. *Science* 296, 2229–2232. <https://doi.org/10.1126/science.1070784>
- Holman, H.-Y.N., Miles, R., Hao, Z., Wozel, E., Anderson, L.M., Yang, H., 2009. Real-Time Chemical Imaging of Bacterial Activity in Biofilms Using Open-Channel Microfluidics and Synchrotron FTIR Spectromicroscopy. *Anal. Chem.* 81, 8564–8570. <https://doi.org/10.1021/ac9015424>
- Horiue, H., Sasaki, M., Yoshikawa, Y., Toyofuku, M., Shigeto, S., 2020. Raman spectroscopic signatures of carotenoids and polyenes enable label-free visualization of microbial distributions within pink biofilms. *Sci. Rep.* 10, 7704. <https://doi.org/10.1038/s41598-020-64737-3>
- Huang, R., Li, M., Gregory, R.L., 2011. Bacterial interactions in dental biofilm. *Virulence* 2, 435–444. <https://doi.org/10.4161/viru.2.5.16140>
- Huang, Y., Chakraborty, S., Liang, H., 2020. Methods to probe the formation of biofilms: applications in foods and related surfaces. *Anal. Methods* 12, 416–432. <https://doi.org/10.1039/C9AY02214G>
- Hutchings, J., Kendall, C., Shepherd, N., Barr, H., Stone, N., 2010. Evaluation of linear discriminant analysis for automated Raman histological mapping of esophageal high-grade dysplasia. *J. Biomed. Opt.* 15, 066015. <https://doi.org/10.1117/1.3512244>
- Ivleva, N.P., Wagner, M., Szkola, A., Horn, H., Niessner, R., Haisch, C., 2010. Label-Free in Situ SERS Imaging of Biofilms. *J. Phys. Chem. B* 114, 10184–10194. <https://doi.org/10.1021/jp102466c>
- James, S.A., Powell, L.C., Wright, C.J., 2016. Atomic Force Microscopy of Biofilms—Imaging, Interactions, and Mechanics, in: *Microbial Biofilms - Importance and Applications*. IntechOpen, London, United Kingdom, pp. 95–118.
- Jansons, V.K., Nickerson, W.J., 1970. Chemical composition of chlamydospores of *Candida albicans*. *J. Bacteriol.* 104, 922–932. <https://doi.org/10.1128/jb.104.2.922-932.1970>
- Jarvis, R.M., Goodacre, R., 2004. Discrimination of Bacteria Using Surface-Enhanced Raman Spectroscopy. *Anal. Chem.* 76, 40–47. <https://doi.org/10.1021/ac034689c>
- Jefferson, K.K., 2004. What drives bacteria to produce a biofilm? *FEMS Microbiol. Lett.* 236, 163–173. <https://doi.org/10.1111/j.1574-6968.2004.tb09643.x>
- Jung, G.B., Nam, S.W., Choi, S., Lee, G.-J., Park, H.-K., 2014. Evaluation of antibiotic effects on *Pseudomonas aeruginosa* biofilm using Raman spectroscopy and multivariate analysis. *Biomed. Opt. Express* 5, 3238. <https://doi.org/10.1364/BOE.5.003238>
- Kahraman, M., Zamaleeva, A.I., Fakhruddin, R.F., Culha, M., 2009. Layer-by-layer coating of bacteria with noble metal nanoparticles for surface-enhanced Raman scattering. *Anal. Bioanal. Chem.* 395, 2559–2567. <https://doi.org/10.1007/s00216-009-3159-0>

## REFERENCES

---

- Karygianni, L., Ren, Z., Koo, H., Thurnheer, T., 2020. Biofilm Matrixome: Extracellular Components in Structured Microbial Communities. *Trends Microbiol.* 28, 668–681. <https://doi.org/10.1016/j.tim.2020.03.016>
- Kawata, S., Ichimura, T., Taguchi, A., Kumamoto, Y., 2017. Nano-Raman Scattering Microscopy: Resolution and Enhancement. *Chem. Rev.* 117, 4983–5001. <https://doi.org/10.1021/acs.chemrev.6b00560>
- Keleştemur, S., Çobandede, Z., Çulha, M., 2020. Biofilm formation of clinically important microorganisms on 2D and 3D poly (methyl methacrylate) substrates: A surface-enhanced Raman scattering study. *Colloids Surf. B Biointerfaces* 188, 110765. <https://doi.org/10.1016/j.colsurfb.2019.110765>
- Kerr, J.R., Taylor, G.W., Rutman, A., Hoiby, N., Cole, P.J., Wilson, R., 1999. *Pseudomonas aeruginosa* pyocyanin and 1-hydroxyphenazine inhibit fungal growth. *J. Clin. Pathol.* 52, 385–387. <https://doi.org/10.1136/jcp.52.5.385>
- Klein, M.I., Hwang, G., Santos, P.H.S., Campanella, O.H., Koo, H., 2015. *Streptococcus mutans*-derived extracellular matrix in cariogenic oral biofilms. *Front. Cell. Infect. Microbiol.* 5. <https://doi.org/10.3389/fcimb.2015.00010>
- Kniggendorf, A.-K., Gaul, T.W., Meinhardt-Wollweber, M., 2011. Hierarchical Cluster Analysis (HCA) of Microorganisms: An Assessment of Algorithms for Resonance Raman Spectra. *Appl. Spectrosc.* 65, 165–173. <https://doi.org/10.1366/10-06064>
- Kniggendorf, A.-K., Meinhardt-Wollweber, M., 2011. Of microparticles and bacteria identification – (resonance) Raman micro-spectroscopy as a tool for biofilm analysis. *Water Res.* 45, 4571–4582. <https://doi.org/10.1016/j.watres.2011.06.007>
- Kokare, C.R., Chakraborty, S., Khopade, A.N., Mahadik, K.R., 2009. Biofilm: Importance and applications. *INDIAN J BIOTECHNOL* 10.
- Kolenbrander, P.E., London, J., 1993. Adhere today, here tomorrow: oral bacterial adherence. *J. Bacteriol.* 175, 3247–3252. <https://doi.org/10.1128/JB.175.11.3247-3252.1993>
- Kommerein, N., Stumpp, S.N., Müsken, M., Ehlert, N., Winkel, A., Häussler, S., Behrens, P., Buettner, F.F.R., Stiesch, M., 2017. An oral multispecies biofilm model for high content screening applications. *PLOS ONE* 12, e0173973. <https://doi.org/10.1371/journal.pone.0173973>
- Kompauer, M., Heiles, S., Spengler, B., 2017. Atmospheric pressure MALDI mass spectrometry imaging of tissues and cells at 1.4- $\mu\text{m}$  lateral resolution. *Nat. Methods* 14, 90–96. <https://doi.org/10.1038/nmeth.4071>
- Koo, H., Xiao, J., Klein, M.I., Jeon, J.G., 2010. Exopolysaccharides Produced by *Streptococcus mutans* Glucosyltransferases Modulate the Establishment of Microcolonies within Multispecies Biofilms. *J. Bacteriol.* 192, 3024–3032. <https://doi.org/10.1128/JB.01649-09>
- Krafft, C., Popp, J., 2019. Micro-Raman spectroscopy in medicine. *Phys. Sci. Rev.* 4. <https://doi.org/10.1515/psr-2017-0047>
- Kriem, L.S., Wright, K., Ccahuana-Vasquez, R.A., Rupp, S., 2021. Mapping of a Subgingival Dual-Species Biofilm Model Using Confocal Raman Microscopy. *Front. Microbiol.* 12, 729720. <https://doi.org/10.3389/fmicb.2021.729720>
- Kriem, L.S., Wright, K., Ccahuana-Vasquez, R.A., Rupp, S., 2020. Confocal Raman microscopy to identify bacteria in oral subgingival biofilm models. *PLOS ONE* 15, e0232912. <https://doi.org/10.1371/journal.pone.0232912>
- Kubryk, P., 2017. Stabilisotopen-Raman-Mikrospektroskopie zur Untersuchung von Mikroorganismen. Technische Universität München, München.
- Kudelski, A., 2008. Analytical applications of Raman spectroscopy. *Talanta* 76, 1–8. <https://doi.org/10.1016/j.talanta.2008.02.042>

## REFERENCES

---

- Kuhar, N., Sil, S., Umapathy, S., 2021. Potential of Raman spectroscopic techniques to study proteins. *Spectrochim. Acta. A. Mol. Biomol. Spectrosc.* 258, 119712. <https://doi.org/10.1016/j.saa.2021.119712>
- Kuhar, N., Sil, S., Verma, T., Umapathy, S., 2018. Challenges in application of Raman spectroscopy to biology and materials. *RSC Adv.* 8, 25888–25908. <https://doi.org/10.1039/C8RA04491K>
- Kumar, S., Matange, N., Umapathy, S., Visweswariah, S.S., 2015. Linking carbon metabolism to carotenoid production in mycobacteria using Raman spectroscopy. *FEMS Microbiol. Lett.* 362, 1–6. <https://doi.org/10.1093/femsle/fnu048>
- Kumar, S., Verma, T., Mukherjee, R., Ariese, F., Somasundaram, K., Umapathy, S., 2016. Raman and infra-red microspectroscopy: towards quantitative evaluation for clinical research by ratiometric analysis. *Chem. Soc. Rev.* 45, 1879–1900. <https://doi.org/10.1039/C5CS00540J>
- Kurouski, D., 2017. Advances of tip-enhanced Raman spectroscopy (TERS) in electrochemistry, biochemistry, and surface science. *Vib. Spectrosc., Prominent Young Vibrational Spectroscopists* 91, 3–15. <https://doi.org/10.1016/j.vibspec.2016.06.004>
- Kusić, D., Kampe, B., Ramoji, A., Neugebauer, U., Rösch, P., Popp, J., 2015. Raman spectroscopic differentiation of planktonic bacteria and biofilms. *Anal. Bioanal. Chem.* 407, 6803–6813. <https://doi.org/10.1007/s00216-015-8851-7>
- Kusić, D., Kampe, B., Rösch, P., Popp, J., 2014. Identification of water pathogens by Raman microspectroscopy. *Water Res.* 48, 179–189. <https://doi.org/10.1016/j.watres.2013.09.030>
- Landau, L.D., Lifshitz, E.M., 1976. *Mechanics*, 3rd. ed. ed. Pergamon Press.
- Lawrence, J.R., Delaquis, P.J., Korber, D.R., Caldwell, D.E., 1987. Behavior of *Pseudomonas fluorescens* within the hydrodynamic boundary layers of surface microenvironments. *Microb. Ecol.* 14, 1–14. <https://doi.org/10.1007/BF02011566>
- Lawrence, J.R., Neu, T.R., Swerhone, G.D.W., 1998. Application of multiple parameter imaging for the quantification of algal, bacterial and exopolymer components of microbial biofilms. *J. Microbiol. Methods* 32, 253–261. [https://doi.org/10.1016/S0167-7012\(98\)00027-X](https://doi.org/10.1016/S0167-7012(98)00027-X)
- Lee, K.S., Landry, Z., Pereira, F.C., Wagner, M., Berry, D., Huang, W.E., Taylor, G.T., Kneipp, J., Popp, J., Zhang, M., Cheng, J.-X., Stocker, R., 2021. Raman microspectroscopy for microbiology. *Nat. Rev. Methods Primer* 1, 80. <https://doi.org/10.1038/s43586-021-00075-6>
- Lemon, K.P., Earl, A.M., Vlamakis, H.C., Aguilar, C., Kolter, R., 2008. Biofilm Development with an Emphasis on *Bacillus subtilis*, in: Romeo, T. (Ed.), *Bacterial Biofilms, Current Topics in Microbiology and Immunology*. Springer Berlin Heidelberg, Berlin, Heidelberg, pp. 1–16. [https://doi.org/10.1007/978-3-540-75418-3\\_1](https://doi.org/10.1007/978-3-540-75418-3_1)
- Lendenmann, U., Grogan, J., Oppenheim, F.G., 2000. Saliva and dental pellicle—a review. *Adv. Dent. Res.* 14, 22–28. <https://doi.org/10.1177/08959374000140010301>
- Lewis, K., 2001. Riddle of Biofilm Resistance. *Antimicrob. Agents Chemother.* 45, 999–1007. <https://doi.org/10.1128/AAC.45.4.999-1007.2001>
- Li, J., Helmerhorst, E.J., Leone, C.W., Troxler, R.F., Yaskell, T., Haffajee, A.D., Socransky, S.S., Oppenheim, F.G., 2004. Identification of early microbial colonizers in human dental biofilm. *J. Appl. Microbiol.* 97, 1311–1318. <https://doi.org/10.1111/j.1365-2672.2004.02420.x>
- Li, M., Canniffe, D.P., Jackson, P.J., Davison, P.A., FitzGerald, S., Dickman, M.J., Burgess, J.G., Hunter, C.N., Huang, W.E., 2012. Rapid resonance Raman microspectroscopy to



## REFERENCES

---

- probe carbon dioxide fixation by single cells in microbial communities. *ISME J.* 6, 875–885. <https://doi.org/10.1038/ismej.2011.150>
- Li, R., Dhankhar, D., Chen, J., Krishnamoorthi, A., Cesario, T.C., Rentzepis, P.M., 2019. Identification of Live and Dead Bacteria: A Raman Spectroscopic Study. *IEEE Access* 7, 23549–23559. <https://doi.org/10.1109/ACCESS.2019.2899006>
- Liu, X.-Y., Guo, S., Bocklitz, T., Rösch, P., Popp, J., Yu, H.-Q., 2022. Nondestructive 3D imaging and quantification of hydrated biofilm matrix by confocal Raman microscopy coupled with non-negative matrix factorization. *Water Res.* 210, 117973. <https://doi.org/10.1016/j.watres.2021.117973>
- Liu, X.-Y., Guo, S., Ramoji, A., Bocklitz, T., Rösch, P., Popp, J., Yu, H.-Q., 2020. Spatiotemporal Organization of Biofilm Matrix Revealed by Confocal Raman Mapping Integrated with Non-negative Matrix Factorization Analysis. *Anal. Chem.* 92, 707–715. <https://doi.org/10.1021/acs.analchem.9b02593>
- Lorenz, B., Wichmann, C., Stöckel, S., Rösch, P., Popp, J., 2017. Cultivation-Free Raman Spectroscopic Investigations of Bacteria. *Trends Microbiol.* 25, 413–424. <https://doi.org/10.1016/j.tim.2017.01.002>
- Lu, X., Al-Qadiri, H.M., Lin, M., Rasco, B.A., 2011. Application of Mid-infrared and Raman Spectroscopy to the Study of Bacteria. *Food Bioprocess Technol.* 4, 919–935. <https://doi.org/10.1007/s11947-011-0516-8>
- Lynge Pedersen, A.M., Belstrøm, D., 2019. The role of natural salivary defences in maintaining a healthy oral microbiota. *J. Dent.* 80, S3–S12. <https://doi.org/10.1016/j.jdent.2018.08.010>
- Madigan, M.T., Bender, K.S., Buckley, D.H., Sattley, W.M., Stahl, D.A., 2018. *Brock Biology of Microorganisms*, 15th ed. Pearson, London, United Kingdom.
- Mah, T.-F., 2012. Biofilm-specific antibiotic resistance. *Future Microbiol.* 7, 1061–1072. <https://doi.org/10.2217/fmb.12.76>
- Maitra, I., Morais, C.L.M., Lima, K.M.G., Ashton, K.M., Bury, D., Date, R.S., Martin, F.L., 2020. Establishing spectrochemical changes in the natural history of oesophageal adenocarcinoma from tissue Raman mapping analysis. *Anal. Bioanal. Chem.* 412, 4077–4087. <https://doi.org/10.1007/s00216-020-02637-1>
- Malik, A., Sahu, A., Singh, S.P., Deshmukh, A., Chaturvedi, P., Nair, D., Nair, S., Murali Krishna, C., 2017. In vivo Raman spectroscopy-assisted early identification of potential second primary/recurrences in oral cancers: An exploratory study. *Head Neck* 39, 2216–2223. <https://doi.org/10.1002/hed.24884>
- Manoharan, R., Ghiamati, E., Dalterio, R.A., Britton, K.A., Nelson, W.H., Sperry, J.F., 1990. UV resonance Raman spectra of bacteria, bacterial spores, protoplasts and calcium dipicolinate. *J. Microbiol. Methods* 11, 1–15. [https://doi.org/10.1016/0167-7012\(90\)90042-5](https://doi.org/10.1016/0167-7012(90)90042-5)
- Maquelin, K., Choo-Smith, L.-P., Endtz, H.P., Bruining, H.A., Puppels, G.J., 2002. Rapid Identification of *Candida* Species by Confocal Raman Microspectroscopy. *J. Clin. Microbiol.* 40, 594–600. <https://doi.org/10.1128/JCM.40.2.594-600.2002>
- Marsh, P., Martin, M., 2009. *Oral microbiology*, 5th ed. ed. Elsevier, Edinburgh ; New York.
- Marsh, P.D., 2004. Dental Plaque as a Microbial Biofilm. *Caries Res.* 38, 204–211. <https://doi.org/10.1159/000077756>
- Marsh, P.D., Moter, A., Devine, D.A., 2011. Dental plaque biofilms: communities, conflict and control: Plaque biofilms and communities. *Periodontol.* 2000 55, 16–35. <https://doi.org/10.1111/j.1600-0757.2009.00339.x>
- McCabe, R.M., Donkersloot, J.A., 1977. Adherence of Veillonella Species Mediated by Extracellular Glucosyltransferase from Streptococcus salivarius. *Infect. Immun.* 18, 726–734. <https://doi.org/10.1128/IAI.18.3.726-734.1977>

## REFERENCES

---

- McDonnell, L.A., Heeren, R.M.A., 2007. Imaging mass spectrometry. *Mass Spectrom. Rev.* 26, 606–643. <https://doi.org/10.1002/mas.20124>
- Mikac, L., Ivanda, M., Gotic, M., Ristic, D., Derek, V., Gebavi, H., Gucciardi, P.G., Trusso, S., D'Andrea, C., 2015. Preparation and characterization of SERS substrates: From colloids to solid substrates, in: 2015 38th International Convention on Information and Communication Technology, Electronics and Microelectronics (MIPRO). Presented at the 2015 38th International Convention on Information and Communication Technology, Electronics and Microelectronics (MIPRO), IEEE, Opatija, Croatia, pp. 9–11. <https://doi.org/10.1109/MIPRO.2015.7160228>
- Myintzu Hlaing, M., Wood, B., McNaughton, D., Ying, D., Augustin, M.A., 2017. Raman spectroscopic analysis of *Lactobacillus rhamnosus* GG in response to dehydration reveals DNA conformation changes. *J. Biophotonics* 10, 589–597. <https://doi.org/10.1002/jbio.201600046>
- Neugebauer, U., Schmid, U., Baumann, K., Ziebuhr, W., Kozitskaya, S., Deckert, V., Schmitt, M., Popp, J., 2007. Towards a Detailed Understanding of Bacterial Metabolism—Spectroscopic Characterization of *Staphylococcus Epidermidis*. *ChemPhysChem* 8, 124–137. <https://doi.org/10.1002/cphc.200600507>
- Nocker, A., Fernández, P.S., Montijn, R., Schuren, F., 2012. Effect of air drying on bacterial viability: A multiparameter viability assessment. *J. Microbiol. Methods* 90, 86–95. <https://doi.org/10.1016/j.mimet.2012.04.015>
- OPLS vs PCA: Explaining Differences or Grouping Data? [WWW Document], 2020. . Sartorius. URL <https://www.sartorius.com/en/knowledge/science-snippets/explaining-differences-or-grouping-data-opls-da-vs-pca-data-analysis-507204> (accessed 12.4.21).
- Pahlow, S., März, A., Seise, B., Hartmann, K., Freitag, I., Kämmer, E., Böhme, R., Deckert, V., Weber, K., Cialla, D., Popp, J., 2012. Bioanalytical application of surface- and tip-enhanced Raman spectroscopy: Bioanalytical application of SERS and TERS. *Eng. Life Sci.* 12, 131–143. <https://doi.org/10.1002/elsc.201100056>
- Pantarella, F., Valenti, P., Natalizi, T., Passeri, D., Berlutti, F., 2013. Analytical techniques to study microbial biofilm on abiotic surfaces: pros and cons of the main techniques currently in use 12.
- Paraskevaidi, M., Matthew, B.J., Holly, B.J., Hugh, B.J., Thulya, C.P.V., Loren, C., StJohn, C., Peter, G., Callum, G., Sergei, K.G., Kamila, K., Maria, K., Kássio, L.M.G., Pierre, M.-H.L., Evangelos, P., Savithri, P., John, A.A., Alexandra, S., Marfran, S., Josep, S.-S., Gunjan, T., Michael, W., Bayden, W., 2021. Clinical applications of infrared and Raman spectroscopy in the fields of cancer and infectious diseases. *Appl. Spectrosc. Rev.* 56, 804–868. <https://doi.org/10.1080/05704928.2021.1946076>
- Paret, M.L., Sharma, S.K., Green, L.M., Alvarez, A.M., 2010. Biochemical Characterization of Gram-Positive and Gram-Negative Plant-Associated Bacteria with Micro-Raman Spectroscopy. *Appl. Spectrosc.* 64, 433–441. <https://doi.org/10.1366/000370210791114293>
- Parthasarathy, R., Thiagarajan, G., Yao, X., Wang, Y.-P., Spencer, P., Wang, Y., 2008. Application of multivariate spectral analyses in micro-Raman imaging to unveil structural/chemical features of the adhesive/dentin interface. *J. Biomed. Opt.* 13, 014020. <https://doi.org/10.1117/1.2857402>
- Pearson, K., 1901. On lines and planes of closest fit to systems of points in space. *Lond. Edinb. Dublin Philos. Mag. J. Sci.* 2, 559–572. <https://doi.org/10.1080/14786440109462720>
- Peleg, A.Y., Hogan, D.A., Mylonakis, E., 2010. Medically important bacterial–fungal interactions. *Nat. Rev. Microbiol.* 8, 340–349. <https://doi.org/10.1038/nrmicro2313>
- Pereira, F.D.E.S., Bonatto, C.C., Lopes, C.A.P., Pereira, A.L., Silva, L.P., 2015. Use of MALDI-TOF mass spectrometry to analyze the molecular profile of *Pseudomonas*

## REFERENCES

---

- aeruginosa biofilms grown on glass and plastic surfaces. *Microb. Pathog.* 86, 32–37. <https://doi.org/10.1016/j.micpath.2015.07.005>
- Pezzotti, G., 2021. Raman spectroscopy in cell biology and microbiology. *J. Raman Spectrosc. jrs.6204*. <https://doi.org/10.1002/jrs.6204>
- Potter, M., Hanson, C., Anderson, A.J., Vargis, E., Britt, D.W., 2020. Abiotic stressors impact outer membrane vesicle composition in a beneficial rhizobacterium: Raman spectroscopy characterization. *Sci. Rep.* 10, 21289. <https://doi.org/10.1038/s41598-020-78357-4>
- Pringle, J.H., Fletcher, M., 1983. Influence of Substratum Wettability on Attachment of Freshwater Bacteria to Solid Surfaces. *APPL Env. MICROBIOL* 45, 7.
- Probst, A.J., Holman, H.-Y.N., DeSantis, T.Z., Andersen, G.L., Birarda, G., Bechtel, H.A., Piceno, Y.M., Sonnleitner, M., Venkateswaran, K., Moissl-Eichinger, C., 2013. Tackling the minority: sulfate-reducing bacteria in an archaea-dominated subsurface biofilm. *ISME J.* 7, 635–651. <https://doi.org/10.1038/ismej.2012.133>
- Puiu, R.A., Dolete, G., Ene, A.-M., Nicoară, B., Vlăsceanu, G.M., Holban, A.M., Grumezescu, A.M., Bolocan, A., 2017. Properties of biofilms developed on medical devices, in: *Biofilms and Implantable Medical Devices*. Elsevier, pp. 25–46. <https://doi.org/10.1016/B978-0-08-100382-4.00002-2>
- Purschke, F.G., 2012. Phänotypische und molekularbiologische Untersuchungen der Interaktionen in gemischten Biofilmen. Phenotypic and molecularbiological analyses of interactions in mixed biofilms. <https://doi.org/10.18419/opus-2014>
- Purschke, F.G., Hiller, E., Trick, I., Rupp, S., 2012. Flexible Survival Strategies of *Pseudomonas aeruginosa* in Biofilms Result in Increased Fitness Compared with *Candida albicans*. *Mol. Cell. Proteomics* 11, 1652–1669. <https://doi.org/10.1074/mcp.M112.017673>
- Raman, C.V., Krishnan, K.S., 1928. A New Type of Secondary Radiation. *Nature* 121, 501–502. <https://doi.org/10.1038/121501c0>
- Ramberg, P., Sekino, S., Uzel, N.G., Socransky, S., Lindhe, J., 2003. Bacterial colonization during de novo plaque formation: Bacteria and developing plaque. *J. Clin. Periodontol.* 30, 990–995. <https://doi.org/10.1034/j.1600-051X.2003.00419.x>
- Ramirez-Mora, T., Dávila-Pérez, C., Torres-Méndez, F., Valle-Bourrouet, G., 2019. Raman Spectroscopic Characterization of Endodontic Biofilm Matrices. *J. Spectrosc.* 2019, 1–7. <https://doi.org/10.1155/2019/1307397>
- Rasband, W.S., 1997. ImageJ. U. S. National Institutes of Health, Bethesda, Maryland, USA.
- Rather, M.A., Gupta, K., Mandal, M., 2021. Microbial biofilm: formation, architecture, antibiotic resistance, and control strategies. *Braz. J. Microbiol.* 52, 1701–1718. <https://doi.org/10.1007/s42770-021-00624-x>
- Rebrošová, K., Šiler, M., Samek, O., Růžička, F., Bernatová, S., Holá, V., Ježek, J., Zemánek, P., Sokolová, J., Petráš, P., 2017. Rapid identification of staphylococci by Raman spectroscopy. *Sci. Rep.* 7, 14846. <https://doi.org/10.1038/s41598-017-13940-w>
- Rebrošová, K., Šiler, M., Samek, O., Růžička, F., Bernatová, S., Ježek, J., Zemánek, P., Holá, V., 2019. Identification of ability to form biofilm in *Candida parapsilosis* and *Staphylococcus epidermidis* by Raman spectroscopy. *Future Microbiol.* 14, 509–517. <https://doi.org/10.2217/fmb-2018-0297>
- Re-discovering Bacterial Biofilm Heterogeneity with MALDI Mass Spectrometry Imaging [WWW Document], n.d. . HTX Imaging. URL <http://www.htximaging.com/htx-an40> (accessed 1.23.22).
- Rinnan, Å., 2014. Pre-processing in vibrational spectroscopy – when, why and how. *Anal Methods* 6, 7124–7129. <https://doi.org/10.1039/C3AY42270D>

## REFERENCES

---

- Römling, U., Kjelleberg, S., Normark, S., Nyman, L., Uhlin, B.E., Åkerlund, B., 2014. Microbial biofilm formation: a need to act. *J. Intern. Med.* 276, 98–110. <https://doi.org/10.1111/joim.12242>
- Rosan, B., Hammond, B.F., 1974. Extracellular Polysaccharides of *Actinomyces viscosus*. *Infect. Immun.* 10, 304–308. <https://doi.org/10.1128/iai.10.2.304-308.1974>
- Rostron, P., Gaber, S., Gaber, D., 2016. Raman spectroscopy, Review. *Int. J. Eng. Tech. Res. IJETR* 6, 50–64.
- Ruiz-Perez, D., Guan, H., Madhivanan, P., Mathee, K., Narasimhan, G., 2020. So you think you can PLS-DA? *BMC Bioinformatics* 21, 2. <https://doi.org/10.1186/s12859-019-3310-7>
- Rusciano, G., Zito, G., Isticato, R., Sirec, T., Ricca, E., Bailo, E., Sasso, A., 2014. Nanoscale Chemical Imaging of *Bacillus subtilis* Spores by Combining Tip-Enhanced Raman Scattering and Advanced Statistical Tools. *ACS Nano* 8, 12300–12309. <https://doi.org/10.1021/nn504595k>
- Rzhevskii, A., 2019. The Recent Advances in Raman Microscopy and Imaging Techniques for Biosensors. *Biosensors* 9, 25. <https://doi.org/10.3390/bios9010025>
- Samek, O., Bernatová, S., Ježek, J., Šiler, M., Šerý, M., Krzyžánek, V., Hrubanová, K., Zemánek, P., Holá, V., Ružicka, F., 2015. Identification of individual biofilm-forming bacterial cells using Raman tweezers. *J. Biomed. Opt.* 20, 051038. <https://doi.org/10.1117/1.JBO.20.5.051038>
- Sánchez, M.C., Romero-Lastra, P., Ribeiro-Vidal, H., Llama-Palacios, A., Figuero, E., Herrera, D., Sanz, M., 2019. Comparative gene expression analysis of planktonic *Porphyromonas gingivalis* ATCC 33277 in the presence of a growing biofilm versus planktonic cells. *BMC Microbiol.* 19, 58. <https://doi.org/10.1186/s12866-019-1423-9>
- Sandt, C., Smith-Palmer, T., Pink, J., Brennan, L., Pink, D., 2007. Confocal Raman microspectroscopy as a tool for studying the chemical heterogeneities of biofilms in situ: Biofilm Raman microspectroscopy. *J. Appl. Microbiol.* 103, 1808–1820. <https://doi.org/10.1111/j.1365-2672.2007.03413.x>
- Santus, W., Devlin, J.R., Behnsen, J., 2021. Crossing Kingdoms: How the Mycobiota and Fungal-Bacterial Interactions Impact Host Health and Disease. *Infect. Immun.* 89. <https://doi.org/10.1128/IAI.00648-20>
- Sato, E.T., Martinho, H., 2018. First-principles calculations of Raman vibrational modes in the fingerprint region for connective tissue. *Biomed. Opt. Express* 9, 1728. <https://doi.org/10.1364/BOE.9.001728>
- Savitzky, Abraham., Golay, M.J.E., 1964. Smoothing and Differentiation of Data by Simplified Least Squares Procedures. *Anal. Chem.* 36, 1627–1639. <https://doi.org/10.1021/ac60214a047>
- Schmid, T., Sebesta, A., Stadler, J., Opilik, L., Balabin, R.M., Zenobi, R., 2010. Tip-enhanced Raman spectroscopy and related techniques in studies of biological materials, in: Dubowski, J.J., Geohegan, D.B., Träger, F. (Eds.), . Presented at the SPIE LASE, San Francisco, California, USA, p. 758603. <https://doi.org/10.1117/12.845471>
- Scholtes-Timmerman, M., Willemse-Erix, H., Schut, T.B., van Belkum, A., Puppels, G., Maquelin, K., 2009. A novel approach to correct variations in Raman spectra due to photo-bleachable cellular components. *The Analyst* 134, 387–393. <https://doi.org/10.1039/B811596F>
- Schwämmle, V., Jensen, O.N., 2010. A simple and fast method to determine the parameters for fuzzy c-means cluster analysis. *Bioinformatics* 26, 2841–2848. <https://doi.org/10.1093/bioinformatics/btq534>
- Scott, E.R., Crone, E.E., 2021. Using the right tool for the job: the difference between unsupervised and supervised analyses of multivariate ecological data. *Oecologia* 196, 13–25. <https://doi.org/10.1007/s00442-020-04848-w>

## REFERENCES

---

- Ščupáková, K., Balluff, B., Tressler, C., Adelaja, T., Heeren, R.M.A., Glunde, K., Ertaylan, G., 2020. Cellular resolution in clinical MALDI mass spectrometry imaging: the latest advancements and current challenges. *Clin. Chem. Lab. Med. CCLM* 58, 914–929. <https://doi.org/10.1515/cclm-2019-0858>
- Seda Keleştemur, Ertug Avci, Mustafa Çulha, 2018. Raman and Surface-Enhanced Raman Scattering for Biofilm Characterization. *Chemosensors* 6, 5. <https://doi.org/10.3390/chemosensors6010005>
- Seredin, P., Goloshchapov, D., Ippolitov, Y., Vongsvivut, J., 2019. Spectroscopic signature of the pathological processes of carious dentine based on FTIR investigations of the oral biological fluids. *Biomed. Opt. Express* 10, 4050. <https://doi.org/10.1364/BOE.10.004050>
- Sharma, G., Prakash, A., 2014. COMBINED USE OF FOURIER TRANSFORM INFRARED AND RAMAN SPECTROSCOPY TO STUDY PLANKTONIC AND BIOFILM CELLS OF CRONOBACTER SAKAZAKII 5.
- Shi, B., Chang, M., Martin, J., Mitreva, M., Lux, R., Klokkevold, P., Sodergren, E., Weinstock, G.M., Haake, S.K., Li, H., 2015. Dynamic Changes in the Subgingival Microbiome and Their Potential for Diagnosis and Prognosis of Periodontitis. *mBio* 6, e01926-14. <https://doi.org/10.1128/mBio.01926-14>
- Shlens, J., 2005. A Tutorial on Principal Component Analysis 13.
- Sil, S., Mukherjee, R., Kumar, N.S., S., A., Kingston, J., Singh, U.K., 2017. Detection and classification of Bacteria using Raman Spectroscopy Combined with Multivariate Analysis. *Def. Life Sci. J.* 2, 435. <https://doi.org/10.14429/dlsj.2.12275>
- Smekal, A., 1923. Zur Quantentheorie der Dispersion. *Naturwissenschaften* 11, 3.
- Smith, A., Mosele, N., L'Imperio, V., Pagni, F., Magni, F., 2018. Tissue MALDI Imaging, in: Vlahou, A., Mischak, H., Zoidakis, J., Magni, F. (Eds.), *Integration of Omics Approaches and Systems Biology for Clinical Applications*. John Wiley & Sons, Inc., Hoboken, NJ, USA, pp. 156–172. <https://doi.org/10.1002/9781119183952.ch9>
- Socransky, S. s., Haffajee, A. d., Cugini, M. a., Smith, C., Kent, R.L., 1998. Microbial complexes in subgingival plaque. *J. Clin. Periodontol.* 25, 134–144. <https://doi.org/10.1111/j.1600-051X.1998.tb02419.x>
- Socrates, G., 2001. *Infrared and Raman characteristic group frequencies: tables and charts*, 3rd ed. ed. Wiley, Chichester ; New York.
- Stîngu, C.S., Rodloff, A.C., Jentsch, H., Schaumann, R., Eschrich, K., 2008. Rapid identification of oral anaerobic bacteria cultivated from subgingival biofilm by MALDI-TOF-MS. *Oral Microbiol. Immunol.* 23, 372–376. <https://doi.org/10.1111/j.1399-302X.2008.00438.x>
- Stöckel, S., Kirchhoff, J., Neugebauer, U., Rösch, P., Popp, J., 2016. The application of Raman spectroscopy for the detection and identification of microorganisms: Raman spectroscopy for microorganism detection and identification. *J. Raman Spectrosc.* 47, 89–109. <https://doi.org/10.1002/jrs.4844>
- Stöhrer, S., 2020. Influence of Different Artificial Saliva Compositions on Subgingival Biofilm Formation. Universität Stuttgart. Master Thesis.
- Stoodley, P., Sauer, K., Davies, D.G., Costerton, J.W., 2002. Biofilms as Complex Differentiated Communities. *Annu. Rev. Microbiol.* 56, 187–209. <https://doi.org/10.1146/annurev.micro.56.012302.160705>
- Strola, S.A., Marcoux, P.R., Schultz, E., Perenon, R., Simon, A.-C., Espagnon, I., Allier, C.P., Dinten, J.-M., 2014. Differentiating the growth phases of single bacteria using Raman spectroscopy, in: Mahadevan-Jansen, A., Petrich, W. (Eds.), . Presented at the SPIE BiOS, San Francisco, California, United States, p. 893905. <https://doi.org/10.1117/12.2041446>

## REFERENCES

---

- Strola, S.A., Schultz, E., Allier, C.P., DesRoches, B., Lemmonier, J., Dinten, J.-M., 2013. Raman microspectrometer combined with scattering microscopy and lensless imaging for bacteria identification, in: Mahadevan-Jansen, A., Vo-Dinh, T., Grundfest, W.S. (Eds.), . Presented at the SPIE BiOS, San Francisco, California, USA, p. 85720X. <https://doi.org/10.1117/12.2002301>
- Svensäter, G., Welin, J., Wilkins, J.C., Beighton, D., Hamilton, I.R., 2001. Protein expression by planktonic and biofilm cells of *Streptococcus mutans*. FEMS Microbiol. Lett. 205, 139–146. <https://doi.org/10.1111/j.1574-6968.2001.tb10937.x>
- Tanner, A., Kent, R., Maiden, M.F.J., Taubman, M.A., 1996. Clinical, microbiological and immunological profile of healthy, gingivitis and putative active periodontal subjects. J. Periodontal Res. 31, 195–204. <https://doi.org/10.1111/j.1600-0765.1996.tb00484.x>
- Tewes, T., 2019. Entwicklung einer Methode zur Identifizierung von Mikroorganismen über Raman-Spektroskopie. Hochschule Rhein-Waal, Kleve.
- Thorpe, K.E., Joski, P., Johnston, K.J., 2018. Antibiotic-Resistant Infection Treatment Costs Have Doubled Since 2002, Now Exceeding \$2 Billion Annually. Health Aff. (Millwood) 37, 662–669. <https://doi.org/10.1377/hlthaff.2017.1153>
- Thurnheer, T., Gmür, R., Guggenheim, B., 2004. Multiplex FISH analysis of a six-species bacterial biofilm. J. Microbiol. Methods 56, 37–47. <https://doi.org/10.1016/j.mimet.2003.09.003>
- Thurnheer, T., Karygianni, L., Flury, M., Belibasakis, G.N., 2019. Fusobacterium Species and Subspecies Differentially Affect the Composition and Architecture of Supra- and Subgingival Biofilms Models. Front. Microbiol. 10, 1716. <https://doi.org/10.3389/fmicb.2019.01716>
- Trygg, J., Wold, S., 2002. Orthogonal projections to latent structures (O-PLS). J. Chemom. 16, 119–128. <https://doi.org/10.1002/cem.695>
- Tsuneda, S., Aikawa, H., Hayashi, H., Yuasa, A., Hirata, A., 2003. Extracellular polymeric substances responsible for bacterial adhesion onto solid surface. FEMS Microbiol. Lett. 223, 287–292. [https://doi.org/10.1016/S0378-1097\(03\)00399-9](https://doi.org/10.1016/S0378-1097(03)00399-9)
- Vacca-Smith, A.M., Bowen, W.H., 1998. Binding properties of streptococcal glucosyltransferases for hydroxyapatite, saliva-coated hydroxyapatite, and bacterial surfaces. Arch. Oral Biol. 43, 103–110. [https://doi.org/10.1016/S0003-9969\(97\)00111-8](https://doi.org/10.1016/S0003-9969(97)00111-8)
- Villa, J.E.L., Quiñones, N.R., Fantinatti-Garboggini, F., Poppi, R.J., 2019. Fast discrimination of bacteria using a filter paper-based SERS platform and PLS-DA with uncertainty estimation. Anal. Bioanal. Chem. 411, 705–713. <https://doi.org/10.1007/s00216-018-1485-9>
- Virdis, B., Millo, D., Donose, B.C., Batstone, D.J., 2014. Real-Time Measurements of the Redox States of c-Type Cytochromes in Electroactive Biofilms: A Confocal Resonance Raman Microscopy Study. PLoS ONE 9, e89918. <https://doi.org/10.1371/journal.pone.0089918>
- Wan, N., Wang, H., Ng, C.K., Mukherjee, M., Ren, D., Cao, B., Tang, Y.J., 2018. Bacterial Metabolism During Biofilm Growth Investigated by <sup>13</sup>C Tracing. Front. Microbiol. 9, 2657. <https://doi.org/10.3389/fmicb.2018.02657>
- Whiteley, R.K., Pajkos, A., Vickery, K., 2002. Biofilms that Impact on Human Health. J. Pharm. Pract. Res. 32, 153–158. <https://doi.org/10.1002/jppr2002322153>
- Wickramasinghe, N.N., Hlaing, M.M., Ravensdale, J.T., Coorey, R., Chandry, P.S., Dykes, G.A., 2020. Characterization of the biofilm matrix composition of psychrotrophic, meat spoilage pseudomonads. Sci. Rep. 10, 16457. <https://doi.org/10.1038/s41598-020-73612-0>
- Wille, G., Hellal, J., Ollivier, P., Richard, A., Burel, A., Jolly, L., Crampon, M., Michel, C., 2017. Cryo-Scanning Electron Microscopy (SEM) and Scanning Transmission

## REFERENCES

---

- Electron Microscopy (STEM)-in-SEM for Bio- and Organo-Mineral Interface Characterization in the Environment. *Microsc. Microanal.* 23, 1159–1172. <https://doi.org/10.1017/S143192761701265X>
- Wolcott, R.D., Rhoads, D.D., Bennett, M.E., Wolcott, B.M., Gogokhia, L., Costerton, J.W., Dowd, S.E., 2010. Chronic wounds and the medical biofilm paradigm. *J. Wound Care* 19, 45–53. <https://doi.org/10.12968/jowc.2010.19.2.46966>
- Wong, L., Sissions, C.H., 2001. A comparison of human dental plaque microcosm biofilms grown in an undefined medium and a chemically defined artificial saliva. *Arch. Oral Biol.* 46, 477–486. [https://doi.org/10.1016/S0003-9969\(01\)00016-4](https://doi.org/10.1016/S0003-9969(01)00016-4)
- Wright, C.J., Shah, M.K., Powell, L.C., Armstrong, I., 2010. Application of AFM from microbial cell to biofilm: AFM from microbial cell to biofilm. *Scanning* 32, 134–149. <https://doi.org/10.1002/sca.20193>
- Wuertz, S., Bishop, P., Wilderer, P., 2005. *Biofilms in Wastewater Treatment: An Interdisciplinary Approach*. IWA Publishing. <https://doi.org/10.2166/9781780402741>
- Xiao, J., Hara, A.T., Kim, D., Zero, D.T., Koo, H., Hwang, G., 2017. Biofilm three-dimensional architecture influences in situ pH distribution pattern on the human enamel surface. *Int. J. Oral Sci.* 9, 74–79. <https://doi.org/10.1038/ijos.2017.8>
- Ximenez-Fyvie, L.A., Haffajee, A.D., Socransky, S.S., 2000. Comparison of the microbiota of supra- and subgingival plaque in health and periodontitis. *J. Clin. Periodontol.* 27, 648–657. <https://doi.org/10.1034/j.1600-051x.2000.027009648.x>
- Yakubovskaya, E., Zaliznyak, T., Martínez Martínez, J., Taylor, G.T., 2019. Tear Down the Fluorescent Curtain: A New Fluorescence Suppression Method for Raman Microspectroscopic Analyses. *Sci. Rep.* 9, 15785. <https://doi.org/10.1038/s41598-019-52321-3>
- Zeiri, L., Bronk, B.V., Shabtai, Y., Czégé, J., Efrima, S., 2002. Silver metal induced surface enhanced Raman of bacteria. *Colloids Surf. Physicochem. Eng. Asp.* 208, 357–362. [https://doi.org/10.1016/S0927-7757\(02\)00162-0](https://doi.org/10.1016/S0927-7757(02)00162-0)
- Zhu, Q., Quivey, R.G., Berger, A.J., 2007. Raman Spectroscopic Measurement of Relative Concentrations in Mixtures of Oral Bacteria. *Appl. Spectrosc.* 61, 1233–1237. <https://doi.org/10.1366/000370207782597021>
- Zhu, Q., Quivey, R.G., Berger, A.J., 2004. Measurement of bacterial concentration fractions in polymicrobial mixtures by Raman microspectroscopy. *J. Biomed. Opt.* 9, 1182. <https://doi.org/10.1117/1.1803844>
- Zijnge, V., Ammann, T., Thurnheer, T., Gmür, R., 2012. Subgingival Biofilm Structure. <https://doi.org/10.1159/000329667>
- Zobell, C.E., Anderson, D.Q., 1936. OBSERVATIONS ON THE MULTIPLICATION OF BACTERIA IN DIFFERENT VOLUMES OF STORED SEA WATER AND THE INFLUENCE OF OXYGEN TENSION AND SOLID SURFACES. *Biol. Bull.* 71, 324–342. <https://doi.org/10.2307/1537438>

## 8 Appendix

### 8.1 Outreach activities

#### Peer-reviewed publications

Kriem, L.S., Wright, K., Ccahuana-Vasquez, R.A., Rupp, S., 2020. Confocal Raman microscopy to identify bacteria in oral subgingival biofilm models. PLOS ONE 12, e0232912. <https://doi.org/10.1371/journal.pone.0232912>

Kriem, L.S., Wright, K., Ccahuana-Vasquez, R.A., Rupp, S., 2021. Mapping of a subgingival dual-species biofilm model using Confocal Raman Microscopy. Front. Microbiol. doi: 10.3389/fmicb.2021.729720

#### Conferences

Kriem, L.S., “The Use of Raman Technologies for Biofilm Mapping.”, EuroBiofilms2022 Conference, Palma de Mallorca (2022)

Kriem, L.S., Rupp, S., Wright, K., Ccahuana-Vasquez, R.A., 2020. “Confocal Raman Microscopy Can Differentiate Oral Multi-Species Biofilms.”, IADR General Meeting, Washington, DC, USA (2020)

Kriem, L.S., “The Skittles Project – Using Raman Technologies for Oral Bacteria Differentiation”, BioClean Dissemination Event, Bari, Italy (2019)

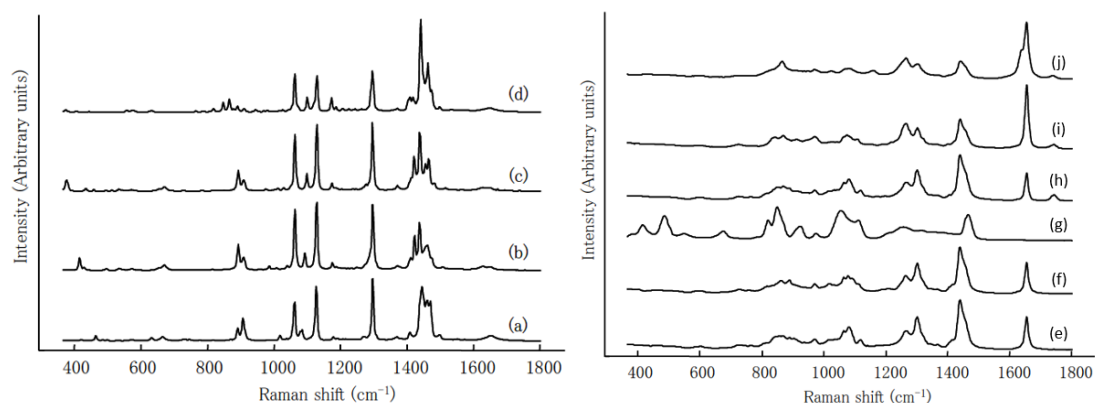
#### Posters

Kriem, L.S., Rupp, S., Schließmann, U., “The Use of Confocal Raman Microscopy for Oral Bacteria Differentiation.”, EuroBiofilms Conference, Glasgow, UK (2019)

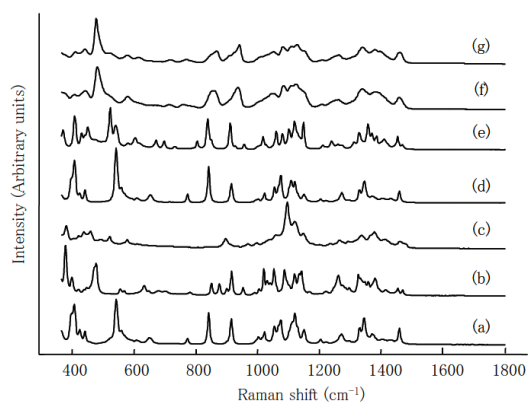


## 8.2 Raman spectra of different biological molecules

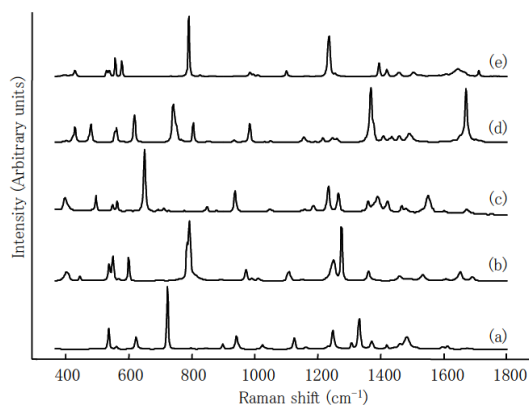
Raman spectra of saturated linear fatty acids: (a) lauric acid, (b) myristic acid, (c) palmitic acid, (d) stearic acid and unsaturated fatty acids: (e) oleic acid, (f) cis-vaccenic acid, (g) glycerol and of the fats (h) triolein, (i) trilinolein, (j) trilinolenin (applied from De Gelder, 2008):



Raman spectra of different saccharides: (a)  $\beta$ -D-glucose, (b) lactose, (c) cellulose, (d) D(+)-dextrose, (e) D(+)-trehalose, (f) amylose, (g) amylopectine (applied from De Gelder, 2008):



Raman spectra of DNA and RNA bases: (a) adenine, (b) cytosine, (c) guanine, (d) thymine, (e) uracil (applied from De Gelder, 2008).



## 8.3 Media recipes

### 8.3.1 Modified Fluid Universal Medium in Sørensen's buffer (pH 7.2):

#### MFUM SOLUTION MIXING RATIOS:

Substance	Mixing ratios
<b>SOLUTION A</b>	<b>8</b>
<b>SOLUTION B</b>	<b>0.5</b>
<b>RTF SOLUTION</b>	<b>1.5</b>

\*\*stored at 4°C for up to 2 weeks\*\*

#### SOLUTION A:

Substance	Final Concentration
Bacto Tryptone	10 g/L
Yeast Extract	5 g/L
KNO <sub>3</sub>	1 g/L
NaCl	2 g/L
Hemin stock	1 ug/L
Sørensen's buffer	800 mL

\*\*autoclave at 120°C\*\*

#### SOLUTION B:

Substance	Final Concentration
Glucose	0.3% (3 g/L)
Cysteine*HCl*H <sub>2</sub> O	0.5 g/L
Na <sub>2</sub> CO <sub>3</sub>	0.5 g/L
Sørensen's buffer	50 mL

\*\*mix with RTF Solution + sterile-filtered with 0.22 µm filter into solution A\*\*

## APPENDIX

### RTF SOLUTION:

Substance	Ratio/Concentration
RTF stock 1	1
RTF stock 2	1
Menadione Stock	2 µg/mL

\*\*mixed with Solution B + sterile-filtered with 0.22 µm filter into solution A\*\*

### Sörensen's Buffer, pH 7,2

Substance	1000mL
KH <sub>2</sub> PO <sub>4</sub>	2.71 g
Na <sub>2</sub> HPO <sub>4</sub>	7.11 g
H <sub>2</sub> O dist.	

\*\*pH check\*\*

\*\*Stored at 4°C\*\*

### RTF 1 Stock Solution

Substance	Concentration
K <sub>2</sub> HPO <sub>4</sub>	6 g/L
Sörensen's buffer	

\*\*Stored at 4°C\*\*

### RTF 2 Stock Solution

Substance	Concentration
KH <sub>2</sub> PO <sub>4</sub>	6 g/L
MgSO <sub>4</sub> *7H <sub>2</sub> O	2.5 g/L
NaCl	12 g/L
(NH <sub>4</sub> )SO <sub>4</sub>	12 g/L
H <sub>2</sub> O dist.	1000 mL

\*\*Stored at 4°C\*\*

### Menadione Stock Solution (0,5 mg/mL)

Substance	50mL
Menadion	25 mg
Ethanol	50 mL

\*\*Stored at 4°C\*\*

**Hemin Stock Solution (1 mg/mL)**

Substance	50mL
KOH 0.1 N	25 mL
Ethanol	12.5 mL
H <sub>2</sub> O dist.	12.5 mL
Hemin chloride	50 mg

\*\*Stored at 4°C\*\*

**8.3.2 Saliva and artificial saliva preparation and evaluation**

Natural saliva was used as reference to evaluate the artificial saliva. Natural saliva was collected from one human donor. The donor was a masculine young adult without acute carious lesions or periodontal disease. Natural saliva was collected at the same daytime at least 1.5 hours after teeth brushing. Salivary flow was stimulated with Parafilm® M (Bemis Company Inc., Neenah, WI, USA). After collection natural saliva was centrifuged at 4000 g<sub>a</sub> and 4 °C for 30 min and the supernatant was filtrated (Sartorius™ Minisart™ NML Syringe Filter, 0.2 µm nonsterile). The solution was stored at 4 °C and used within a week.

For 1 L of phosphate buffered saline (PBS), 0.29 g monobasic potassium phosphate, 1.19 g dibasic potassium phosphate and 4.93 g sodium chloride was dissolved in dd water and autoclaved. PBS contained 93.32 mM salt.

Hahnel's saliva was applied from (Hahnel, 2007):

Substance	Concentration (mg/L)
Albumin	40.000
Lysozyme (1400 U/mL)	10.000
A-Amylase (50 U/mL)	1.000
Mucin	850

\*\*Stored at 4°C for up to two weeks\*\*

## APPENDIX

DMM saliva was applied from (Wong and Sissions, 2001):

Substance	Concentration (mg/L)
Calcium chloride dihydrate	147,02
Magnesium chloride	50,57
Potassium dihydrogen phosphate	476
Di-potassium hydrogen phosphate	261
Sodium chloride	584
Potassium chloride	1118
Ammonium chloride	107
Mucin	2500
Urea	60

\*\*Stored at 4°C for up to two weeks\*\*

In total, three artificial saliva substitutes (Hahnel, DMM and PBS) mixed with mFUM were compared to mimic natural saliva based on their subgingival bacterial adhesion properties and biofilm formation. Hahnel artificial saliva has first been described by Hahnel in 2007 with the recipe in Chapter 8.3.2 (Appendix). DMM as an artificial saliva was first described by Wong and Sissions in 2001 with the recipe in Chapter 8.3.2 (Appendix). Additionally, PBS was considered as an alternative that doesn't contain additional proteins besides the amount present in the mFUM medium (see Chapter 8.3.2 in the Appendix).

Artificial saliva were evaluated in comparison to natural saliva based on their total bacterial concentration in a biofilm (Figure 41) and their ratios of *A.denticolens*, *S.oralis* and *V.dispar* within the biofilms (Figure 42). Biofilms were quantified using RT-PCR with calibration curves found in Chapter 8.6 of the Appendix using gBlocks™ (described in Chapter 3.2.4).

Quantification of biofilms grown with natural saliva had a total mean concentration of  $1.51 \times 10^8$  ( $\pm 1.37 \times 10^8$ ) bacteria while artificial saliva showed concentrations of  $2.71 \times 10^8$  ( $\pm 1.04 \times 10^8$ ) bacteria for DMM:mFUM,  $4.37 \times 10^7$  ( $\pm 2.66 \times 10^7$ ) bacteria for Hahnel:mFUM and  $1.20 \times 10^8$  ( $\pm 8.71 \times 10^7$ ) bacteria for PBS:mFUM (Figure 41). In comparison to the biofilms in natural saliva:mFUM, DMM:mFUM increases the bacterial concentration by 80.37%, while concentrations with the use of Hahnel:mFUM and PBS:mFUM artificial saliva were reduced by 71.02% and 20.60% respectively. In conclusion, out of the three selected artificial saliva, PBS in a 50:50 ratio with mFUM medium shows the closest bacterial concentration to natural saliva.

In addition to total biofilm bacteria concentrations, biofilms grown with natural saliva showed a bacterial distribution of *A.denticolens*, *S.oralis* and *V.dispar* of 27.69% : 70.45% : 1.86%.

APPENDIX

Biofilms cultivated in DMM:mFUM showed percentages of 18.73% : 79.86% : 1.42%, Hahnel:mFUM percentages of 38.99% : 55.11% : 5.90% and PBS:mFUM percentages of 24.93% : 73.37% : 1.69%. Biofilms with DMM:mFUM showed an overpopulation of *S.oralis* and underpopulation of *A.denticolens* when compared to natural saliva, while Hahnel:mFUM saliva showed the opposite effect. Only PBS:mFUM showed representative ratios compared to natural saliva mixed with mFUM with population differences of only about 3% (Figure 42).

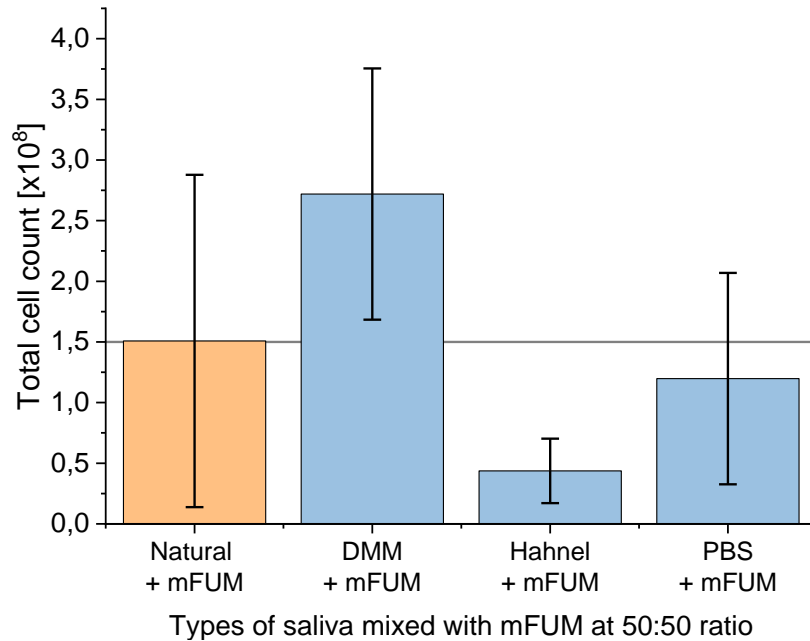


Figure 41: Total concentration of bacteria in a multi-species biofilm consisting of *A.denticolens*, *S.oralis* and *V.dispar*. For every type of saliva a total of 10 samples were evaluated using RT-PCR.

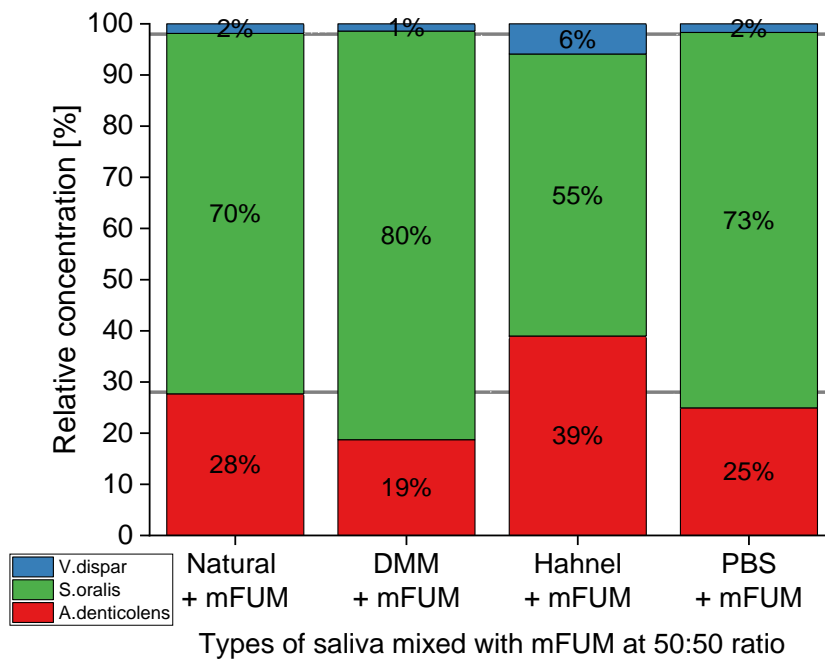


Figure 42: Ratio of bacterial species within a biofilm cultivated with different types of saliva (natural and artificial) and mFUM medium at a 50:50 ratio. Relative concentrations are based on RT-PCR data generated from 10 samples for each type of saliva.

Comparing the three selected artificial saliva to natural saliva in terms of biofilm growth and species distribution, only PBS:mFUM showed similar characteristics to natural saliva and mFUM.

## 8.4 Fluorescent *in-situ* hybridization

### 4% PFA (Paraformaldehyde)/ PBS

- Heat 200 mL distilled water to 60°C
- Add 10g PFA and 5 drops of 1 M NaOH (NO OVERHEATING)
- Let PFA dissolve in 2min and add 5 mL 10X PBS
- Adjust to pH 7.2 with HCl and fill up to 250 mL with DI water
- Store at 4°C but not longer than 6 months

### Oligonucleotide

Bacteria	Probe	Label	Probe conc. (ug/mL of hybridization buffer)	Formamide conc. (%)
<i>S.oralis</i>	MIT447	6-FAM	20	20-30
<i>A.denticolens</i>	ACT476	Cy3	20	25-35

### Hybridization Buffer for 200 µL:

	Formamide concentration (units in µL)								
	20%			30%			40%		
	200uL	1mL	2mL	200uL	1mL	2mL	200uL	1mL	2mL
<b>5M NaCl</b>	36	180	360	36	180	360	36	180	360
<b>1M Tris-HCl</b>	4	20	40	4	20	40	4	20	40
<b>10% SDS</b>	0.2	1	2	0.2	1	2	0.2	1	2
<b>Formamide</b>	<b>40</b>	<b>200</b>	<b>400</b>	<b>60</b>	<b>300</b>	<b>600</b>	<b>80</b>	<b>400</b>	<b>800</b>
<b>ddH<sub>2</sub>O</b>	<b>114</b>	<b>570</b>	<b>1140</b>	<b>94</b>	<b>470</b>	<b>940</b>	<b>74</b>	<b>370</b>	<b>740</b>
<b>Any FISH Probe</b>	6	30	60	6	30	60	6	30	60

### Washing Buffer for 50 mL:

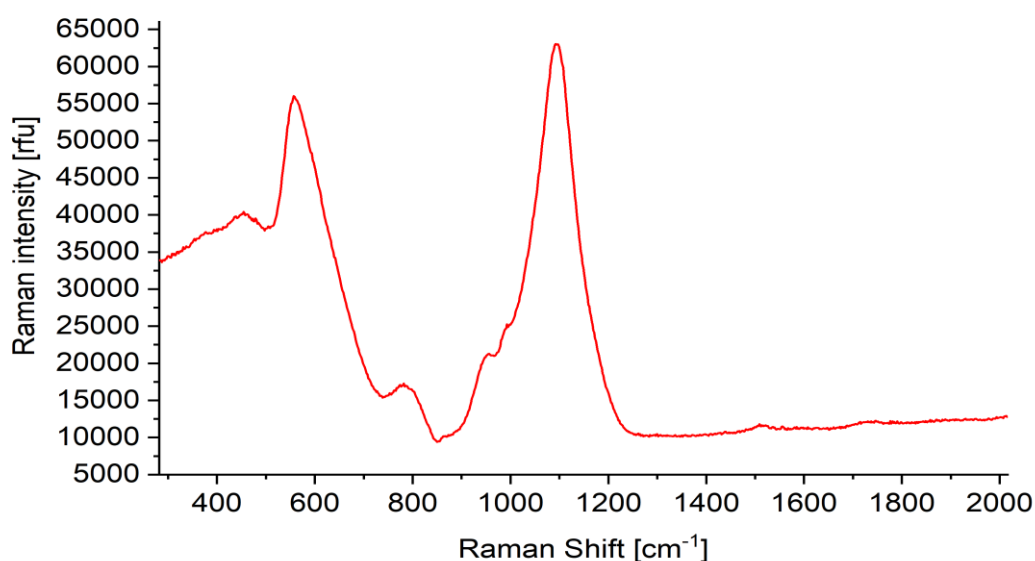
	Formamide concentration (units in mL)					
	20%		30%		40%	
<b>5M NaCl</b>	2,15	0,43	1,02	0,204	0,46	0,092
<b>1M Tris-HCl</b>	1	0,2	1	0,2	1	0,2
<b>0.5M EDTA</b>	0,5	0,1	0,5	0,1	0,5	0,1
<b>ddH<sub>2</sub>O</b>	46,35	9,27	47,35	9,496	48,1	9,608
<b>10% SDS</b>	50 uL	10 uL	50 uL	10 uL	50 uL	10 uL
<b>TOTAL</b>	<b>50</b>	<b>10</b>	<b>50</b>	<b>10</b>	<b>50</b>	<b>10</b>

**Mowiol® 4-88:**

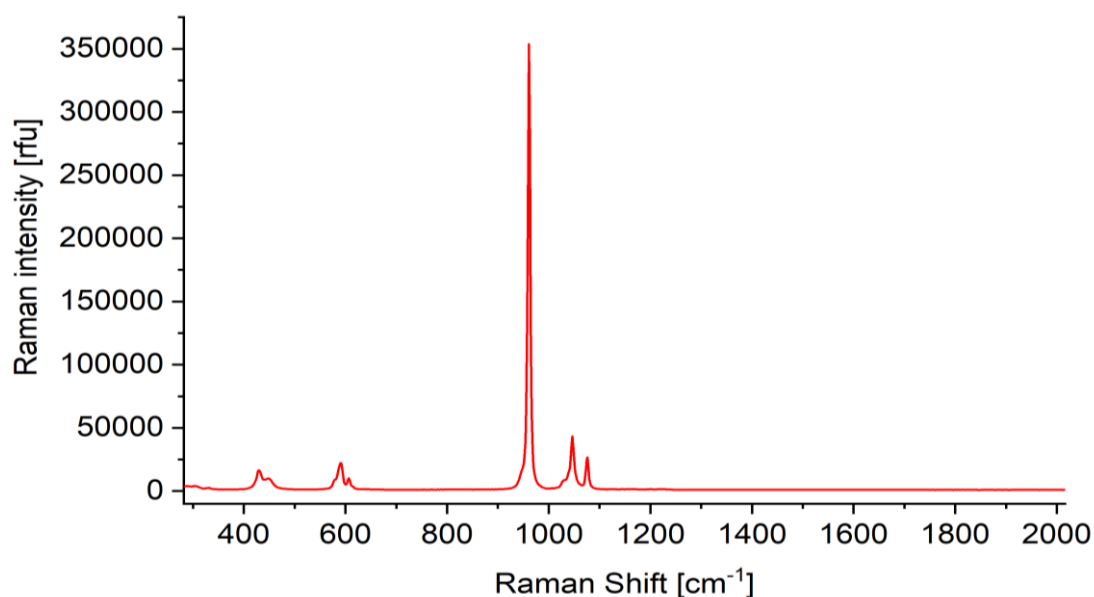
- Weigh 2.4 g Mowiol® 4-88 and add 6 g Glycerol and 6 mL DI water and mix
- add 9.6 ml DI water and 2.4 ml Tris-HCl (1 M, pH 8.5)
- Mix for 5h and then let it rest for 2h
- incubate for 10 min at 50 °C
- centrifuge for 15 min at 5000 xg
- aliquot supernatant in Eppendorf vials and keep at -20°C

## 8.5 Raman spectra

### 8.5.1 Borosilicate glass spectrum



### 8.5.2 Hydroxyapatite disc spectrum





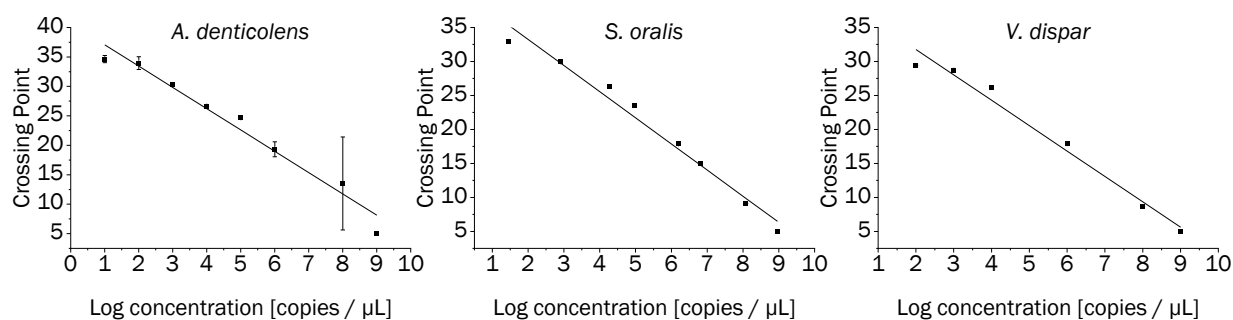
### 8.5.3 Peak assignment of Raman spectra for medical microorganisms

The table shows major peak assignments for the two species of interest for the differentiation of medical biofilms. (s) = small peak, (m) = medium peak, (l) = large peak.

Band [ $\text{cm}^{-1}$ ]		Peak assignments for biochemical compounds
<i>P.aeruginosa</i>	<i>C.albicans</i>	
607 (s)	-	Phenylalanine
623 (s)	623 (s)	Phenylalanine
640 (s)	642 (s)	Tyrosine
722 (s)	722 (s)	Adenine
749 (l)	749 (l)	Thymine (ring breathing)
783 (s)	782 (m)	Cytosine (ring breathing)
848 (m)	853 (s)	Proteins
894 (s)	894 (s)	$\gamma(\text{CN})$ , $\gamma(\text{CON})$ symmetric, $\delta(\text{CCH})$ aliphatic
-	974 (s)	Polysaccharide
986 (m)	-	Polysaccharide
1003 (s)	1003 (m)	Phenylalanine ( $\gamma(\text{CC})$ aromatic ring)
1128 (l)	1128 (l)	C-C, C-N stretch of proteins
1157 (s)	1156 (s)	Amide III
1169 (s)	1173 (s)	Phospholipids
1207 (s)	1207 (s)	Phenylalanine, Tyrosine
1229 (s)	1229 (s)	Amide III (CN in plane bend)
1312 (m)	1312 (s)	Amide III
1340 (s)	1339 (m)	Tryptophane (C-H <sub>2</sub> twist)
1397 (s)	1397 (s)	COO <sup>-</sup> sym./CH <sub>2</sub> asym. def.
1455 (m)	1458 (l)	C-H <sub>2</sub> deformation (scissoring from Lipids, assym. Def. of amino acid side chains)
1527 (s)	1527 (s)	C=C stretch
1585 (m)	1585 (m)	Amide II
1659 (m)	1659 (m)	Amide I
1746 (m)	1746 (s)	CH <sub>2</sub> bending

### 8.6 RT-PCR calibration curves

The used sequences for calibration is described in Chapter 3.2.4 where a gBlocks™ sequence was selected containing all three sequences for *A.denticolens*, *S.oralis* and *V.dispar*.

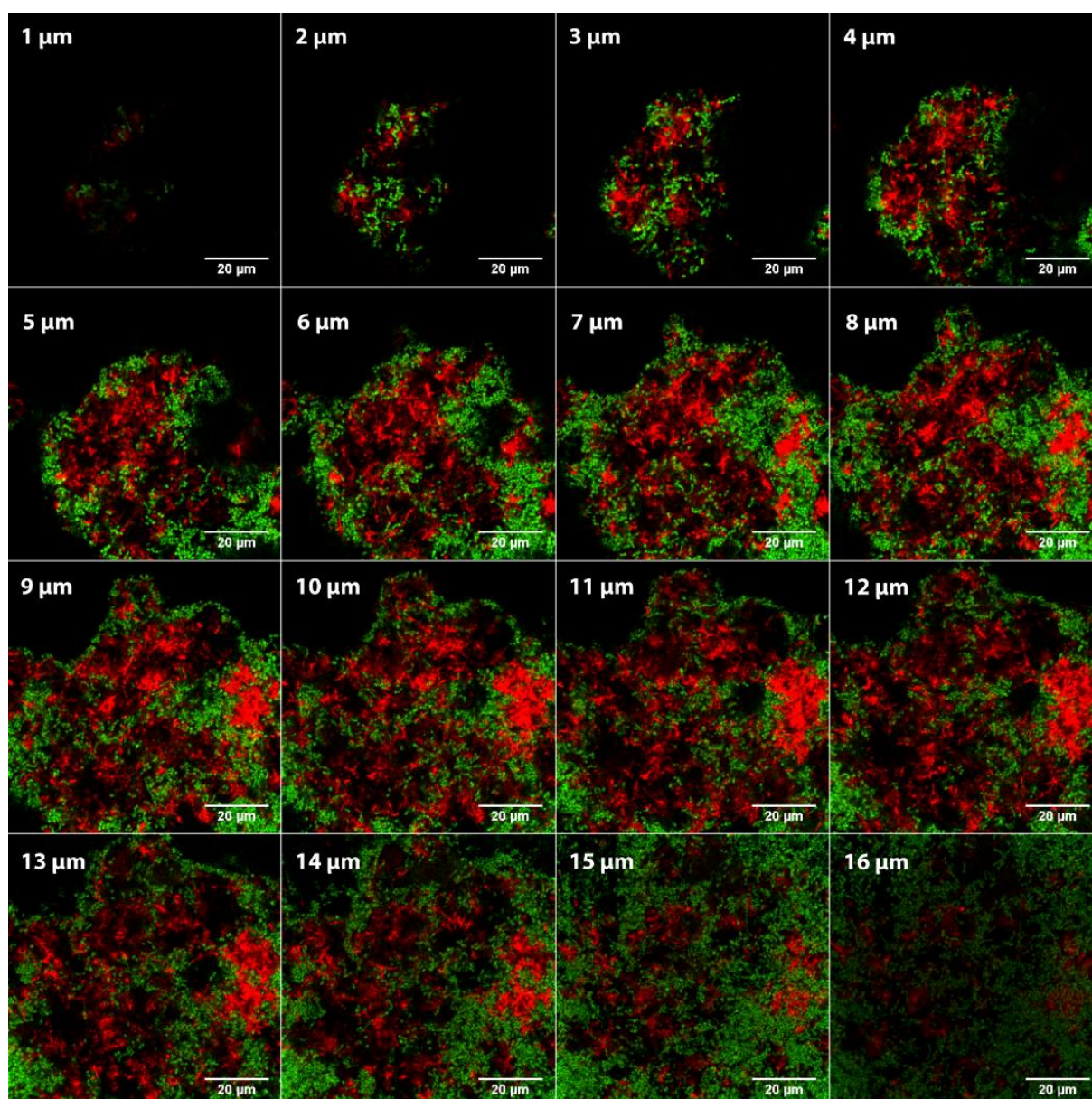


## APPENDIX

RT-qPCR calibration characteristics. The formula shows the slope and y-intercept with its standard errors:

Species	Formula	Pearson's r
<i>A.denticolens</i>	$y = -3.61 \pm 0.11 x + 40.70 \pm 0.59$	0.97
<i>S.oralis</i>	$y = -3.84 \pm 0.10 x + 40.92 \pm 0.58$	0.98
<i>V.dispar</i>	$y = -3.73 \pm 0.13 x + 39.22 \pm 0.79$	0.98

### 8.7 Individual images of FISH staining



## 8.8 Bacteria coverage for different samples that were analyzed through morphology and Raman analysis

Total quantitative results of bacteria coverage for the different samples analyzed in Figure 33. Negative values in total differences indicate under-identification of the species in Raman analysis compared to morphology analysis while a positive value indicates over-identification. Values in the column different area classification morphology vs. Raman indicate coverage of blue area from overlapped images of morphology and Raman in Figure 33 and indicates the different locational identification in comparison to total coverage.

Sample	Morphology area in %		Raman area in %			Difference in %		Different classification Morphology vs. Raman in %
	<i>A.denticolens</i>	<i>S.oralis</i>	<i>A.denticolens</i>	<i>S.oralis</i>	Unidentified	<i>A.denticolens</i>	<i>S.oralis</i>	
1	61.67	38.33	62.01	31.01	6.98	0.35	-7.33	27.47
2	30.48	69.52	42.42	57.58	0.00	11.94	-11.94	24.33
3	33.83	66.17	37.86	62.14	0.00	4.03	-4.03	27.28
4	63.98	36.02	66.72	26.52	6.76	1.94	-9.44	31.54
5	63.16	36.85	69.72	27.11	3.18	6.56	-9.74	27.06
6	31.12	68.88	33.62	66.38	0.00	2.49	-2.49	30.09
7	63.01	36.99	55.20	44.80	0.00	-7.81	7.81	24.45
8	51.45	48.55	51.80	48.20	0.00	0.35	-0.35	28.57
9	39.10	60.90	41.03	58.97	0.00	1.93	-1.93	29.78
10	46.40	53.60	32.98	67.02	0.00	-13.42	13.42	21.82
11	43.04	56.96	40.41	59.59	0.00	-2.63	2.63	26.71
12	38.80	61.20	36.08	63.92	0.00	-2.72	2.72	17.66
13	45.41	54.59	54.57	45.43	0.00	9.16	-9.16	30.68
14	47.11	52.89	50.54	49.46	0.00	3.44	-3.44	26.24
15	37.28	62.72	39.82	60.18	0.00	2.54	-2.54	27.00

## **Declaration of Authorship**

### **Declaration of Authorship**

I hereby certify that the dissertation entitled: “The Use of Raman Microscopy for the Evaluation of *In-Vitro* Biofilm Model Structures“ is entirely my own work except where otherwise indicated. Passages and ideas from other sources have been clearly quoted.

### **Erklärung über die Eigenständigkeit der Dissertation**

Ich versichere, dass ich die vorliegende Arbeit mit dem Titel: „The Use of Raman Microscopy for the Evaluation of *In-Vitro* Biofilm Model Structures“ selbständig verfasst und keine anderen als die angegebenen Quellen und Hilfsmittel benutzt habe; aus fremden Quellen entnommene Passagen und Gedanken sind als solche kenntlich gemacht.

Name/Name: Lukas Kriem

Signature/Unterschrift: \_\_\_\_\_

Date/Datum: